Modeling auditory processing and speech perception in hearing-impaired listeners

Jepsen, Morten Løve; Pedersen, Michael Syskind; Dau, Torsten

Publication date:
2010

Document Version
Publisher's PDF, also known as Version of record

Technical University of Denmark

CONTRIBUTIONS TO
HEARING RESEARCH

Volume 7

Morten Løve Jepsen

Modeling auditory processing and speech perception in hearing-impaired listeners

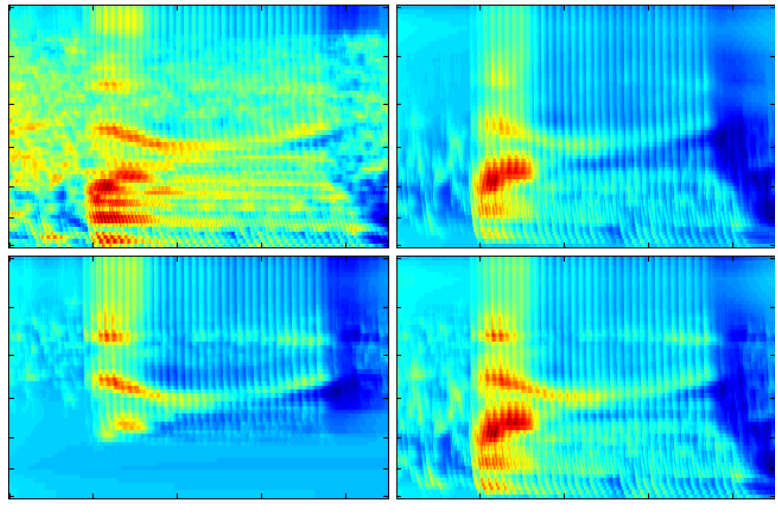

Centre for Applied Hearing Research
Department of Electrical Engineering

Modeling auditory processing and speech perception in hearing-impaired listeners

Ph.D. thesis by
Morten Løve Jepsen

Technical University of Denmark
2010

Printed in Denmark by Rosendahls - Schultz Grafisk A/S.
The defense was held on May 27, 2010.

Denne ph.d.-afhandling er indleveret til bedømmelse til Institut for Elektroteknologi på Danmarks Tekniske Universitet.

Projektet er hovedsageligt udført hos Center for anvendt høreforskning, Institut for Elektroteknologi på Danmarks Tekniske Universitet. Dele af projektet er udført på Hearing Research Center ved Boston University, Massachusetts, USA.

Vejledere:

Hovedvejleder:
Professor Torsten Dau
Center for anvendt høreforskning, DTU Elektro
Lyngby, Danmark

Medvejledere:
Lars Bramsløw, Ph.D. and Michael S. Pedersen, Ph.D.
Oticon
Smørum, Danmark

Vejleder på delprojekt på Boston University:
Dr. Oded Ghitza
Hearing Research Center, Boston University
Boston, Massachusetts, USA

Finansiering:

Projektet var finansieret gennem Oticon Fonden, Forskerskolen SNAK (Sanser, nerver, adfærd og kommunikation) og Ministeriet for videnskab, teknologi og udvikling.

Et eksternt forskningsophold blev endvidere støttet af Oticon Fonden, Otto Mønsteds Fond og Kaj og Hermilla Ostenfeld's Fond.

4. Februar, 2010

.

_____

Morten Løve Jepsen, forfatter

To my son
Tobias

Abstract

A better understanding of how the human auditory system represents and analyzes sounds and how hearing impairment affects such processing is of great interest for researchers in the fields of auditory neuroscience, audiology, and speech communication as well as for applications in hearing-instrument and speech technology. In this thesis, the primary focus was on the development and evaluation of a computational model of human auditory signal-processing and perception. The model was initially designed to simulate the normal-hearing auditory system with particular focus on the nonlinear processing in the inner ear, or cochlea. The model was shown to account for various aspects of spectro-temporal processing and perception in tasks of intensity discrimination, tone-in-noise detection, forward masking, spectral masking and amplitude modulation detection. Secondly, a series of experiments was performed aimed at experimentally characterizing the effects of cochlear damage on listeners' auditory processing, in terms of sensitivity loss and reduced temporal and spectral resolution. The results showed that listeners with comparable audiograms can have very different estimated cochlear input-output functions, frequency selectivity, intensity discrimination limens and effects of simultaneous- and forward masking. Part of the measured data was used to adjust the parameters of the stages in the model, that simulate the cochlear processing. The remaining data were used to evaluate the fitted models. It was shown that an accurate simulation of cochlear input-output functions, in addition to the audiogram, played a major role in accounting both for sensitivity and supra-threshold processing. Finally, the model was used as a front-end in a framework developed to predict consonant discrimination in a diagnostic rhyme test. The framework was constructed such that discrimination errors originating from the front-end and the back-end were separated. The front-end was fitted to individual listeners with cochlear hearing loss according to non-speech data, and speech data were obtained in the same listeners. It was shown that most observations in the measured consonant discrimination error patterns were predicted by the model, although error rates were systematically underestimated by the model in few particular acoustic-phonetic features. These results reflect a relation between basic auditory processing deficits and reduced speech perception performance in the listeners with cochlear hearing loss. Overall, this work suggests a possible explanation of the variability in consequences of cochlear hearing loss. The proposed model might be an interesting tool for, e.g., evaluation of hearing-aid signal processing.

Resumé

Der er stor interesse for en bedre forståelse af hvordan menneskets hørelse analyserer og repræsenterer lyde og for at forstå hvordan høretab påvirker signalbehandlingen og opfattelsen af lyd. Disse aspekter er særligt interessante for forskere indenfor neurovidenskab, audiologi, talekommunikation og i anvendelsesområder som i høreapparats og tale-teknologi. Det primære fokus i denne afhandling var udvikling og evaluering af en beregningsmodel for auditiv signalbehandling og lydopfattelse hos mennesker. Modellen blev først udviklet til at simulere det normalthørende auditive system med fokus på den ikke-lineære processering i det indre øre (cochlea). Det blev vist, at modellen kunne forklare aspekter der vedrører spektro-temporal processering, såsom intensitets-diskrimination, detektering af toner i støj, tids-maskering (forward masking), spektral maskering samt detektering af amplitude-modulation. Dernæst blev det undersøgt hvordan man ved hjælp af psykoakustiske eksperimenter kan karakterisere den auditive signalbehandling hos hørehæmmede med høretab i det indre øre. Disse eksperimenter testede hørbarhed samt eventuelt reduceret opløsning i tid og frekvens. Resultaterne viste at personer med sammenlignelige audiogrammer havde vidt forskellige udfald i forhold input-output funktioner i cochlea, frekvens-selektivitet, intensitets-diskrimination samt simultan maskering og tids-maskering. En del af data blev brugt til at tilpasse parametre i de trin i modellen der simulerer det indre øres funktion og formålet var at beskrive signalbehandlingen hos de målte individer. De resterende data blev brugt til at evaluere de tilpassede modeller. Udover audiogrammet, viste det sig at være vigtigt at kunne simulere cochlear processeringen præcist for at kunne beskrive både hørbarhed og såkaldt "supra-tærskel" processering. Til sidst blev modellen brugt som "front-end" i et talegenkendelses-system målrettet mod at kunne forudsige data fra et specifikt taleeksperiment (diagnostic rhyme test). Systemet var udviklet til at kunne separere konsonant-diskriminations fejl i forhold til om de stammede fra modellens front-end eller detektor (back-end). Modellens front-end blev på baggrund af maskeringsdata tilpasset til personer med høretab i det indre øre, og fejlrater i tale-eksperimentet blev målt i de samme personer. Modellen kunne i de fleste betingelser forudsige mønsteret i de målte konsonant-diskriminations fejl. Disse resultater afspejler at der er en sammenhæng mellem den forringede signalbehandling i hørelsen og forværret taleopfattelse hos hørehæmmede.

Samlet set bliver der i denne afhandling foreslået en række mulige forklaringer på variationen i hørehæmmedes lydopfattelse. Derudover kan den foreslåede model muligvis være interessant i anvendelse som et værktøj, eksempelvis til at evaluere signalbehandlingen i høreapparater.

Forord

Det er min overbevisning, at tiden går hurtigt hvis man nyder hvad man laver. Det er netop hvad der er sket for mig i de sidste 3 år. Det har været en fornøjelse at møde på arbejde hver dag i forbindelse med dette projekt. Den primære årsag har vært de mennesker som har omgivet mig på kontoret og privat.

Jeg takker Torsten Dau for at have været min inspiration til at gå i gang med et forskningsprojekt. Hans engagement og den energi han har lagt i vejledningen er uvurderlig. Måden hvorpå han involverer sig som kollega og ven har gjort det til en fornøjelse at arbejde på projektet.

Adskillige folk og medstuderende har skabt et enestående arbejdsmiljø på Center for anvendt høreforskning (CAHR), både fagligt og socialt. For at nævne nogle få: Claus, Eric, Filip, Iris, Olaf, Sarah, Sebastien, Sylvain og Tobias... Tak. Også en tak til Martin, Sven og Anders for nogle underholdende timer i pauserne.

Jeg er taknemmelig overfor min familie, især mine forældre. I har været en uundværlig støtte, og jeg havde ikke kunne udføre dette arbejde uden jeres hjælp og fleksibilitet.

Mine medvejledere hos Oticon, Lars og Michael, har vist stor interesse i projektets forløb, og var en stor hjælp i projektet indledende fase i forhold til planlægning og til at vælge en indholdsmæssig relevant retning.

The people at Boston University were very welcoming, and made my visit in Boston during the fall of 2008 a great experience from day one. Thank you, Oded and Steve.

Tak til alle forsøgspersonerne der har deltaget i mine lytteforsøg. Resultaterne fra målingerne er selvfølgelig en vigtig del af hele projektet.

Og mest af alle vil jeg takke min søn, Tobias, for alle de dejlige dage som har fjernet mine tanker fra arbejdet når det var nødvendigt. Disse år havde ikke været så sjove og lykkelige uden dig.

Morten Løve Jepsen, 4. februar, 2010

List of publications

Journal articles:

Jepsen, M. L., Ewert, S. D. and Dau, T. **(2008)**, ”A computational model of human auditory signal processing and perception”, J. Acoust. Soc. Am. 124, 422-438.

Moore, B. C. J., Glasberg, B. R., and Jepsen, M. L. **(2009)**, ”Effects of pulsing of the target tone on the audibility of partials in inharmonic complex tones”, J. Acoust. Soc. Am. 125, 3194-3204.

Jepsen, M. L., and Dau, T. **(2010)**, “Characterizing auditory processing and perception in individual listeners with sensorineural hearing loss”, J. Acoust. Soc. Am., *Submitted*.

Conference articles:

Dau, T., Jepsen, M. L., and Ewert, S. D. **(2007)**, ”Modeling spectral and temporal masking in the human auditory system”, Proceedings of the 19th International Congress on Acoustics, ICA ’07, Madrid, Spain.

Dau, T., Jepsen, M. L., and Ewert, S. D. **(2008)**, ”Spectral and temporal processing in the human auditory system”, Proceedings of the International Symposium on Auditory and Audiological Research (ISAAR), Helsingør, Denmark.

Jepsen, M. L., and Dau, T. **(2008)**, ”Modeling auditory signal processing in hearing-impaired listeners”, Proceedings of the International Symposium on Auditory and Audiological Research (ISAAR), Helsingør, Denmark.

Jepsen, M. L., and Dau, T. **(2010)**, ”Modeling a damaged cochlea: beyond non-speech psychophysics”, International Symposium on Auditory and Audiological Research (ISAAR), Helsingør, Denmark. *Submitted*.

Published abstracts:

Jepsen, M. L., and Dau, T. **(2008)**, ”Estimating the basilar-membrane input-output function in normal-hearing and hearing-impaired listeners using forward masking”, J. Acoust. Soc. Am. 123, 3859. Acoustics ’08, Paris, France.

Jepsen, M. L., and Dau, T. **(2008)**, ”Modeling auditory perception of individual hearing-impaired listeners”, International Hearing Aid Research Conference (IHCON), Lake Tahoe, CA, USA.

Dau, T. and Jepsen, M. L. **(2010)**, ”Modeling Individual Hearing Impairment with a Physiologically-Based Auditory Perception Model”, Association for Research in Otolaryngology (ARO), Midwinter Meeting, February 2010, Anaheim, CA, USA.

Contents

List of abbreviations

AM	Amplitude modulation
AN	Auditory nerve
BM	Basilar membrane
CASP	Computational Auditory Signal-processing and Perception
CF	Characteristic frequency
CM	Compactness
DRNL	Dual-resonance nonlinear
DRT	Diagnostic rhyme test
ERB	Equivalent rectangular bandwidth
GOM	Growth-of-masking
GV	Graveness
HI	Hearing impaired
HL	Hearing level
HL_{TOT}	Total hearing loss
HL_{OHC}	Hearing loss due to outer hair-cell loss
HL_{IHC}	Hearing loss due to inner hair-cell loss
IHC	Inner hair cell
I/O	Input-output
IR	Internal representation
JND	Just noticeable difference

MSE	Mean squared error
MSI	Masker-signal interval
NH	Normal hearing
NN	Noise signal and noise masker
NS	Nasality
NT	Noise signal and tone masker
OHC	Outer hair cell
rms	Root-mean-square
roex	Rounded exponential
SAM	Sinusoidally amplitude modulated
SB	Sibilation
SD	Standard deviation
SL	Sensation level
SNHL	Sensorineural hearing loss
SNR	Signal-to-noise ratio
SPL	Sound pressure level
SRT	Speech reception threshold
ST	Sustention
TFS	Temporal fine structure
TMC	Temporal masking curve
TMTF	Temporal modulation transfer function
TN	Tone signal and noise masker
TT	Tone signal and tone masker
VC	Voicing

1

General introduction

Hearing loss affects the life of millions of people throughout the world. The increasing population of elderly people and the present day noise exposure of young people are likely to further increase the number of people with hearing impairment (HI) over the next years. Impaired hearing ability has major consequences for every-day life, since acoustic communication is a primary source of information. Hearing-aid technology has experienced a great evolution in the last decades, and modern hearing aids undoubtedly help a large part of the HI people to restore their ability to function in every-day situations. However, the performances in day-to-day tasks which involve hearing, e.g., understanding an acoustic message or speech in a noisy environment, vary substantially among hearing-aid users. Some experience more benefit than others.

There has been extensive research on understanding the function of hearing and how the human auditory system analyzes acoustic signals. A lot has been learned over the years but many aspects still remain unclear. The normally functioning auditory system has an impressive capability to extract information from a mixture of sounds from an acoustic environment. The challenges are to identify a sound source and disregard the irrelevant information, while still being attentive to new potentially important acoustic events. Psychoacoustic measurements are usually used in research on the processing in the human auditory systems. Several experiments, such as the measurement of signal-detection thresholds in the presence of a masker, have been developed to gain insight into basic auditory function. For example, notched-noise masking and forward masking have typically been used to measure the spectral and temporal resolution of the system, respectively. The aim of models of auditory processing and perception has been to match the human performance in tasks like these.

Computer models of the auditory system become more complex the more we understand about the underlying mechanisms of hearing, and the models can account for several fundamental aspects when simulating the performances of humans in certain tasks. However, there is still room for substantial improvement, especially regarding generalized models that can account for a broad variety of data. Most existing models can be expected to simulate the particular aspects which they were specifically designed for. For example, models that have focused on the simulation of precise temporal processing in the auditory periphery are not necessarily successful when considering the auditory spectral analysis.

The signal processing of the inner ear, the cochlea, and in particular the basilar membrane (BM) is of great importance for understanding the capability of the auditory periphery to process complex sounds. The BM basically realizes a frequency analyzer which is highly nonlinear and has level-dependent compression. This feature partly explains our ability to perceive a wide dynamic range of input sound pressure levels which allows the subsequent neural system that has a very limited dynamic range to further process the incoming information. The nonlinearity has several consequences on spectro-temporal auditory processing. The sharpness of the auditory filters reflects the ability of frequency selectivity, and their bandwidths are level-dependent. The cochlea also realizes a nonlinear gain which effectively amplifies low-level input signals. It thus seems that an appropriate simulation of the processing on the BM is a key element in a successful model of the auditory system.

The most typical type of hearing loss is the so-called sensorineural hearing loss (SNHL), which is a consequence of a dysfunction of sensory hair-cells within the cochlea. A typical consequence of hair-cell loss is an abnormal BM processing. Although there are substantial individual differences among the people with this type of hearing loss, the nonlinear gain is typically reduced. Changes in the compressive behavior of the BM affect the tuning of the auditory filters, which have been observed to be broader in listeners with SNHL. Such effects have dramatic perceptual consequences for the HI listeners, since their ability to resolve sounds in time and frequency is degraded. Individual differences in the basic auditory processing may explain the variability in the severity of communication problems across HI listeners as well as the varying benefit from compensation by hearing-

aids. It is likely that an individual characterization of cochlear processing is important for a better understanding of the perceptual consequences of cochlear damage or SNHL. Such characterization needs a set of critical experiments, psychoacoustic or objective measures, and provides an "auditory profile" for each individual HI listener, including substantial information in addition to the conventional audiogram. Auditory processing models of individual hearing loss may be particularly interesting for the evaluation of novel hearing-aid processing and compensation strategies, or the prediction of implications of hearing loss on speech intelligibility and sound quality.

The most serious consequence of hearing loss is probably the reduced ability to understand speech information in noisy backgrounds or in conditions with multiple speech sources. This has often been referred to as the "cocktail party problem". Psychoacoustic measures of speech intelligibility typically estimate the signal-to-noise ratio (SNR) at which a pre-defined amount of words, presented in a masking condition, is correctly identified. This is reflected in measures of the speech reception threshold (SRT), hence it reflects an average long-term performance. Other behavioral measures of speech perception extract more detailed information about specific speech recognition errors. For example, measures of consonant identification in noise provide detailed consonant confusion patterns. It is likely that there is a relation between these speech measures and the outcomes of the non-speech psychophysics described earlier. A computational model which appropriately simulates the processing in normal-hearing (NH) and HI listeners and further includes an appropriate "central operator", such as an optimal detector or a recognizer, would provide a very powerful tool to explain the observed variation in the data, particularly among the HI listeners. The work presented in this thesis attempted to provide a step in this direction in addition to the capability to explain non-speech data.

This thesis presents the results of four interconnected studies. In **Chapter 2**, a model of computational auditory signal processing and perception (CASP) is described. It was developed to account for a variety of masking and discrimination data by simulating the monaural signal processing of the normally-functioning auditory system. It represents a further development of an existing model of auditory processing and the major modifications addressed the nonlinear cochlear processing stage and the processing of amplitude modulations beyond the cochlear stage. The

model is tested in conditions that critically depend on the appropriate simulation of BM compression and spectral- and temporal resolution. The experimental test conditions are intensity discrimination, tone-in-noise detection, spectral masking, forward masking and the detection of amplitude modulations.

In **Chapter 3**, a method to estimate BM processing in terms of its input-output (I/O) function is suggested. The results obtained with this method provide valuable information about the state of the cochlea and can be used for an individual characterization of hearing loss. The method is based on a forward masking paradigm and allows robust estimates of BM compression in humans both with normal and impaired hearing. The method further provides an estimate of the "knee point" and that allows estimation of an individual BM I/O function covering a wider range of input levels compared to the existing method.

Chapter 4 describes a method to experimentally characterize individual SNHL in terms of spectro-temporal processing and intensity resolution. The experimental conditions include; the pure-tone audiogram, forward masking, notched-noise masking and intensity discrimination. Data are collected from ten listeners with SNHL and three NH listeners. The measures of sensitivity to pure tones (audiogram) and forward-masking thresholds are used to adjust the cochlear parameters of the CASP model in order to account for individual hearing loss; one parameter set for each listener. The analysis is focused on obtaining individual estimates and appropriate simulations of outer- and inner hair-cell losses. The individually fitted models are evaluated in terms of predicted sensitivity, BM tuning as well as simultaneous- and forward masking measured in a separate masking experiment.

In order to investigate the relation between auditory processing and perception of speech, the CASP model for normal and impaired hearing is used as a front-end to a speech recognizer in **Chapter 5**. Psychoacoustic measures of forward masking and pure-tone sensitivity are performed in three listeners with SNHL. The procedure presented in Chapter 4 is used to adjust the front-end parameters. Data from a speech task are obtained by using the diagnostic rhyme test (DRT). The DRT data provide a detailed error pattern of consonant confusion. It is investigated how the measured error patterns match to the error patterns produced by the model. If individual error patterns can be accounted for by the model, then this would indicate

a clear relation between speech and non-speech psychophysics. Within the modeling framework it is required that errors from the front-end and back-end processing are clearly separated. Otherwise it will not be possible to conclude whether the model's internal representation appropriately reflects the perceptual relevant features.

Finally, **Chapter 6** summarizes the main findings and conclusions from the four studies. Possible implications as well as an outlook at potential applications are discussed.

2

A computational model of human auditory signal processing and perception[1]

A model of computational auditory signal processing and perception (CASP) is presented that accounts for various aspects of simultaneous and non-simultaneous masking in human listeners. The model is based on the modulation filterbank model described by Dau *et al.* [J. Acoust. Soc. Am., **102**, 2892-2905 (1997)] but includes major changes at peripheral and more central stages of processing. The model contains outer- and middle-ear transformation, a nonlinear basilar-membrane processing stage, a hair-cell transduction stage, a squaring expansion, an adaptation stage, a 150-Hz lowpass modulation filter, a bandpass modulation filterbank, a constant-variance internal noise and an optimal detector stage. The model was evaluated in experimental conditions that reflect, to a different degree, effects of compression and spectral and temporal resolution in auditory processing. The experiments include intensity discrimination with pure tones and broadband noise, tone-in-noise detection, spectral masking with narrowband signals and maskers, forward masking with tone signals and tone or noise maskers, and amplitude modulation detection with narrow and wideband noise carriers. The model can account for most of the key properties of the data and is more powerful than the original model. The model might be useful as a front-end in technical applications.

[1] This chapter was published as Jepsen *et al.* (2008).

2.1 Introduction

There are at least two reasons why auditory processing models are constructed: to represent the results from a variety of experiments within one framework and to explain the functioning of the system. Specifically, processing models help generate hypotheses that can be explicitly stated and quantitatively tested for complex systems. Models of auditory processing may be roughly classified into biophysical, physiological, mathematical (or statistical) and perceptual models, depending on which aspects of processing are considered. Most of the models can be broadly referred to as functional models, that is, they simulate experimentally observed input-output behavior of the auditory system without explicitly modeling the precise internal biophysical mechanisms involved.

The present study deals with the modeling of perceptual masking phenomena, with focus on effects of intensity discrimination and spectral and temporal masking. Explaining basic auditory masking phenomena in terms of physiological mechanisms has a long tradition. There have been systematic attempts at predicting psychophysical performance limits from the activity of auditory nerve (AN) fibers (e.g., Siebert, 1965, 1970; Heinz *et al.*, 2001a,b; Colburn *et al.*, 2003), combining analytical and computational population models of the AN with statistical decision theory. A general result has been that those models that make optimal use of all available information from the AN (e.g., average rate, synchrony, and nonlinear phase information) typically predict performance that is 1-2 orders of magnitude better than human performance, while the trends often match well to human performance.

Other types of auditory masking models are to a lesser extent inspired by neurophysiological findings and make certain simplifying assumptions about the auditory processing stages. Such an "effective" modeling strategy does not allow conclusions about the details of signal processing at a neuronal level. On the other hand, if the effective model accounts for a variety of data, this suggests certain general processing principles. These, in turn, may motivate the search for neural circuits in corresponding physiological studies. Models of temporal processing typically consist of an initial stage of bandpass filtering, reflecting a simplified action of basilar membrane (BM) filtering. Each filter is followed by a nonlinear device. In recent

models, the nonlinear device typically includes two processes, half-wave rectification and a compressive nonlinearity, resembling the compressive input-output function on the BM (e.g., Ruggero and Rich, 1991; Oxenham and Moore, 1994; Oxenham and Plack, 1997; Plack and Oxenham, 1998; Plack *et al.*, 2002). The output is fed to a smoothing device implemented as a lowpass filter (Viemeister, 1979) or a sliding temporal integrator (e.g., Moore *et al.*, 1988). This is followed by a decision device, typically modeled as the signal-to-noise ratio. Forward and backward masking have been accounted for in terms of the build-up and decay processes at the output of the sliding temporal integrator. The same model structure has also been suggested to account for other phenomena associated with temporal resolution, such as gap detection and modulation detection (e.g., Viemeister, 1979).

An alternative way of describing forward masking is in terms of neural adaptation (e.g., Jesteadt *et al.*, 1982; Nelson and Swain, 1996; Oxenham, 2001; Meddis and O'Mard, 2005). A few processing models include adaptation and account for several aspects of forward masking (e.g., Dau *et al.*, 1996a,b; Buchholz and Mourjoloulus, 2004a,b; Meddis and O'Mard, 2005). It appears that the two types of models, temporal integration and adaptation, can lead to similar results even though seemingly conceptually different (Oxenham, 2001; Ewert *et al.*, 2007).

Dau *et al.* (1996a) proposed a model to account for various aspects of simultaneous and non-simultaneous masking using one framework. The model includes a linear one-dimensional transmission line model to simulate BM filtering (Strube, 1985), an inner-hair-cell transduction stage, an adaptation stage (Püschel, 1988) and an 8-Hz modulation lowpass filter, corresponding to an integration time constant of 20 ms. The adaptation stage in that model is realized by a chain of five simple nonlinear circuits, or feedback loops (Püschel, 1988; Dau *et al.*, 1996a). An internal noise is added to the output of the preprocessing that limits the resolution of the model. Finally, an optimal detector is attached that acts as a matched filtering process. An important general feature of the model of Dau *et al.* (1996a) is that, once it is calibrated using a simple intensity discrimination task to adjust its internal noise variance, it is able to quantitatively predict data from other psychoacoustic experiments without further fitting. Part of this flexibility is caused by the use of the matched filter in the decision process. The optimal detector automatically "adapts" to the current task and is based

on the cross-correlation of a template, a supra-threshold representation of the signal to be detected in a given task, with the internal signal representation at the actual signal level.

In a subsequent modeling study (Dau *et al.*, 1997a,b), the gammatone filterbank model of Patterson *et al.* (1995) was used instead of Strube's transmission-line implementation, because its algorithm is more efficient and the bandwidths matched estimates of auditory-filter bandwidths more closely. The modulation lowpass filter was replaced by a modulation filterbank, which enables the model to reflect the auditory system's high sensitivity to fluctuating sounds and to account for amplitude modulation (AM) detection and masking data (e.g., Bacon and Grantham, 1989; Houtgast, 1989; Dau *et al.*, 1997a; Verhey *et al.*, 1999; Piechowiak *et al.*, 2007). The modulation filterbank realizes a limited-resolution decomposition of the temporal modulations and was inspired by neurophysiological findings in the auditory brainstem (e.g., Langner and Schreiner, 1988; Palmer, 1995). The parameters of the filterbank were fitted to perceptual modulation masking data and are not directly related to the parameters from physiological models that describe the transformation from a temporal neural code into a rate based representation of AM in the auditory brainstem (Langner, 1981; Hewitt and Meddis, 1994; Nelson and Carney, 2004; Dicke *et al.*, 2007).

The preprocessing of the model described by Dau *et al.* (1996a, 1997a) has been used in a variety of applications, e.g., for assessing speech quality (Hansen and Kollmeier, 1999, 2000), predicting speech intelligibility (Holube and Kollmeier, 1996), as a front-end for automatic speech recognition (Tchorz and Kollmeier, 1999), for objective assessment of audio quality (Huber and Kollmeier, 2006) and signal-processing distortion (Plasberg and Kleijn, 2007). The model has also been extended to predict binaural signal detection (Breebaart *et al.*, 2001a,b,c) and across-channel monaural processing (Piechowiak *et al.*, 2007).

However, despite some success with the model of Dau *et al.* (1997a), there are major conceptual limitations of the approach. One of these is that the model does not account for nonlinearities associated with basilar-membrane processing, since it uses the (linear) gammatone filterbank (Patterson *et al.*, 1995). Thus, for example, the model must fail in conditions which reflect level-dependent frequency selectivity,

such as in spectral masking patterns. Also, even though the model includes effects of adaptation which account for certain aspects of forward masking, it must fail in those conditions that directly reflect the nonlinear transformation on the BM. This, in turn, implies that the model will not be able to account for consequences of sensorineural hearing impairment for signal detection, since a realistic cochlear representation of the stimuli in the normal system is missing as a reference.

Implementing a nonlinear BM processing stage in the framework of the model is a major issue, since the interaction with the successive static and dynamic processing stages can strongly affect the internal representation of the stimuli at the output of the preprocessing, depending on the particular experimental condition. For example, how does the level-dependent cochlear compression affect the results in conditions of intensity discrimination? To what extent are the dynamic properties of the adaptation stage affected by the fast-acting cochlear compression? What is the influence of the compressive peripheral processing on the transformation of modulations in the model? In more general terms, the question is whether a modified model that includes a realistic (but more complex) cochlear stage can *extend* the predictive power of the original model. If this cannot be achieved, major conceptual changes of the modeling approach would most likely be required.

In an earlier study (Derleth *et al.*, 2001), it was suggested how the model of Dau *et al.* (1997a,b), referred to in the following as the "original model", could be modified to include fast-acting compression, as found in BM processing. Different implementations of fast-acting compression were tested, either through modifications of the adaptation stage, or by using modified, level-dependent, gammatone filters (Carney, 1993). Derleth *et al.* (2001) found that the temporal adaptive properties of the model were strongly affected in all implementations of fast-acting compression; their modified model thus failed in conditions of forward masking. It was concluded that, in the given framework, the model would only be able to account for the data when an expansion stage after BM compression was assumed (which would then partly compensate for cochlear compression). However, corresponding explicit predictions were not generated in their study.

Several models of cochlear processing have been developed recently (e.g., Heinz *et al.*, 2001b; Meddis *et al.*, 2001; Zhang *et al.*, 2001; Bruce *et al.*, 2003; Irino and

Patterson, 2006) which differ in the way that they account for the nonlinearities in the peripheral transduction process. In the present study, the dual-resonance nonlinear (DRNL) filterbank described by Meddis *et al.* (2001) was used as the peripheral BM filtering stage in the model - instead of the gammatone filterbank. In principle, any of the above cochlear models could instead have been integrated in the present modeling framework. The DRNL was chosen since it represents a computationally efficient and relatively simple functional model of peripheral processing. It can account for several important properties of BM processing, such as frequency- and level-dependent compression and auditory-filter shape in animals (Meddis *et al.*, 2001). The DRNL structure and parameters were adopted to develop a human cochlear filterbank model by Lopez-Poveda and Meddis (2001), on the basis of pulsation-threshold data.

In addition to the changes at BM level, several other substantial changes in the processing stages of the original model were made. The motivation was to incorporate findings from other successful modeling studies in the present framework. Models of human outer- and middle-ear transformations were included in the current model, none of which were considered in the original model. An expansion stage, realized as a squaring device, was assumed after BM processing, as in the temporal-window model (Plack and Oxenham, 1998; Plack *et al.*, 2002). Also, certain aspects of modulation processing were modified in the processing, motivated by recent studies on modulation detection and masking (Ewert and Dau, 2000; Kohlrausch *et al.*, 2000). The general structure of the original perception model, however, was kept the same.

The model developed in this study, referred to as the computational auditory signal processing and perception (CASP) model in the following, was evaluated using a set of critical experiments, including intensity discrimination using tones and broadband noise, tone-in-noise detection as a function of the tone duration, spectral masking patterns with tone and narrow-band noise signals and maskers, forward masking with noise and tone maskers, and amplitude modulation detection with wide- and narrow-band noise carriers. The experimental data from these conditions can only be accounted for if the compressive characteristics and the spectral and temporal properties of auditory processing are modeled appropriately. To the knowledge of the authors, no model is currently available that can account for the data from all the

conditions listed above, without changing the model parameters substantially from one condition to the next.

2.2 Description of the model

2.2.1 Overall structure

Figure 2.1 shows the structure of the CASP model[2]. The first stages represent the transformations through the outer and the middle ear, which were not considered in Dau *et al.* (1997a,b). A major change to the original model was the implementation of the DRNL filterbank. The hair-cell transduction, i.e., the transformation from mechanical vibrations of the BM into inner hair-cell receptor potentials, and the adaptation stage are the same as in the original model. However, a squaring expansion was introduced in the model after hair-cell transduction, reflecting the square-law behavior of rate-versus-level functions of the neural response in the auditory nerve (Yates *et al.*, 1990; Muller *et al.*, 1991). In terms of envelope processing, a 1st-order 150-Hz lowpass filter was introduced in the processing prior to the modulation bandpass filtering. This was done in order to limit sensitivity to fast envelope fluctuations, as observed in amplitude-modulation detection experiments with tonal carriers (Ewert and Dau, 2000; Kohlrausch *et al.*, 2000). The transfer functions of the modulation filters and the optimal detector are the same as used in the original model. The details of the processing stages are presented below.

2.2.2 Processing stages in the model

Outer- and middle-ear transformations

The input to the model is a digital signal, where an amplitude of 1 corresponds to a maximum sound pressure level of 100 dB. The amplitudes of the signal are scaled to be represented in units of Pa prior to the outer-ear filtering. The first stage of auditory processing is the transformation through outer and middle ear. As in the study of Lopez-Poveda and Meddis (2001), these transfer functions were realized by two linear-phase finite impulse response (FIR) filters. The outer-ear filter was a

[2] MATLAB implementations of the model stages are available under the name 'Computational Auditory Signal-processing and Perception (CASP) model' on our lab's website: http://www.dtu.dk/centre/cahr/downloads.aspx. Implementations of stages from earlier papers are also included, e.g. Dau *et al.* (1996a, 1997a)

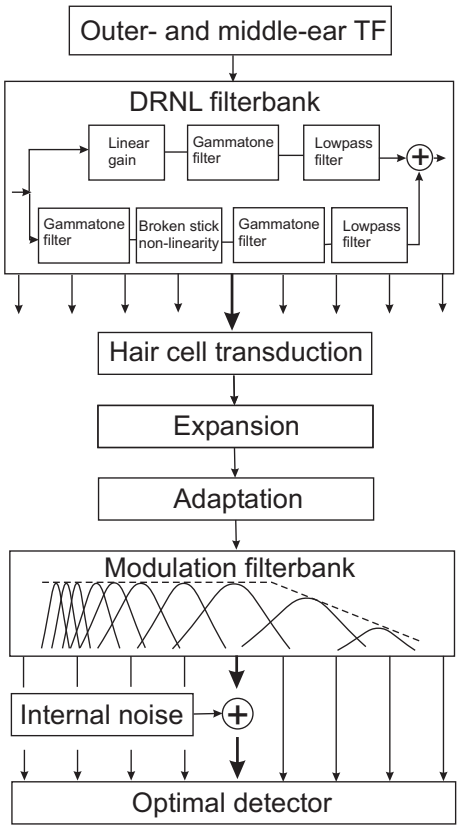

Figure 2.1: Block diagram of the model structure. See text for a description of each stage.

headphone-to-eardrum transfer function for a specific pair of headphones (Pralong and Carlile, 1996). It was assumed that the headphone brand only has a minor influence, as long as circumaural, open and diffuse-field equalized, quality headphones are considered, as was done in the present study. The middle-ear filter was derived from human cadaver data (Goode *et al.*, 1994) and simulates the mechanical impedance change from the outer ear to the middle ear. The outer- and middle-ear transfer functions correspond to those described in Lopez-Poveda and Meddis (2001, their Fig. 2). The combined function has a symmetric bandpass characteristic with a

maximum at about 800 Hz and slopes of 20 dB/decade. The output of this stage is assumed to represent the peak velocity of vibration at the stapes as a function of frequency.

The dual-resonance nonlinear (DRNL) filterbank

Meddis *et al.* (2001) developed an algorithm to mimic the complex nonlinear BM response behavior of physiological chinchilla and guinea pig observations. This algorithm includes two parallel processing paths, a linear one and a compressive nonlinear one, and its output represents the sum of the outputs of the two paths. The complete unit has therefore been called the dual-resonance nonlinear (DRNL) filter. The structure of the DRNL filter is illustrated in Fig. 2.1. The linear path consists of a linear gain function, a gammatone bandpass filter and a lowpass filter. The nonlinear path consists of a gammatone filter, a compressive function which applies an instantaneous broken-stick nonlinearity, another gammatone filter and, finally, a lowpass filter. The output of the linear path dominates the sum at high signal levels (above 70-80 dB SPL). The nonlinear path behaves linearly at low signal levels (below 30-40 dB SPL) and is compressive at medium levels (40-70 dB SPL). In Meddis *et al.* (2001), the model parameters were fitted to physiological data so that the model accounted for a range of phenomena, including iso-velocity contours, input-output functions, phase responses, two-tone suppression, impulse responses and distortion products. In a subsequent study, the DRNL filterbank was modified in order to simulate the properties of the *human* cochlea (Lopez-Poveda and Meddis, 2001), by fitting the model parameters to psychophysical pulsation threshold data (Plack and Oxenham, 2000). These data have been assumed to estimate the amount of peripheral compression in human cochlear processing. The parameters of their model were estimated for different signal frequencies and Lopez-Poveda and Meddis (2001) suggested how to derive the parameters for a complete filterbank.

The CASP model includes the digital time-domain implementation of the DRNL filterbank described by Lopez-Poveda and Meddis (2001). However, slight changes in some of the parameters were made. The amount of compression was adjusted to stay constant above 1.5 kHz, whereas it was assumed to increase continuously in the original parameter set. This modification is consistent with recent findings of

Lopez-Poveda *et al.* (2003) and Rosengard *et al.* (2005), where a constant amount of compression was estimated at signal frequencies of 2 and 4 kHz, based on forward masking experiments. A table containing the parameters that were modified is given in Sec. 2.7. For implementation details, the reader is referred to Lopez-Poveda and Meddis (2001).

Some of the key properties of the implemented DRNL filter are reflected in the input/output (I/O) functions at different characteristic frequencies (CF). Figure 2.2A shows I/O functions of the filters at 0.25, 0.5, 1 and 4 kHz. The 0.25-kHz function (dotted curve) is linear up to an input level of 60 dB SPL, and becomes compressive at the highest levels. With increasing CF, the level at which compression begins to occur decreases. It is well known that the compressive characteristics of the BM are most prominent near CF (0.2-0.5 dB/dB), at least for CFs above about 1 kHz, whereas the response is close to linear (0.8-1.0 dB/dB) for stimulation at frequencies well below CF (e.g., Ruggero *et al.*, 1997). Figure 2.2B shows the I/O functions for the filter centered at 4 kHz in response to tones with several input frequencies (1, 2.4, 4, 8 kHz). It can be seen that the largest response is generally produced by on-frequency stimulation (4 kHz). The I/O functions for stimulation frequencies below CF are linear. The response to a tone with a frequency one octave above CF (8 kHz) is compressive (dotted curve), but at a very low level.

Associated with the compressive transformation for on-frequency stimulation and the less compressive (close to linear) response to off-frequency stimulation is the level-dependent magnitude transfer function of the filter. The transfer function (normalized to the maximal tip gain) for the DRNL filter tuned to 1 kHz (solid curves) is shown for input levels of 30 dB SPL (panel C), 60 dB SPL (panel D) and 90 dB SPL (panel E). For comparison, the dashed curves indicate the transfer function of the 4th-order gammatone filter at the same CF. At the lowest level, 30 dB SPL, the transfer function of the DRNL is very similar to that of the gammatone filter. The bandwidth of the DRNL filter increases with level and the filter becomes increasingly asymmetric. With increasing level, the best frequency, i.e., the stimulus frequency that produces the strongest response, shifts toward lower frequencies, similar to physiological data from animals at higher frequencies (e.g., Ruggero *et al.*, 1997). Behavioral data from Moore and Glasberg (2003) indicated that this shift may not occur at the 1-kHz site

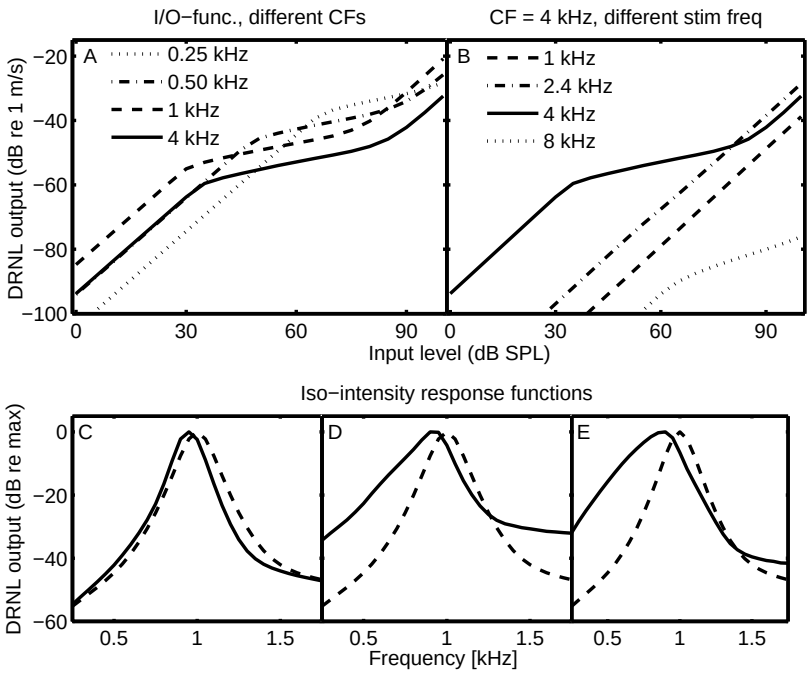

Figure 2.2: Properties of the DRNL filterbank. Panel A shows the input/output functions for on-frequency stimulation at different characteristic frequencies (CF). Panel B shows the input/output functions for the filter with CF = 4 kHz, for tones with frequencies of 1, 2.4, 4 and 8 kHz. The solid curves in panels C, D and E show the normalized magnitude transfer functions of the DRNL filter tuned to 1 kHz for input levels of 30, 60 and 90 dB SPL, respectively. The dashed curves indicate the transfer function of the corresponding 4th-order gammatone filter.

in humans. Nevertheless, the implementation as suggested in Lopez-Poveda and Meddis (2001) was kept in the present study. The output of the DRNL filterbank is a multi-channel representation, simulating the temporal output activity in various frequency channels. Each channel is processed independently in the following stages. The distance between center frequencies in the filterbank is one equivalent rectangular bandwidth, representing a measure of the critical bandwidth of the auditory filters as defined by Glasberg and Moore (1990).

Mechanical-to-neural transduction and adaptation

The hair-cell transduction stage in the model roughly simulates the transformation of the mechanical BM oscillations into receptor potentials. As in the original model, this transformation is modeled by half-wave rectification followed by a 1st-order lowpass filter (Schroeder and Hall, 1974) with a cutoff frequency at 1 kHz. The lowpass filtering preserves the temporal fine structure of the signal at low frequencies and extracts the envelope of the signal at high frequencies (Palmer and Russell, 1986). The output is then transformed into an intensity-like representation, by applying a squaring expansion. This step is motivated by physiological findings of Muller *et al.* (1991) and Yates *et al.* (1990) which provided evidence for a square-law behavior of rate-versus-level functions of auditory-nerve fibers near AN threshold (in guinea pigs). The output of the squaring device serves as the input to the adaptation stage of the model which simulates adaptive properties of the auditory periphery. Adaptation refers to dynamic changes of the gain in the system in response to changes in input level. Adaptation has been found physiologically at the level of the auditory nerve (e.g., Smith, 1977; Westermann and Smith, 1984). In the present model, the effect of adaptation is realized by a chain of five simple nonlinear circuits, or feedback loops, with different time constants as described by Püschel (1988) and Dau *et al.* (1996a, 1997a). Each circuit consists of a lowpass filter and a division operation. The lowpass filtered output is fed back to the denominator of the divisor element. For a stationary input signal, each loop realizes a square-root compression. Such a single loop was first suggested by Siebert (1968) as a phenomenological model of auditory-nerve adaptation. The output of the series of five loops approaches a logarithmic compression for stationary input signals. For input variations that are rapid compared to the time constants of the low-pass filters, the transformation through the adaptation loops is more linear, leading to an enhancement of fast temporal variations or onsets and offsets at the output of the adaptation loops. The time constants, ranging between 5 and 500 ms, were chosen to account for perceptual forward masking data (Dau *et al.*, 1996a). In response to signal onsets, the output of the adaptation loops is characterized by a pronounced overshoot. In Dau *et al.* (1997a), this overshoot was limited, such that the maximum ratio of onset response amplitude and steady-state

response amplitude was 10. This version of the adaptation stage was also used in the CASP model.

Modulation processing

The output of the adaptation stage is processed by a 1st-order lowpass filter with a cutoff frequency at 150 Hz. This filter simulates a decreasing sensitivity to sinusoidal modulation as a function of modulation frequency (Ewert and Dau, 2000; Kohlrausch *et al.*, 2000). The lowpass filter is followed by a modulation filterbank. The highest modulation filter center frequencies in the filterbank are limited to one quarter of the center frequency of the peripheral channel driving the filterbank, and maximally to 1000 Hz, motivated by results from physiological recordings of Langner and Schreiner (1988) and Langner (1992). The lowest modulation filter is a 2nd-order lowpass filter with a cutoff frequency at 2.5 Hz. The modulation filters tuned to 5 and 10 Hz have a constant bandwidth of 5 Hz. For modulation frequencies at and above 10 Hz, the modulation filter center frequencies are logarithmically scaled and the filters have a constant Q value of 2. The magnitude transfer functions of the filters overlap at their -3 dB points. As in the original model, the modulation filters are complex frequency-shifted first-order lowpass filters. These filters have a complex valued output and either the absolute value of the output or the real part can be considered. For the filters centered above 10 Hz, the absolute value is considered. This is comparable to the Hilbert envelope of the bandpass filtered output and only conveys information about the presence of modulation energy in the respective modulation band, i.e., the modulation phase information is strongly reduced. This is in line with the observation of decreasing monaural phase discrimination sensitivity for modulation frequencies above about 10 Hz (Dau *et al.*, 1996a; Thompson and Dau, 2008). For modulation filters centered at and below 10 Hz, the real part of the filter output is considered. In contrast to the original model, the output of modulation filters above 10 Hz was attenuated by a factor of $\sqrt{2}$, so that the rms value at the output is the same as for the low-frequency channels in response to a sinusoidal AM input signal of the same modulation depth.

The decision device

In order to simulate limited resolution, a Gaussian-distributed internal noise is added to each channel at the output of the modulation filterbank. The variance of the internal noise was the same for all peripheral channels and was adjusted so that the model predictions followed Weber's law in an intensity discrimination task. Specifically, predictions were fitted to intensity discrimination data of a 1-kHz pure-tone at 60 dB SPL and of broadband noise at medium sound pressure levels. The representation of the stimuli after the addition of the internal noise is referred to as the "internal representation". The decision device is realized as an optimal detector, as in the original model. Within the model, it is assumed that the subject is able to create a "template" of the signal to be detected. This template is calculated as the normalized difference between the internal representation of the masker plus a suprathreshold signal representation and that of the masker alone. The template is a three-dimensional pattern, with axes time, frequency and modulation frequency. During the simulation procedure, the internal representation of the masker alone is calculated and subtracted from the internal representation in each interval of a given trial. Thus, in the signal interval, the difference contains the signal, embedded in internal noise, while the reference interval(s) contain internal noise only. For stochastic stimuli, the reference and signal intervals are affected both by internal noise and by the external variability of the stimuli. The (non-normalized) cross-correlation coefficient between the template and the difference representations is calculated, and a decision is made on the basis of the cross-correlation values obtained in the different intervals. The interval that produces the largest value is assumed to be the signal interval. This corresponds to a matched-filtering process (e.g., Green and Swets, 1966) and is described in more detail in Dau *et al.* (1996a).

2.3 Experimental method

The experimental method, stimulus details and simulation parameters are described below. In the present study, data were collected for tone-in-noise detection and forward masking, while the data on intensity discrimination, spectral masking and modulation detection were taken from the literature (Houtsma *et al.*, 1980; Moore *et al.*, 1998; Dau *et al.*, 1997a; Viemeister, 1979).

2.3.1 Subjects

Four normal-hearing listeners, aged between 24 and 28 years, participated in the experiments. They had pure-tone thresholds of 10 dB HL or better for frequencies between 0.25 and 8 kHz. One subject was the first author and had experience with psychoacoustic experiments. The other three subjects had no prior experience in listening tests. These three subjects were paid for their participation on an hourly basis and received 30 minute training sessions before each new experiment. There were no systematic improvements in thresholds during the course of the experiments. Measurement sessions ranged from 30 to 45 minutes depending of the subject's ability to focus on the task. In all measurements, each subject completed at least three runs for each condition.

2.3.2 Apparatus and procedure

All stimuli were generated and presented using the AFC-Toolbox for Matlab (Mathworks), developed at the University of Oldenburg, Germany, and the Technical University of Denmark (DTU). The sampling rate was 44.1 kHz and signals were presented through a personal computer with a high-end, 24-bit soundcard (RME DIGI 96/8 PAD) and headphones (Sennheiser HD-580). The listeners were seated in a double-walled, sound insulated booth with a computer monitor, which displayed instructions and gave visual feedback.

A three-interval, three-alternative forced choice (3-AFC) paradigm was used in conjunction with an adaptive 1-up-2-down tracking rule. This tracked the point on the psychometric function corresponding to 70.7% correct. The initial step size was

4 dB. After each second reversal, the step size was halved until a minimum step size of 0.5 dB was reached. The threshold was calculated as the average of the level at six reversals at the minimum step size. The computer monitor displayed a response box with three buttons for the stimulus intervals in a trial. The subject was asked to indicate the interval containing the signal. During stimulus presentation, the buttons in the response box were successively highlighted in time with the appropriate interval. The subject responded via the keyboard and received immediate feedback on whether the response was correct or not.

2.3.3 Stimuli

Intensity discrimination of pure tones and broadband noise

The data on intensity discrimination of a 1-kHz tone and broadband noise were taken from Houtsma *et al.* (1980). The just noticeable level difference was measured as a function of the standard (or reference) level of the tone or noise, which was 20, 30, 40, 50, 60 or 70 dB SPL. The duration of the tone was 800 ms, including 125-ms onset and offset raised-cosine ramps. The noise had a duration of 500, including 50-ms raised-cosine ramps.

Tone-in-noise simultaneous masking

Detection thresholds of a 2-kHz signal in the presence of a noise masker were measured for signal durations from 5 to 200 ms, including 2.5-ms raised-cosine ramps. The masker was a Gaussian noise that was bandlimited to a frequency range from 0.02 to 5 kHz. The masker was presented at a level of 65 dB SPL and had a duration of 500 ms including 10-ms raised-cosine ramps. The signal was temporally centered in the masker.

Spectral masking with narrowband signals and maskers

The data from this experiment were taken from Moore *et al.* (1998). The signal and the masker were either a tone or an 80-Hz wide Gaussian noise. All four signal-masker combinations were considered: tone signal and tone masker (TT), tone signal

and noise masker (TN), noise signal and tone masker (NT), and noise signal and noise masker (NN). In the TT-condition, a 90-degree phase shift between signal and masker was chosen, while the other conditions used random onset phases of the tone. The masker was centered at 1 kHz, and the signal frequencies were 0.25, 0.5, 0.9, 1.0, 1.1, 2.0, 3.0 and 4.0 kHz. The signal and the masker were presented simultaneously. Both had a duration of 220 ms including 10-ms raised-cosine ramps. Here, only the masker levels of 45 and 85 dB SPL were considered, whereas the original study also used a level of 65 dB SPL.

Forward masking with noise and tone maskers

In the first forward masking experiment, the masker was a broadband Gaussian noise, bandlimited to the range from 0.02 to 8 kHz. The steady-state masker duration was 200 ms and 2-ms raised-cosine ramps were applied. Three masker levels were used: 40, 60, and 80 dB SPL. The signal was a 4-kHz tone. It had a duration of 10 ms and a Hanning window was applied over the entire signal duration. Thresholds were obtained for temporal separations between the masker offset and the signal onset of -20 ms to 150 ms. For separations between -20 and -10 ms, the signal was presented completely in the masker, i.e., these conditions reflected simultaneous masking.

The second experiment involved forward masking with pure-tone maskers. The stimuli were similar to those used by Oxenham and Plack (2000). Two conditions were used: in the on-frequency condition, the signal and the masker were presented at 4 kHz. In the off-frequency condition, the signal frequency remained at 4 kHz whereas the masker frequency was 2.4 kHz. The signal was the same as in the first experiment. The signal and the masker had random onset phases in both conditions. The signal level at masked threshold was obtained for several masker levels. In the on-frequency condition, the masker was presented at levels from 30 to 80 dB SPL, in 10-dB steps. For the off-frequency condition, the masker was presented at 60, 70, 80 and 85 dB SPL. The separation between masker offset and signal onset was either 0 or 30 ms.

Modulation detection

The data for the modulation detection experiments were taken from Dau *et al.* (1997a) for the narrowband-noise carriers and from Viemeister (1979) for the broadband-noise carriers. For the narrowband carriers, a bandlimited Gaussian noise, centered at 5 kHz, was used as the carrier. The carrier bandwidths were 3, 31 or 314 Hz. The carrier level was 65 dB SPL. The overall duration of the stimuli was 1 s, windowed with 200-ms raised-cosine ramps. Sinusoidal amplitude modulation (SAM) with a frequency in the range from 3 to 100 Hz was applied to the carrier. The duration of the signal modulation was equal to that of the carrier. In the case of the 314-Hz wide carrier, the modulated stimuli were limited to the original (carrier) bandwidth to avoid spectral cues. To eliminate potential level cues, all stimuli were adjusted to have equal power (for details, see Dau *et al.*, 1997a).

For the broadband noise carrier, a Gaussian noise with a frequency range from 1 to 6000 Hz was used. The carrier was presented at a level of 77 dB SPL and had a duration of 800 ms. The signal modulation had the same duration and the stimulus was gated with 150-ms raised-cosine ramps, resulting in a 500-ms steady-state portion. Sinusoidal signal modulation, ranging from 4 to 1000 Hz, was imposed on the carrier. There was no level compensation, i.e., the overall level of the modulated stimuli varied slightly depending on the imposed modulation depth.

2.3.4 Simulation parameters

The model was calibrated by adjusting the variance of the internal noise so that the model predictions satisfied Weber's law for the intensity discrimination task. When setting up the simulations, the frequency range of the relevant peripheral channels and the supra-threshold signal level for the generation of the template need to be specified. The range of channels was chosen such that potential effects of off-frequency listening were included in the simulations. The on-frequency channel may not always represent the channel with the best signal-to-noise ratio, particularly in the present model where the best frequency of the nonlinear peripheral channels depends on the stimulus level.

The following frequency ranges and supra-threshold signal levels were used in the simulations: For intensity discrimination with tones, the peripheral channels from

one octave below to one octave above the signal frequency (1 kHz) were considered. For the broadband noise, all peripheral channels centered from 0.1 to 8 kHz were used. For both experiments, the signal level for the template was chosen to be 5 dB above the standard level. For tone-in-noise masking, the channels from one octave below to one octave above the 2-kHz signal frequency were considered. The signal level for the template was set to 75 dB SPL which is about 10 dB higher than the highest expected masked threshold in the data. For the spectral masking experiments, the channels from half an octave below to one octave above the signal frequency were considered. For the forward masking experiment with a broadband noise masker and a 4-kHz signal, the channels from 3.6 to 5 kHz were used. The signal level for the template was chosen to be 10 dB above the masker level. For the forward-masking experiments with pure-tone maskers, only the channel tuned to the signal frequency (4 kHz) was used and the template level was 10 dB above the masker level. In the modulation detection experiment with narrow-band carriers centered at 5 kHz, the channel at 5 kHz was considered as in the study of Dau *et al.* (1997a) in order to directly compare with the results with the original simulations. For this experiment, the simulations showed a standard deviation that was larger than in the data. To reduce the standard deviation, simulated thresholds were averages of 20 runs instead of only three runs as for all other simulations. For the broadband-noise carrier condition, the channels from 0.1 to 8 kHz were used. In both cases, the modulation depth for the template was chosen to be -6 dB.

2.4 Results

In this section, measured data are compared with simulations. The data are represented by open symbols while simulations are shown as filled symbols. For comparison, gray symbols indicate simulations obtained with the original model. Differences between the predictions of the two models are discussed in more detail in Sec. 2.5.

2.4.1 Intensity discrimination

For pure-tone and broadband noise stimuli, the smallest detectable change in intensity, ΔI, is, to a first approximation, a constant fraction of the standard intensity, I, of the stimulus (e.g., Miller, 1947). This is referred to as Weber's law. As in many other studies, intensity differences are described in the following as just noticeable differences (JNDs) in level, ΔL.

The broadband noise JND at medium levels (from 30 to 60 dB) was used to calibrate the model, i.e., to adjust the variance of the internal noise in the model. In the original model, the combination of the logarithmic compression of (the stationary parts of) the stimuli, realized in the adaptation loops, and the constant-variance internal noise produced a constant Weber fraction (for noise) throughout the entire level range.

Figure 2.3 shows the JNDs for the 1-kHz tone (panel A) and for broadband noise (panel B). The simulations (filled circles) are shown together with average data (open squares) taken from Houtsma *et al.* (1980). For the pure tone, the simulated JND is about 0.5 dB for all standard levels considered here. For the levels from 20 to 40 dB SPL, the simulated JNDs lie about 0.5 dB below the data. At higher standard levels, the simulations agree well with the data. The simulation does not reflect the near-miss to Weber's law observed in the measured data, i.e., the decrease of threshold with increasing standard level. This is discussed in detail in Sec. 2.5.1. The original model (gray symbols) accounts well for the data at 20 dB SPL and above 50 dB SPL, while the JND for 40 dB SPL lies 0.5 dB below the measured JND.

The measured JNDs for broadband noise (panel B) are about 0.6 dB for levels from 30 to 50 dB SPL. There is a slight increase at the lowest and the highest levels in the data, resulting in a JND of about 0.8 dB. The simulations agree very well with the

data for levels from 30 to 60 dB SPL. For the lowest level (20 dB SPL), the simulated JND lies 0.3 dB below the measured JND, while it is about 0.2 dB above the measured value at the highest level. The simulations obtained with the original model show essentially the same results.

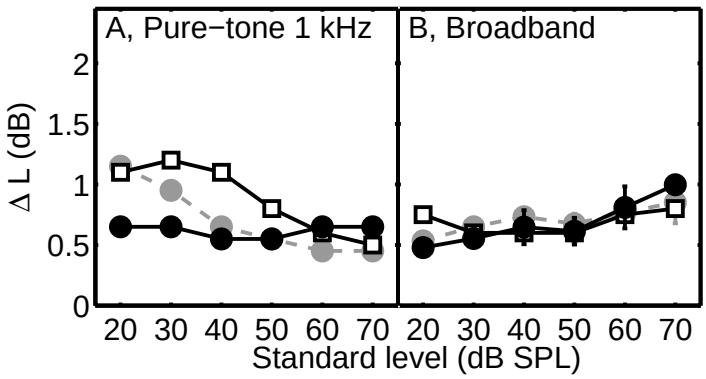

Figure 2.3: Intensity discrimination thresholds for a 1-kHz tone (left panel) and broadband noise (right panel) as a function of the standard level. Model predictions (closed symbols) are shown along with measured data (open symbols) taken from Houtsma *et al.* (1980). The gray symbols represent simulations obtained with the model of Dau *et al.* (1997a).

2.4.2 Tone-in-noise simultaneous masking

Figure 2.4 shows the average thresholds of the four listeners from the present study for tone-in-noise masking (open circles). The error bars indicate $\pm$ one standard deviation across subjects, which is typically less than 1 dB, but amounts to about 2 dB for the shortest signal duration of 5 ms. For signal durations in the range from 5 to 20 ms, the threshold decreases by about 4-5 dB per doubling of signal duration, while the decrease is about 3 dB per doubling for durations above 20 ms. The data are consistent with results from earlier studies on signal integration in tone-in-noise masking (e.g., Dau *et al.*, 1996b; Oxenham and Plack, 1997; Oxenham, 1998). The simulations (filled circles) show a constant decay of 3 dB per doubling of signal duration. This agrees nicely with the measured data for durations at and above 15 ms.

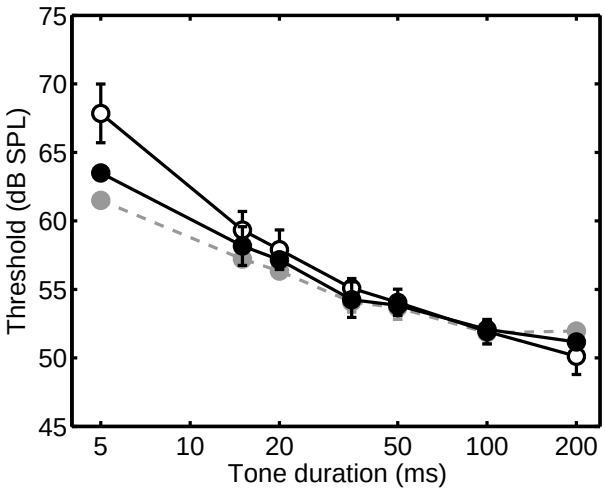

Figure 2.4: Results from the tone-in-noise masking experiment with a broadband noise masker at 65 dB SPL. The signal was a 2-kHz pure tone. The open circles show the mean detection thresholds for the four subjects as a function of signal duration. The error bars indicate one standard deviation. The closed circles indicate the predicted thresholds for the CASP model (black) and the original model (gray).

At signal durations of 200 ms and above (not shown), the simulations are consistent with the prediction of 48 dB obtained with the classical power spectrum model of masking (Patterson and Moore, 1986), assuming a threshold criterion of 1.5 dB increase of power (due to the addition of the signal to the noise) in the passband of the 2-kHz gammatone filter. For the shortest signal duration of 5 ms, the CASP model underestimates the measured threshold by 4 dB. This results from the 3-dB per doubling decay in the simulations observed also for the short durations (5-20 ms) while the data show a somewhat larger slope in this region. The simulations with the original model (gray symbols) show similar results[3] as the CASP model.

[3] The same condition was earlier tested using the model described by Dau *et al.* (1996a). The model produced a much too shallow decay of the threshold function with increasing signal duration. This was mainly caused by the excessive overshoot produced by the adaptation stage in response to the signal onset, such that information from the steady-state portion of the signal hardly contributed to the detection of the signal. The onset response of the adaptation stage was therefore limited in Dau *et al.* (1997a) in order to obtain a more realistic ratio of onset and steady-state amplitude.

The actual integration of signal information in the model is realized in the optimal detector. The matched filtering process implies that a variable time constant is available that is matched to the signal duration. The integration of the cross correlator in the detector is similar to the classic notion of temporal integration, but no fixed integration time constant is necessary for long-term integration. It is the temporal extension of the template which automatically determines the weighting of the stimuli across time. This concept is effectively close to the "multiple-looks" strategy discussed by Viemeister and Wakefield (1991). Time constants that are related to the "hard-wired" part of signal processing within the model represent a lower limit of temporal acuity. The modulation filterbank represents a set of time constants that are, however, too short to account for the long-term integration data. Thus, it is the decision device that inherently accounts for the long effective time constants observed in the present experiment. The result of the decision process depends critically on the properties of the internal representation of the stimuli which forms the input to the detector. The combination of peripheral processing, adaptation, modulation filtering and decision making, assumed in the present model, leads to a good agreement of the predictions with the data in this experimental condition.

2.4.3 Spectral masking patterns with narrowband signals and maskers

Masking patterns represent the amount of masking of a signal as a function of signal frequency in the presence of a masker with fixed frequency and level. The shapes of these masking patterns are influenced by several factors, such as occurrence of combination tones or harmonics produced by the peripheral nonlinearities, and by beating cues (Moore and Glasberg, 1987; van derHeijden and Kohlrausch, 1995). Additionally, the width and shape of the masking patterns are level dependent as a consequence of the level-dependent auditory filters. Moore *et al.* (1998) measured masking patterns using pure tones and narrow-band noises as signals and pure tones and narrow-band noises as maskers, for masker levels of 45, 65 and 85 dB SPL. They found that temporal fluctuations (beats) had a strong influence on the measured masking patterns for sinusoidal maskers, for masker-signal frequency separations

up to a few hundred Hertz. The data also indicated some influence of beats for the conditions with narrow-band noise maskers. The simulations obtained with the present model are compared here with the data of Moore *et al.* (1998) and with simulations of Derleth and Dau (2000) using the original model.

The open symbols in Fig. 2.5 show the mean data of Moore *et al.* (1998). The four panels show the results for conditions TT, TN, NT and NN. The masking patterns for masker levels of 45 and 85 dB SPL are indicated by squares and circles, respectively. The ordinate represents masking, defined as the difference between the masked threshold and the absolute threshold at each signal frequency. The masking patterns generally show a maximum at the masker frequency. The amount of masking generally decreases with increasing spectral separation between the signal and the masker. For the TT condition, the peak in the masking patterns is particularly pronounced, since beating between the signal and the masker for frequency separations of a few hundred Hz provides a very effective detection cue in this condition (e.g., Moore *et al.*, 1998). The 45-dB SPL masker produces a symmetric pattern in all conditions, whereas the pattern for the 85-dB SPL masker is asymmetric with a considerable broadening on the high-frequency side.

The filled symbols in Fig. 2.5 show the model predictions. In the TT condition, the predictions agree well with the experimental data, except for the signal frequencies 500 and 750 Hz for the 85-dB SPL masker, where the amount of masking is overestimated. The simulations at this masker level otherwise show the asymmetry found in the measured masking pattern, which in the model is a direct consequence of the level-dependent BM filter shapes. The gray symbols plot the simulated pattern from Derleth and Dau (2000). Using level-invariant, linear gammatone filters, these predictions underestimate the amount of masking at high signal frequencies.

The two filled upward-pointing triangles in panel A indicate simulations that were obtained considering only the first 8 modulation filters (with center frequencies ranging from 0 to 130 Hz), while neglecting activity in the remaining modulation filters tuned to modulation rates above 130 Hz. These predictions exceed measured thresholds by up to 15 dB. Within the model, the reason for this deviation from the data is that the beats between the signal and the masker at rates of 150-200 Hz are not represented and cannot contribute to signal detection. Thus, in the framework of the

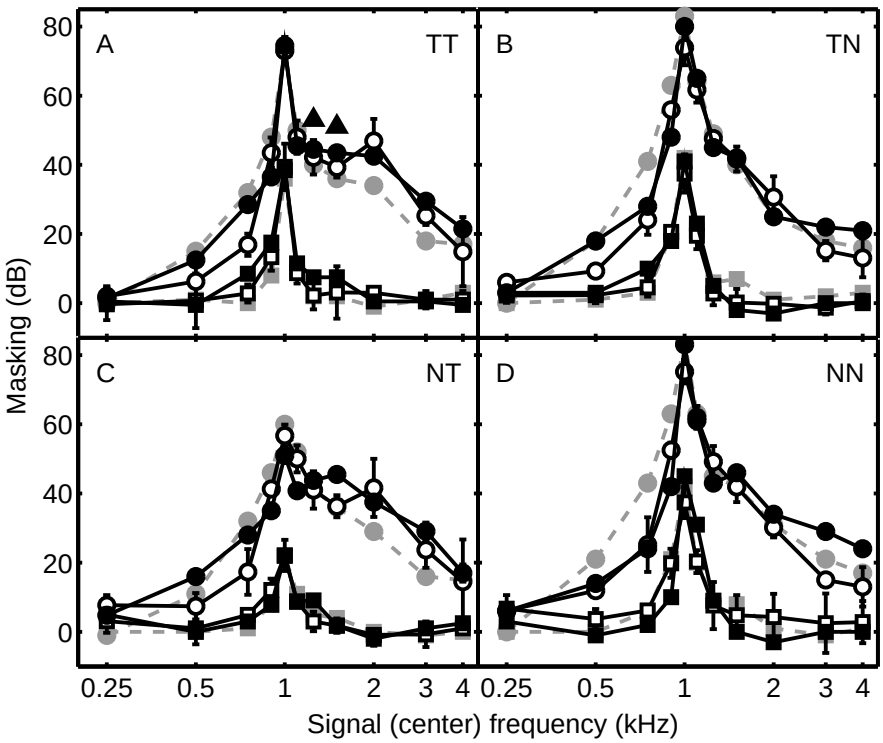

Figure 2.5: Spectral masking patterns for the four stimulus conditions. Masking in dB is the difference between the masked and the absolute threshold. The masker was centered at 1 kHz. Squares and circles indicate masker levels of 45 and 85 dB SPL, respectively. Open symbols indicate the measured data (Moore *et al.*, 1998). Closed symbols indicate the simulated patterns. Panel A represents the TT-condition. The upward triangles indicate predicted masking where the modulation filters were limited to have a maximum center frequency of 130 Hz. Panels B, C and D show the patterns in the TN, NT, and NN conditions, respectively. The gray symbols indicate predictions from Derleth and Dau (2000)

present model, the inclusion of higher-frequency modulation filters between 130 and 250 Hz is crucial to account for the tone-on-tone masking pattern.

The masking patterns for condition TN are shown in panel B. For signal frequencies close to the masker frequency, they are broader than for the TT condition.

The sharp peak at 2 kHz that occurred for the tonal masker is not present for the noise masker. This is also the case in the simulated pattern since the beating cue for small masker-signal frequency separations is less pronounced than in the case of the tonal masker. On the low-frequency side of the masker, the predictions of the CASP model are considerably better than those obtained by Derleth and Dau (2000), where masking was overestimated by up to 18 dB. Thus, as expected, in this condition where energy cues play the most important role, the shapes of the level-dependent BM filters are mainly responsible for the good agreement between the data and the simulations.

Panel C shows the results for condition NT. When the signal and masker are centered at the same frequency, the amount of masking is about 20 dB lower than for the TN and TT conditions. This "asymmetry" of masking has been reported previously and explained by temporal envelope fluctuations introduced by the noise signal (e.g., Hellman, 1972; Hall, 1997; Moore *et al.*, 1998; Gockel *et al.*, 2002; Verhey, 2002). The simulated patterns agree very well with the data, except for signal (center) frequencies of 500 and 750 Hz at the high masker level, where masking is overestimated by about 10 dB. Again, the agreement between simulations and data is better for the current model than for the original model which assumed linear BM filters.

Finally, the masking patterns for the NN condition are shown in panel D. The results are similar to those for the TN condition. The simulations agree very well with the measured patterns, except for the signal center frequencies of 3 and 4 kHz, where the masking is overestimated by about 11 dB for the 85-dB masker. The simulations using the original model (Derleth and Dau, 2000, Fig. 4) showed a considerable overestimation of the masking on the low-frequency side of the masker (up to about 20 dB).

In summary, the masking patterns simulated with the CASP model agree well with the measured data in the four masking conditions. For the 45-dB masker, the predictions were similar to those obtained by Derleth and Dau (2000). For the 85-dB masker, however, the simulations were clearly improved as a consequence of the more realistic simulation of level-dependent cochlear frequency selectivity. However, it is the combination of audio-frequency selectivity and the sensitivity to temporal cues,

such as beating between the signal and the masker, that is crucial for a successful simulation of masking patterns.

2.4.4 Forward masking with noise and on- versus off-frequency tone maskers

The forward masking experiments of the present study were conducted to test the ability of the CASP model to account for data that have been explained in terms of nonlinear cochlear processing. Figure 2.6 shows the mean masked thresholds for the four subjects (open symbols) for three masker levels (40, 60, 80 dB SPL), as a function of the offset-onset interval between the masker and the signal. The error bars indicate $\pm$ one standard deviation. The mean absolute threshold of the subjects for the brief signal was 12 dB SPL and is indicated in Fig. 2.6 by the gray horizontal lines. In the simultaneous-masking conditions, represented by the negative offset-onset intervals, the masked thresholds lie slightly below the level of the masker. As expected, the thresholds decrease rapidly for short delays, and more slowly for larger delays. At a masker-signal separation of 150 ms, the three forward masking curves converge at the absolute threshold of the signal. The simulated forward masking curves are indicated by the filled symbols in Fig. 2.6. The model accounts quantitatively for the measured thresholds for all three masker levels. The simulations obtained with the original model (gray symbols) show clear deviations from the data, with a decrease that is too shallow in the 0- to 40-ms region of the forward-masking curve for the highest masker level (panel C).

In the CASP model, peripheral compression influences the thresholds in this region, since the signal level falls in the compressive region around 50 dB SPL. Large changes in the input level are thus required to produce small changes in the internal representation of the signal, resulting in a faster decay of forward masking.

Oxenham and Plack (2000) presented data that demonstrated the role of level-dependent BM processing in forward masking. Similar experiments, using on- and off-frequency pure-tone maskers in forward masking, were conducted here. The hypothesis was that GOM functions in forward masking should depend on whether the masker and/or the signal level fall within the compressive region of the BM input-

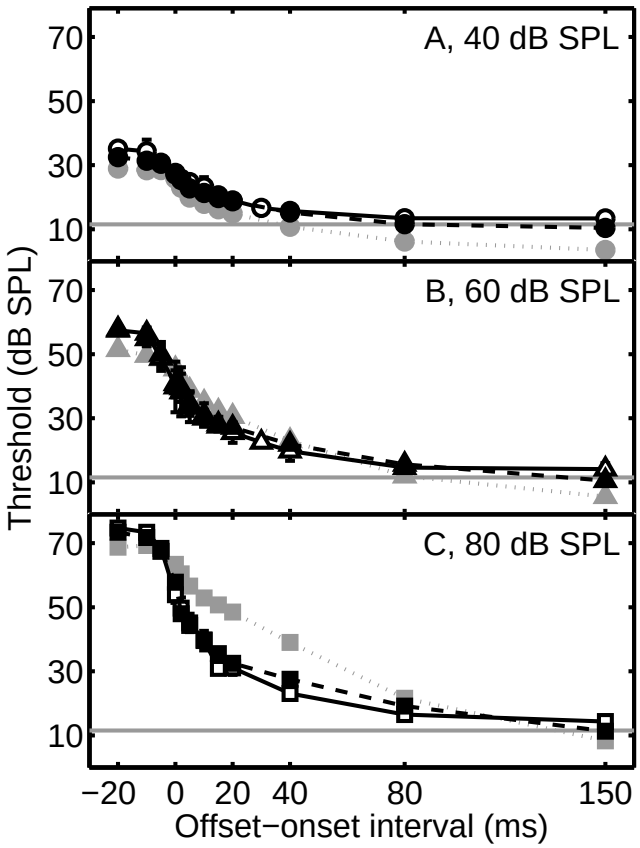

Figure 2.6: Forward masking thresholds obtained with a 10-ms 4-kHz pure-tone signal and a broadband noise masker. Results for masker levels of 40, 60 and 80 dB SPL are indicated in panels A, B and C, respectively. Open symbols represent the mean data from four subjects, while closed symbols represent predicted thresholds. Predictions of the original model are given in gray. The abscissa represents the time interval between the masker offset and the signal onset. The horizontal gray lines indicate the absolute threshold of the signal.

output function. If the masker and the signal levels both fall in the compressive region, which is typically the case for very short masker-signal separations, and if the compression slope is assumed to be constant, the signal level at threshold should change linearly with changing masker level. On the other hand, for larger masker-

signal separations, the masker level may fall in the compressive region while the signal level falls in the linear region of the BM input-output function. In this case, a given change in masker level will produce a smaller change of the signal level at threshold, leading to a shallower slope of the GOM function.

For off-frequency stimulation with a masker frequency well below the signal frequency, the BM response at the signal frequency is assumed to be linear at all levels. The slope of the curves should therefore be roughly independent of the masker-signal interval for off-frequency stimulation. The data presented in Oxenham and Plack (2000) provided evidence for such behavior of the GOM functions, using on- and off-frequency pure-tone maskers. Figure 2.7 shows the GOM functions from the second forward masking experiment of the present study, averaged across the four subjects. Panels A and B show the results for the on- and off-frequency conditions, respectively. Thresholds corresponding to masker-signal intervals of 0 and 30 ms are indicated by triangles and circles, respectively. In the on-frequency condition, the measured GOM function is close to linear ($\approx$ 0.9 dB/dB) for the 0-ms interval. For the masker-signal interval of 30 ms, the slope of the GOM function is shallower ($\approx$ 0.25 dB/dB). This was expected since the signal and masker can be assumed to be processed in different level regions of the BM input-output function. The data agree with the results of Oxenham and Plack (2000) in terms of the slopes of the GOM functions (0.82 dB/dB for the 0-ms interval, and 0.29 dB/dB for the 30-ms interval).

The corresponding simulated GOM functions (filled symbols) for both masker-signal intervals are very close to the measured data. This supports the hypothesis that the nonlinear BM stage can account for the different shapes for different intervals. Since the BM stage in the earlier model processes sound linearly, the slopes of the predicted GOM functions (gray symbols) are similar for the two masker-signal intervals. The failure of the original model to correctly predict the GOM slope for the 30-ms interval was also observed in the first forward masking experiment for the 30-ms interval for the 80-dB masker from the previous experiment (Fig. 2.6, Panel C).

For the off-frequency masker, the slope of the GOM function for the 0-ms interval is about 1.2 dB/dB, while it is 0.5 dB/dB for the 30-ms interval. These data are not consistent with the hypothesis that the GOM function for off-frequency stimulation should be independent of the interval. The variability of the average data is very

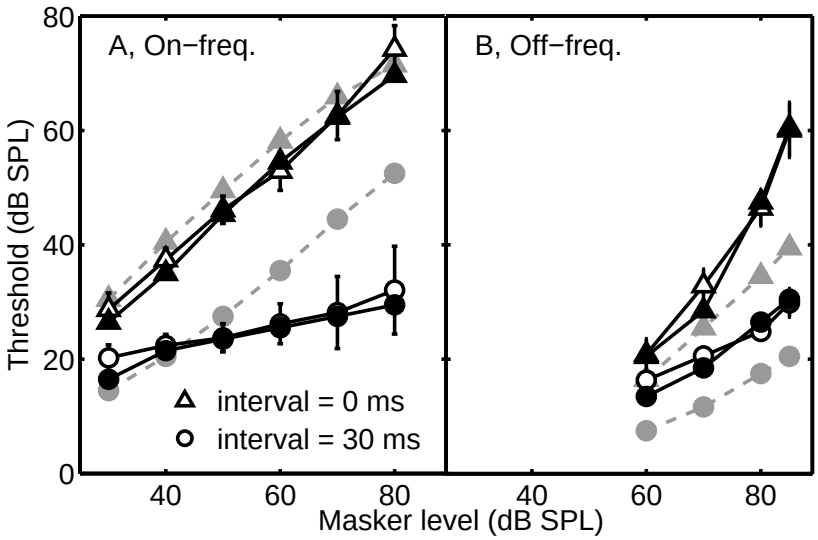

Figure 2.7: Panel A shows the growth of masking (GOM) curves obtained in the forward masking experiment, where a 10-ms, 4-kHz pure-tone signal was masked by an on-frequency forward masker. Triangles and circles represent thresholds when the masker-signal interval was 0 and 30 ms, respectively. Open symbols show the mean data of four subjects. Black and gray symbols show simulated thresholds using the CASP and the original model, respectively. In panel B, GOM curves for an off-frequency masker at 2.4 kHz are shown using the same symbols and notation as for panel A.

low, with a standard deviation of only 1-2 dB. The data also differ from the average data of Oxenham and Plack (2000, their Fig. 3). They found GOM functions in this condition with a mean slope close to unity for all masker-signal separations. However, there was substantial variability in slope across subjects; some showed a clearly compressive GOM function while other subjects showed a linear or slightly expansive GOM function.

The initial hypothesis was that both the signal and the masker were processed linearly in the off-frequency condition. However, this is not always the case: the signal level can be above 30-40 dB and thus fall in the compressive region of the BM

input/output function, while the off-frequency masker is still processed linearly. Such a situation would lead to a GOM function with a slope greater than 1, a trend which is observed in the data in panel B for the 0-ms separation, at least for the two highest masker levels. The data of Oxenham and Plack (2000) for the same interval support this idea, but this was not explicitly discussed in their study.

The simulations for the off-frequency condition closely follow the measured data. The CASP model predicts a GOM function with a slope below one for the 30-ms interval, as observed in the data. This is caused by the adaptation stage, which compresses the long-duration off-frequency masker slightly more than the short-duration signal. This slight compression can also be seen in the simulations obtained with the original model (gray circles). For the 0-ms interval, some of the signal thresholds lie in the compressive part ($>$30 dB SPL) of the BM input/output function (see also Fig. 2.2A). As a consequence, the GOM function has a slope above one, since the masker is still processed linearly. The corresponding simulations obtained from the original model show a function which is essentially parallel to the 30-ms function. This model thus fails to account for the different slopes for the two masker-signal intervals.

2.4.5 Modulation detection with noise carriers of different bandwidth

In the following, amplitude modulation detection with random noise carriers of different bandwidth is considered. Figure 2.8 shows the average data (open symbols) from Dau *et al.* (1997a) for carrier bandwidths of 3 Hz, 31 Hz, and 314 Hz. Panel D shows the "classical" temporal modulation transfer function (TMTF) using a broadband noise carrier, taken from Viemeister (1979, open symbols). The modulation depth at threshold, in dB ($20 \log m$), is plotted as a function of the modulation frequency. The simulations (closed symbols) for the 3-Hz wide carrier account for the main characteristics of the data. The simulated TMTF shows a slightly shallower threshold decrease with increasing signal modulation frequency than the measured function. For the 31-Hz wide carrier, the simulated TMTF follows the high-pass characteristic observed in the data; only at 50 Hz is the measured threshold

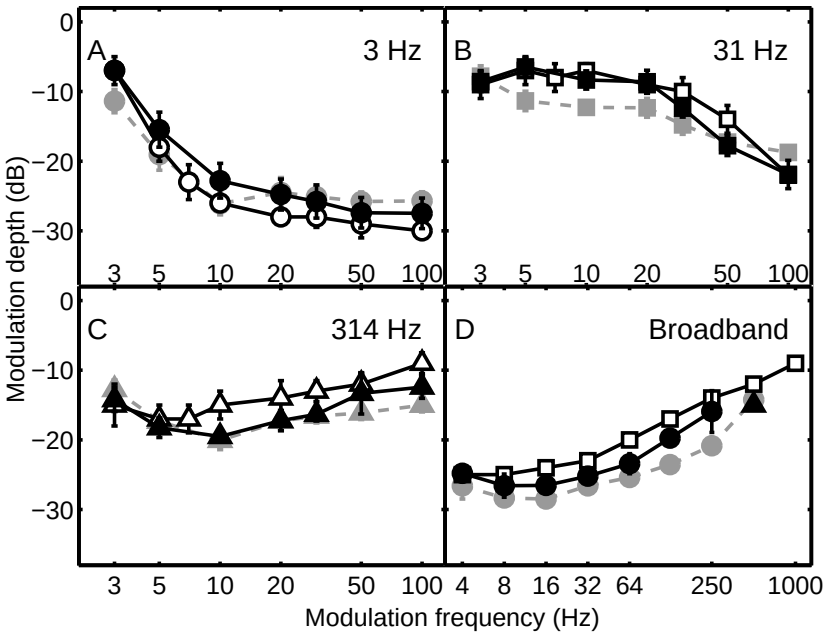

Figure 2.8: Temporal modulation transfer functions (TMTFs) for sinusoidal amplitude modulation imposed on noise carriers of different bandwidths. In panels A, B, and C, the measured data of Dau *et al.* (1997a) are indicated as open symbols for carrier bandwidths of 3, 31 and 314 Hz, respectively. Panel D shows measured data from Viemeister (1979) as open symbols. The black filled symbols represent the simulated TMTFs obtained with the present model. Gray symbols indicate the simulations obtained with the original model. The black triangle indicates the predicted threshold for the 500-Hz modulation frequency when no limiting 150-Hz modulation lowpass filter was used.

underestimated by 3-4 dB. For the 314-Hz wide carrier, the simulated thresholds roughly follow the shape of the measured TMTF, but predicted thresholds are typically 1-3 dB below the data. The agreement of the simulations with the data is slightly worse for the original model than for the present model, except for the 3-Hz bandwidth, where the agreement is similar.

Finally, the broadband TMTF (panel D) shows a low-pass characteristic with a cut-off frequency of about 64 Hz. Thresholds are generally lower than for the 314-Hz

wide carrier, which is a consequence of the lower envelope power spectrum density resulting from intrinsic fluctuations in the carrier. Since the envelope spectrum of the carrier extends to the carrier bandwidth, the power density in the envelope spectrum is lower (given that the overall level of the carriers is similar in these two conditions) and stretches over a broader frequency region in the case of the broadband noise carrier. If the model was based on a broad "predetection" filter instead of a peripheral filterbank, the distribution of power in the envelope spectrum would directly relate to the lower thresholds in the broadband condition. In the model, however, the auditory filters limit the bandwidths of the internal signals and thus the frequency range of their envelope spectra. The lower thresholds obtained with the broadband carriers result from across-frequency integration of modulation information in the model, as shown by Ewert and Dau (2000). The predicted and measured TMTFs have similar shapes for frequencies up to 250 Hz, but the simulated TMTF (closed symbols) lies 1-3 dB below the data. At 500 and 1000 Hz, the modulation is undetectable for the model (even at a modulation depth of 0 dB) and no predicted threshold is shown. This is related to the modulation lowpass filter, which reduces the sensitivity to modulation frequencies above 150 Hz. The filled triangle indicates the simulated threshold for 500 Hz when the limiting lowpass filter was left out. In this case, the result is close to the measured threshold and also similar to the simulated threshold obtained with the original model. However, both the CASP model and the original model fail to predict the measured threshold for the 1000-Hz modulation frequency. It is possible that other cues contribute to detection at these high modulation rates which are not reflected in the modulation filterbank of the present model, such as pitch (e.g., Burns and Viemeister, 1981; Fitzgerald and Wright, 2005).

2.5 Discussion

In this section, the effects of the modifications introduced in the CASP model and their interaction with the remaining processing stages are considered. The limitations of the present modeling approach are discussed and potentials for further model investigations addressed.

2.5.1 Role of nonlinear cochlear processing in auditory masking

The original model (Dau *et al.*, 1997a) is quite successful when predicting simultaneous and nonsimultaneous discrimination and masking data, even though the model's linear processing at the BM level is not realistic. The study of Derleth *et al.* (2001) demonstrated fundamental problems when trying to implement BM nonlinearity in a straightforward way in the model: when the gammatone filterbank was replaced by a nonlinear cochlear stage, the model could not account for forward masking, since the temporal-adaptive properties were substantially affected. One might argue that the assumed processing in the model, particularly the processing in the adaptation stage, is inappropriate, since it leads to successful predictions only when combined with a linear BM simulation. However, the simulations obtained with the CASP model demonstrate that forward masking actually can be accounted for including the adaptation stage. One of the reasons for this result is the squaring device that simulates the expansive transformation from inner hair-cell potentials into auditory-nerve rate functions. The expansion reduces the amount of (instantaneous) compression introduced by the compressive BM stage while the overall compression in the CASP model is kept level dependent, which is different from the original model. A squaring stage was also included by Plack *et al.* (2002) in their temporal-window model and was crucial for the success of their model when describing forward masking.

In several of the experimental conditions considered here, the CASP model produced very similar predictions to the original model. In the level discrimination task, the predicted just-noticeable difference in level depends on the overall steady-state compression in the model, which is dominated by the logarithmic compression in the adaptation stage. This leads to a roughly constant discrimination threshold in the

model, independent of level (see Fig. 2.3). The level-dependent compression realized in the cochlear processing does not affect the model predictions for broadband noise. For pure tones, the present model predicts slightly lower JNDs than the original model for the lowest standard levels of 20 and 30 dB SPL.

The original model correctly describes Weber's law within each channel, consistent with intensity discrimination data in notched noise (Viemeister, 1983). With increasing spread of activity into different auditory channels in the multi-channel simulation shown here (2.3, gray symbols), the original model predicts the near miss to Weber's law. The CASP model can no longer predict Weber's law within an individual channel as a consequence of the BM compression at mid levels. An analysis of the model's behavior revealed that, when only a single peripheral channel (centered at the signal frequency) was considered, the pure-tone JNDs were elevated in the mid-level region (50-70 dB SPL) by 0.3-0.4 dB to a maximum of about 1 dB. If a channel tuned to a higher center frequency was analyzed, for which the tone fell in the region of linear processing, the JNDs were level independent. When using an auditory filterbank (as in the simulations shown in Fig. 2.3), the level-independent JND contributions from the off-frequency channels produce essentially a constant JND across levels, thus minimizing the effect of on-frequency peripheral compression. Thus, the combination of information across frequency leads here to the prediction of Weber's law but does not account for the near-miss to Weber's law. This result is consistent with simulations by Heinz *et al.* (2001b) when considering only AN firing rate information (average discharge counts) and disregarding nonlinear phase information. AN fibers with CFs above and below the tone frequency have phase responses that change with level (e.g., Ruggero *et al.*, 1997) and thus contribute information. In their modeling framework, Heinz *et al.* (2001b) showed that the inclusion of nonlinear phase information (at low and moderate CFs where phase information is available) as well as rate-based information can account for the near miss to Weber's law, using an across-frequency coincidence mechanism evaluating this information. Thus, it appears that the lack of such an evaluation of nonlinear phase effects across CF is responsible for the inability of the CASP model to account for the near-miss to Weber's law.

The predicted detection of amplitude modulation is not affected by the amount of cochlear compression in the CASP model, consistent with earlier results of Ewert

and Dau (2000) for broadband TMTFs. Since both signal modulation and inherent carrier modulations are compressed in the same way, the signal-to-noise ratio (at the output of the modulation filters) does not change. This is also consistent with the observation that sensorineural hearing-impaired listeners often show about the same sensitivity to modulation, independent of the amount of hearing loss (e.g., Bacon and Viemeister, 1985; Formby, 1987; Bacon and Gleitman, 1992), at least for narrowband noise carriers, and for broadband-noise carriers as long as the hearing loss is relatively flat. Accordingly, the characteristics of the spectral masking patterns (as in Fig. 2.5) that are associated with temporal envelope (beating) cues do not strongly depend on peripheral compression, i.e., the simulations obtained with the present model are very similar to earlier simulations using the gammatone filterbank. For example, the sharp tuning of the masking pattern for the tone signal and the tone masker and the asymmetry of masking effect for tone-on-noise versus noise-on-tone masking can be accounted for by both models.

However, cochlear nonlinear processing *does* play a crucial role in the other conditions considered in the present study. For the spectral masking patterns obtained with the high masker level (85 dB SPL), the effect of upward spread of masking is accounted for by the level-dependent frequency selectivity in the BM stage, which was not implemented in the original model. In the forward-masking conditions, where the signal and the masker were processed in different regions of the BM input-output function, the results obtained with the CASP model showed much better agreement with the data than the original model. Specifically, in the conditions with an on-frequency tone masker, the measured slopes of the GOM function strongly depend on the masker-signal interval, an effect explained by cochlear compression (Oxenham and Plack, 2000).

In the forward-masking condition with the broadband noise masker, the present model was able to account for the data for all masker levels. In contrast, the original model overestimated forward masking by 15 to 20 dB for masker-signal intervals of 10-40 ms at the highest masker level (80 dB SPL). These deviations are directly related to the deviations observed in the GOM functions for the tonal masker.

Ewert *et al.* (2007) compared forward-masking simulations from an earlier version of the CASP model with predictions from the temporal-window model (e.g.,

Oxenham and Moore, 1994; Oxenham, 2001). They investigated whether forward masking was better explained by the concept of neural persistence or temporal integration, as reflected in the temporal-window model, or by the concept of neural adaptation, as reflected in the CASP model. Ewert *et al.* (2007) showed that the two models produce essentially equivalent results and argued that the temporal-window model can be considered a simplified model of adaptation. The reason for the similarity of the two models is that the signal-to-noise ratio based decision criterion at the output of the temporal-window model acts in a way that corresponds to the division process in the adaptation stage of the present model.

The remaining difference is that the CASP model includes adaptation effects of the signal itself since the model contains a feedback mechanism in the adaptation loops. In contrast, the temporal-window model only mimics adaptation effects caused by the masker which are modeled using a feed-forward mechanism (Ewert *et al.*, 2007).

2.5.2 Effects of other changes in the processing on the overall model performance

The transformations through the outer and middle ear were not considered and absolute sensitivity as a function of frequency was only approximated in the original model. In the current model, an outer-ear and a middle-ear transfer function were implemented. In the experiments considered here, the effect of the absolute threshold was only observed in the forward-masking condition at the largest masker-signal intervals.

The 150-Hz modulation lowpass filter was included in the CASP model to simulate the auditory system's limited sensitivity to high-frequency envelope fluctuations. The filter was chosen based on the results of studies on modulation detection with tonal carriers where performance was limited by internal noise rather than any external statistics of the stimuli. The model accounts well for the broadband noise TMTF for AM frequencies up to 250 Hz (see Fig. 2.8). However, the 150-Hz lowpass filter caused predicted thresholds to be too high for high-rate modulations. Additional model predictions for a 500-Hz modulation rate without the 150-Hz filter were very

close to those obtained with the original model and the experimental data. This suggests that the slope of the 150-Hz lowpass filter (6 dB/oct) might be too steep. A shallower slope of 3-4 dB/oct would most likely not affect other simulations in the present study substantially while it would still be in line with the modulation detection data for pure-tone carriers of Kohlrausch *et al.* (2000). However, it is also possible that other cues, like pitch, contribute to the detection of high-frequency modulations. It has been shown that sinusoidal amplitude modulation of broadband noise allows melody recognition, even though the pitch is weak (e.g., Burns and Viemeister, 1981; Fitzgerald and Wright, 2005). The model does not contain any pitch detection mechanism and is therefore not able to account for potential effects of pitch on amplitude modulation detection. There might be an additional process responsible for the detection of temporal envelope pitch and (fine-structure) periodicity pitch (Stein *et al.*, 2005). Such a process might already be effective at modulation rates above the lower limit of pitch (of about 30 Hz), but particularly at high modulation rates (above about 200 Hz) which are not represented or are strongly attenuated in the internal representation of the stimuli in the CASP model.

Another modification of the original model was that the center frequencies of the modulation filters were restricted to one quarter of the center frequency of the corresponding peripheral channel, but never exceeded 1 kHz. In the spectral masking experiment of the present study, with a masker centered at 1 kHz, the simulations showed very good agreement with the data, suggesting that beating cues up to about 250 Hz can contribute to signal detection, at least in the high-level masker condition. However, it is difficult to determine the upper limit of the "existence region" of modulation filters, since the sidebands are typically either spectrally resolved by the auditory filters (for tonal carriers), or the modulation depth required for detection is very large (for broadband noise carriers), such that there is not enough dynamic range available to accurately estimate any meaningful modulation filter characteristic (Ewert and Dau, 2000; Ewert *et al.*, 2002). The combination of the first-order 150-Hz modulation low-pass filter (that provides the "absolute" threshold for AM detection) and the modulation bandpass filtering (over a modulation frequency range that scales with the carrier or "audio" frequency), appears to be successful in various experimental conditions.

2.5.3 Limitations of the model

Several studies of modulation depth discrimination (e.g., Wakefield and Viemeister, 1990; Lee and Bacon, 1997; Ewert and Dau, 2004) showed that Weber's law holds for most modulation depths, i.e., the just noticeable difference of AM depth is proportional to the reference modulation depth. A modified internal-noise source would be required in the model to account for these data (Ewert and Dau, 2004). Such a noise could be modeled either by a multiplicative internal noise at the output of the modulation filters or by a logarithmic compression of the *rms* output of the modulation filter (see Ewert and Dau, 2004). Neither the original model nor the CASP model can predict Weber's law in this task, since a level-independent fixed-variance internal noise is assumed. As described earlier, both models do account for Weber's law in classic intensity discrimination, since the preprocessing realizes a logarithmic compression for stationary signals (due to the adaptation stage). However, the AM depth for input fluctuations with rates higher than 2 Hz (which are represented in the modulation bandpass filters) is transformed almost linearly by the adaptation stage. Thus, the CASP model fails in these conditions. This might be improved by including an additional nonlinearity in the modulation domain. Such a modification was considered beyond the scope of the present study.

Shamma and colleagues (e.g., Chi *et al.*, 1999; Elhilali *et al.*, 2003) described a model that is conceptually similar to the CASP model but includes an additional "dimension" in the signal analysis. They suggested a spectro-temporal analysis of the envelope, motivated by neurophysiological findings in the auditory cortex (Schreiner and Calhoun, 1995; deCharms *et al.*, 1998). In their model, a "spectral" modulation filterbank was combined with the temporal modulation analysis, resulting in 2-dimensional spectro-temporal filters. Thus, in contrast to the implementation presented here, their model contains joint (and inseparable) spectral-temporal modulations. In conditions where both temporal and spectral features of the input are manipulated, the two models respond differently. The model of Shamma and co-workers has been utilized to account for spectro-temporal modulation transfer functions, for the assessment of speech intelligibility (Chi *et al.*, 1999; Elhilali *et al.*, 2003), the prediction of musical timbre (Ru and Shamma, 1997), and the perception of certain complex sounds (Carlyon and Shamma, 2003). The CASP model is

sensitive to spectral envelope modulation which is reflected as a variation of the energy (considered at the output of the modulation lowpass filter) as a function of the audio-frequency (peripheral) channel. For temporal modulation frequencies below 10 Hz, where the phase of the envelope is preserved, the present model could thus use spectro-temporal modulations as a detection cue. The main difference to the model of Chi *et al.* (1999), however, is that the CASP model does not include joint spectro-temporal channels. It is not clear to the authors of the present study to what extent detection or masking experiments can assess the existence of joint spectro-temporal modulation filters. The assumption of the CASP model that (temporal) modulations are processed independently at the output of each auditory filter implies that no across-channel modulation processing can be accounted for. This reflects a limitation of this model.

2.5.4 Perspectives

Recently, comodulation masking release (CMR) has been modeled using an equalization-cancellation (EC) mechanism for the processing of activity across audio frequencies (Piechowiak *et al.*, 2007). The EC process was assumed to take place at the output of the modulation filterbank for each audio-frequency channel. In that model, linear BM filtering was assumed. The model developed in the present study will allow a quantitative investigation of the effects of nonlinear BM processing, specifically the influence of level-dependent frequency selectivity, compression and suppression, on CMR. The model might be valuable when simulating the numerous experimental data that have been described in the literature, and might in particular help interpreting the role of within- versus across-channel contributions to CMR.

Another challenge will be to extend the model to binaural processing. The model of Breebaart *et al.* (2001a) accounted for certain effects of binaural signal detection, while their monaural preprocessing was based on the model of Dau *et al.* (1996a), i.e., without BM nonlinearity and without the assumption of a modulation filterbank. Effects of BM compression Breebaart *et al.* (2001a) and the role of modulation frequency selectivity (Thompson and Dau, 2008) in binaural detection have been discussed, but not yet considered in a common modeling framework.

An important perspective of the CASP model is the modeling of hearing loss and

its consequences for perception. This may be possible because the model now includes realistic cochlear compression and level-dependent cochlear tuning. Cochlear hearing loss is often associated with lost or reduced compression (Moore, 1995). Lopez-Poveda and Meddis (2001) suggested how to reduce the amount of compression in the DRNL to simulate a loss of outer hair-cells for moderate and severe hearing loss. This could be used in the present modeling framework as a basis for predicting the outcome of a large variety of psychoacoustic tasks in (sensorineural) hearing-impaired listeners (see Chapter 4; Jepsen and Dau, 2010).

2.6 Summary

- A computational auditory signal processing and perception (CASP) model was developed, representing a major modification of the modulation filterbank model of Dau *et al.* (1997a). The CASP model includes an outer- and middle-ear transformation and a nonlinear cochlear filtering stage, the DRNL, that replaces the linear gammatone filterbank used in the original model. A squaring expansion was included before the adaptation stage and a modulation lowpass filter at 150 Hz was used prior to the modulation bandpass filterbank. The adaptation stage, the main parameters of the modulation filterbank and the optimal detector were the same as in the original model.

- Model simulations were compared with data for intensity discrimination with tones and broadband noise, tone-in-noise detection as a function of tone duration, spectral masking with tonal and narrow-band noise signals and maskers, forward masking with tone signals and (on- and off-frequency) noise and tone maskers, and amplitude modulation detection using narrowband and wideband noise carriers.

- The model was shown to account well for most aspects of the data. In some cases (intensity discrimination, signal integration in noise, amplitude modulation detection), the simulation results were similar to those for the original model. In other cases (forward masking with noise and tone maskers, spectral masking at high masker levels) the CASP model showed much better agreement with the data than the original model, mainly as a consequence of the level-dependent compression and frequency selectivity in the cochlear processing.

2.7 Appendix: DRNL parameters of the model

The parameters of the human dual resonance nonlinear filterbank used in the CASP model were slightly different from those in (Lopez-Poveda and Meddis, 2001, Table III, average response). Table 2.1 shows the original parameters (Lopez-Poveda *et al.*, 2001, left column) and the parameters used here (right column). They were calculated from regression-line coefficients of the form $\log_{10}(\text{parameter}) = p_0 + m \log_{10}(\text{BF})$, where BF is expressed in Hertz. Parameters a and b are the same as the original for BFs below 1.5 kHz. For larger BFs they are set to be constant to reduce the amount of compression. The original value of the compression exponent c was 0.25 and is unchanged. The amount of compression is not determined by c alone, but by a combination of parameters a, b and c, as a consequence of the parallel processing structure of the DRNL algorithm.

	original		present	
Parameter	p_0	m	p_0	m
BW_{lin}	0.03728	0.78563	0.03728	0.75
BW_{nlin}	-0.03193	0.77426	-0.03193	0.77
$\text{LP}_{\text{lin cutoff}}$	-0.06762	1.01673	-0.06762	1.01
$a_{\text{CF} > 1.5\text{ kHz}}$	1.40298	0.81916	4.00471	0.00
$b_{\text{CF} > 1.5\text{ kHz}}$	1.61912	-0.81867	-0.98015	0.00

Table 2.1: The left column shows the original values of the DRNL filterbank parameters which were changed in the present study to reduce the filter bandwidths and the amount of compression at BFs higher than 1.5 kHz. The right column shows the new values.

3

Estimating basilar-membrane input-output functions using forward masking[4]

To characterize the function of human cochlear processing, it would be beneficial to behaviorally estimate the basilar membrane (BM) input-output (I/O) function. Such estimates would also be useful for auditory modeling when simulating individual cochlear hearing loss. In recent studies, forward masking has been used to estimate BM compression. If an on-frequency masker is processed compressively, while an off-frequency masker provides a linear processing reference, then the ratio between the slopes of growth of masking (GOM) functions reflects an estimate of BM compression. In this study, this paradigm was extended to also estimate the knee point of the I/O-function. If a low-level signal is masked by an on-frequency masker, such that the signal is processed linearly and the masker compressively according to the I/O function, then a steeper GOM function is expected than that obtained for a high-level signal where both masker and signal are processed compressively. The knee point can then be estimated at the input level where the GOM slope changes significantly. In order to find this, data were collected from 7 normal-hearing (NH) and 5 hearing-impaired (HI) listeners with a mild to moderate sensorineural hearing loss. Both groups show large across-listener but low within-listener variability. For these HI listeners for whom a knee point could be estimated, the knee point level was similar to or shifted up to about 30 dB higher than the level for the NH listeners. The amount of compression for the HI listeners was similar to or smaller than for that found in NH listeners. The method was shown to provide estimates of the BM I/O function for a wider range of input levels, due to the additional estimates of the knee points.

[4] The data from this chapter were presented at Acoustics '08, Paris (Jepsen and Dau, 2008).

3.1 Introduction

Basilar-membrane (BM) nonlinearity is known to influence several aspects of auditory perception and the performance in various psychoacoustic tasks. Normal-functioning BM compression is responsible for our ability to extract information from an impressively large dynamic range of acoustic sound-pressure levels. A consequence of BM compression is level-dependent tuning of the BM filters which determine the frequency selectivity of the auditory system. Temporal masking aspects, such as forward masking, have been shown to be influenced by the compressive properties of the BM (Oxenham and Plack, 2000). The function of the outer hair-cells (OHCs) is mainly responsible for the compressive properties of BM processing. The consequences of damage to the OHCs are a reduced or lost compression and, in turn, reduced frequency selectivity and degraded temporal resolution such as a slower recovery from forward masking. These aspects may be critical for our ability to understand speech in noisy environments or to segregate sound sources, since it becomes harder to exploit the spectral and temporal cues from the target. Loss of OHCs also causes reduced sensitivity, since the effect nonlinear gain is reduced or absent. Another perceptual aspect associated with loss of compression is abnormal growth of loudness or loudness recruitment.

The nonlinear features of BM processing have been investigated in physiological animal studies. It was found that compression is present at the characteristic frequency (CF) when using on-frequency stimulation, while the processing is more linear using off-frequency stimulation (Ruggero *et al.*, 1997). It was also observed that compression generally occurs for mid- and high-level stimulation, while more linear processing was observed at the lowest stimulation levels. Some studies suggested that compressive processing is only present for at mid- and high CFs, but this remain unclear due to technical limitations in measuring in the apical parts of the cochlea. Behavioral studies indicated that off-frequency compression might also exist in the apical parts of the cochlea (Lopez-Poveda *et al.*, 2003)

A quantitative characterization of the BM behavior can be realized by the BM I/O-function which is assumed to have close-to-linear processing for low stimulation levels, and approximately constant compressive processing for mid- and

high levels (e.g., Ruggero *et al.*, 1997). The input-level at the transition between the linear and compressive processing regions is referred to as the "knee point" throughout this chapter. Studies of BM compression in human listeners have suggested to use behavioral techniques such as measurement of pulsation thresholds (Plack and Oxenham, 2000) and forward masking (Oxenham and Plack, 1997, 2000; Nelson *et al.*, 2001). Oxenham and Plack (1997) developed a forward masking paradigm to estimate the amount of BM compression. Temporal masking is interesting here since it eliminates effects of suppression. Using a tonal signal masked by an on-frequency tone or an off-frequency masker at a lower frequency as a linear reference, Oxenham and Plack (1997) assumed that the ratio of the slopes of masking functions provides an estimate of BM compression. This method will throughout this chapter be referred to as the growth-of-masking (GOM) method. It is though limited to estimate compression only at and above 1 kHz, where an appropriate off-frequency masker can be used as a linear reference. The forward masking paradigms, in general, have limited ability to produce reliable results at low signal frequencies because of the ringing of the auditory filters. Oxenham and Plack (1997) collected data from both NH and HI listeners. NH listeners showed estimates of compression of about 0.15-0.30 dB/dB. HI listeners showed a substantially reduced amount of compression or no compression. Oxenham and Plack (2000) further investigated the role of cochlear compression in forward masking in NH listeners, where they varied the masker-signal interval in their stimuli. For an on-frequency masking condition, their data showed decreasing slopes of the GOM functions with increasing masker-signal interval. In an off-frequency masking condition, they found that the slopes of GOM functions were independent of the masker-signal interval, indicating near to linear processing. This encouraged the idea of using an off-frequency masker at a lower frequency as a linear reference.

Nelson *et al.* (2001) suggested an alternative forward masking approach to estimate BM compression. They argued that the estimates from the method of Oxenham and Plack (1997) are influenced by the spread of excitation produced by signals at the different levels. Nelson *et al.* suggested to use a fixed low-level signal (10 dB SL) and to measure the masker level at threshold as a function of the masker-signal interval. These are referred to as temporal masking curves (TMC). They derived I/O response growth curves as estimates of BM I/O functions. The rationale

assumes that, at a given masker-signal interval, the effective response produced by an off-frequency masker is the same as produced by an on-frequency masker at the signal-frequency place. An increase of the masker-signal interval, for an off-frequency masker, results in a linear increase in the effective output level at the signal-frequency place. Therefore, the changes in masker input level with masker-signal interval will be the same as the changes in effective output level that occur at the probe frequency place. A compressively processed on-frequency masker will produce less change in the effective output level at the same masker-signal intervals. The I/O function thus represents a plot of the off-frequency output levels against the on-frequency masker input level. This method was used in, Nelson *et al.* (2001); Lopez-Poveda *et al.* (2003); Rosengard *et al.* (2005) to measure compression for a wide range of frequencies in NH listener as well as in HI listeners (Moore *et al.*, 1999; Nelson and Carney, 2004; Plack *et al.*, 2004; Rosengard *et al.*, 2005; Stainsby and Moore, 2006). Plack *et al.* (2004) obtained estimates of BM I/O functions in listeners with mild-to-moderate hearing loss. In their data, a general trend was observed: Several listeners had compression exponents in the normal range. However, their knee points were shifted towards higher input levels, implying that the nonlinear cochlear gain might be unchanged at high input levels.

Rosengard *et al.* (2005) compared the methods of Oxenham and Plack (1997) and Nelson *et al.* (2001) using the same NH and HI listeners. The two methods produced similar estimates of the amount of compression. Their main conclusions were that: (1) The method of Oxenham and Plack produces stable estimates of compression, with small confidence intervals compared to the method of Nelson *et al.*. (2) The tested levels can be predefined, whereas pilot testing is required in the method of Nelson *et al.*. (3) The method of Nelson et al. uses a low-level signal, which avoids concerns of off-frequency listening effects. (4) The TMC method provided estimates of the I/O function knee point due to multi-segment curve-fitting. Wojtczak and Oxenham (2009) showed further that the recovery from forward masking with on- versus off-frequency maskers was different, especially at high masker levels. This violates the basic assumption of these forward masking paradigms, which assumes a frequency and level-independent recovery. As a consequence, compression might be

overestimated by the TMC method by up to a factor of two (Wojtczak and Oxenham, 2009).

An estimate of the BM I/O-function would be useful for auditory modeling when simulating individual hearing impairment. Quantitative estimates of the amount of compression and the knee point would provide useful information for adjusting the parameters of a nonlinear cochlear processing stage (see chapter 4 of this thesis).

In this study, the idea was to characterize the BM I/O function by two sequential forward masking experiments. The motivation was to establish experiments with a low within-listener variability in the data. Furthermore, the amount of necessary training should be low. Experiment 1 was similar to the GOM experiment suggested in Oxenham and Plack (1997) and was conducted to estimate the amount of compression in the compressive region of the BM. This experiment was chosen because it produces very robust data compared to other paradigms (Rosengard *et al.*, 2005). Experiment 2 was designed to estimate the knee point of the I/O-function. This experiment was inspired by the hypothesis in Oxenham and Plack (2000) suggesting that differences in GOM will occur if the signal and the masker are processed differently on the BM.

Here, the hypothesis was that a GOM function will have a transition point, due to differences in the underlying BM I/O function, as illustrated in Fig. 3.1. This will occur when the masker-signal interval (MSI) is larger than about 10 ms, such that the absolute levels of the signal and the masker are sufficiently different. In condition A1, the levels of both, masker and signal at masked threshold, fall in the compressive region on the BM I/O function. A change in input signal and masker level would lead to identical changes in the BM response ($\Delta S_i = \Delta M_i$ for $\Delta S_o = \Delta M_o$). This produces a certain slope of the GOM function. At the lower signal level, in condition A2, the presented signal falls in the linear region of the BM I/O function, while the masker still falls in the compressive processing region. This implies that a smaller change in signal input level is necessary to produce a similar change in BM response level between signal and masker ($\Delta S_i < \Delta M_i$ for $\Delta S_o = \Delta M_o$). This will produce a steeper GOM curve, which is presumably divided in two segments. Differences in the slopes indicate whether the data-points were produced from condition A1 or A2. At low input levels, the GOM curve will be steeper than at higher input levels. The transition point between the two segments provides an estimate of the knee point of the

BM I/O function. In the most widely used GOM method (Oxenham and Plack, 1997), and in experiment 1 here, the MSIs were small (about 0 to 2 ms), and it is therefore likely that signal and masker were both processed in the linear or compressive region at all tested levels, such that no transition point appears.

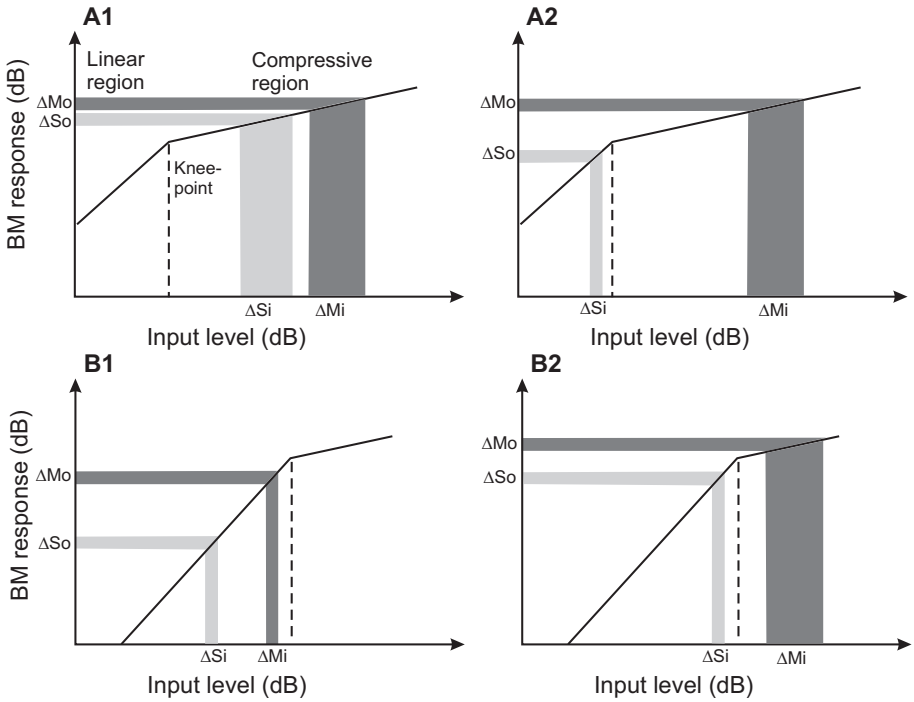

Figure 3.1: Schematic diagram of the BM response changes in probe- and masker tone levels. A change in signal input level (light gray regions, ΔS_i) and masker input level (dark gray regions, ΔM_i) produces corresponding changes in output level (ΔS_o and ΔM_o). The top row represents condition with a normal BM I/O function, while the bottom row shows examples where the knee point has shifted towards higher levels. A1: probe and masker are both processed in the compressive region. A2: The signal is processed in the linear region while the masker is processed compressively. B1:Signal and masker are both processed in the linear region. B2: The signal is processed in the linear region while the masker is processed compressively.

Consider the hypothetical I/O function observed in HI listeners where the compression exponent is near normal and the knee point is shifted towards higher input levels (Plack *et al.*, 2004). This is illustrated in panels B1 and B2 in Fig 3.1. The

dynamic range of signal levels that will force the masker to fall in the compressive region is now narrower (B2), and will produce slopes of the GOM function similar to that obtained in condition A2 ($\Delta S_i < \Delta M_i$ for $\Delta S_o = \Delta M_o$). In condition B1, both masker and signal will be processed linearly leading to a shallower steepness of the GOM function ($\Delta S_i = \Delta M_i$ for $\Delta S_o = \Delta M_o$). Thus, in this particular situation, the complete GOM function would have a shallow slope at low input levels, while a steeper slope at higher input levels. Again, the transition level indicates the knee-point.

3.2 Experimental methods

3.2.1 Listeners

Seven normal-hearing and five hearing-impaired listeners participated in the measurements. The NH listeners were between 20 and 26 years of age, and all had pure-tone thresholds of 10 dB HL or better at frequencies between 0.125 and 8 kHz. One was the first author and had previous experience in psychoacoustic experiments. The others had no prior experience in listening tests. The five HI listeners had mild-to-moderate sensorineural hearing loss at the test frequencies. Their pure-tone audiograms are shown in Fig. 3.2 and additional information can be found in Sec. 3.6. They were between 53 and 73 years of age. Listeners were paid for their participation on an hourly basis, except for the author. They all received training-sessions of about two hours in forward masking before the measurements were conducted. There were no systematic improvements in thresholds during the course of the experiments. Measurement sessions ranged from 30 to 60 minutes depending on the listener's ability to focus on the task. In all measurements, each subject completed at least three runs for each condition. The total testing time, including training, was 6 to 8 hrs.

3.2.2 Apparatus and procedure

Measurements were carried out in a double-walled sound insulated booth with a computer monitor to provide instructions and visual feedback. The computer keyboard was used to obtain the responses. The stimuli were presented monaurally via Sennheiser HD580 headphones. Signals were generated in MATLAB on a personal computer and converted to analogue signals by a 24-bit soundcard (RME DIGI 96/8). The sampling rate was at 44.1 kHz. FIR equalization filters were applied to obtain a flat frequency response at the headphone output. A three-interval tree-alternative forced choice paradigm combined with a 2-up-1-down tracking rule was used such that thresholds reflect the 70.7% point on the psychometric function and represent the mean of at least three measurements. The step size was varied adaptively, starting

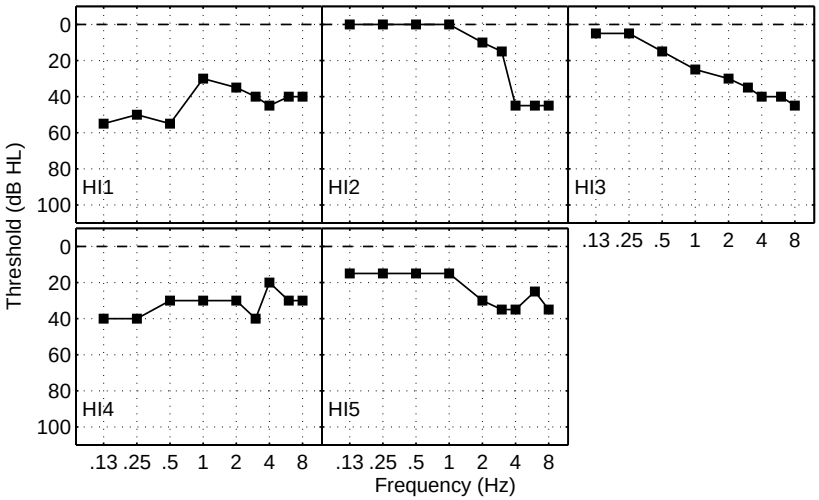

Figure 3.2: Audiograms of the measured ears of the five HI listeners. Thresholds are shown in dB hearing level (HL).

at 4 dB and ending at 1 dB. Thresholds were an average of the levels at the last six reversals with the final step size.

3.2.3 Stimuli

Experiment 1 was used to estimate BM compression. Forward masking of a brief probe tone was measured as a function of the signal level. The masker-signal interval (MSI) was fixed. The masker level was adaptively changed in order to reach the masked threshold. The parameters were similar to those of Rosengard *et al.* (2005), with slight changes to the probe duration and MSI. The probe signal was a 5-ms tone burst at a frequency (f_{sig}) of 1 or 4 kHz, Hanning windowed over its duration. The masker was also a pure tone with a duration of 110 ms and 5-ms raised-cosine on- and off ramps were applied. The masker frequency (f_m) was equal to f_{sig} in the on-frequency condition and $0.55 \cdot f_{sig}$ in the off-frequency condition. The MSI was fixed at 2 ms. The signal level ranged from 40 to 85 dB SPL, and the individual levels were

chosen for each listener in a pilot experiment. The lower limit was typically 40 dB SPL for the NH listeners since it was intended to measure the amount of compression in the compressive region of the BM I/O function. The upper limit for the level was found such that masker levels did not become uncomfortably loud. These levels were 95 dB SPL for NH listeners and 100 dB SPL for the HI listeners. In order to prevent off-frequency listening effects, an ipsi-lateral high-pass noise was presented at a spectrum level of 40 dB (60 dB for HI listeners) below the signal level. The noise had a frequency range from $1.2 \cdot f_{sig}$ to 6.0 kHz and a duration of 200 ms including 50 ms raised-cosine on- and off-frequency ramps. To prevent detection of the contra-lateral ear, a noise was presented with frequencies ranging from $0.8 \cdot f_{sig}$ to $1.2 \cdot f_{sig}$ presented at a spectrum level 20 dB (50 dB for HI listeners) lower than the signal level.

Experiment 2 was used to estimate the knee point of the BM I/O function. Most experimental parameters in this experiment were identical to those of experiment 1, i.e., the duration and frequencies of the on- and off-frequency maskers as well as the ipsi- and contra-lateral noise maskers. However, the probe duration was 10 ms and Hanning-windowed over its duration. The masker-signal interval (MSI) was chosen, such that there was sufficient dynamic range of the input levels in condition A2 for NH listeners. If the MSI was too short, then the levels of the masker and the signal were too similar, and no transition point would be found. If the masker-signal interval was too long the sound pressure level of the masker approached the maximally allowed presentation level, which, in turn, reduced the dynamic range of the data in condition A1, especially when measuring HI listeners with reduced compression. The other issue was that the level of the signal in condition A2/B2 can be very close to its threshold in quiet. This made the task more demanding to the listeners and training could presumably not resolve this. Here, the MSI was 12 ms. The tested signal levels ranged from 18 to 60 dB SPL for NH listeners and from 30 to 85 dB for the HI listeners. Measurable levels in the experimental conditions for each listener were found in a pilot run of the experiment.

3.3 Results

3.3.1 BM I/O functions in NH listeners

Figure 3.3 shows the results of experiment 1 for the NH listeners. The first two rows show the data measured with f_{sig} at 1 kHz while the two lower rows show results where f_{sig} was 4 kHz. Circles indicate GOM functions obtained with on-frequency masking and the squares show GOM functions obtained with off-frequency masking. The solid lines show linear functions fitted to the data. The slopes of the on-frequency GOM function are generally steeper than the off-frequency slopes. The ratio of the slopes of the fitted curves was calculated and provides an estimate of BM compression. The compression estimates are listed in Table 3.1. In some cases (e.g., NH2 and NH4 at 1 kHz), the on-frequency GOM functions cross the off-frequency curves, however this does not affect the estimate of compression. The compression estimates was in the range from 0.34 to 0.63 dB/dB (mean = 0.48) at 1 kHz and from 0.17 to 0.45 dB/dB (mean = 0.30) at 4 kHz. The 1 kHz values are slightly higher than those found in other studies (e.g., Rosengard *et al.*, 2005). The 4 kHz values are in good agreement with previous results. Error bars indicate $\pm$ one standard deviation and are typically within the size of the symbols.

Knee points were estimated from the data in Fig. 3.4. The shape of the obtained GOM functions support the hypothesis described in the introduction and visualized in Fig. 3.1 (panels A1 and A2). A two-line multi-phase linear regression analysis was performed, and the fitted linear curves are plotted as the solid curves. In cases where the slopes of the two lines were significantly different, an estimate of the knee point was obtained. This was possible in 10 of the 14 cases. The short vertical lines indicate the input level at these knee points. The estimated values are provided in the plots and listed in Table 3.1. The obtained estimates are comparable at the two tested frequencies and are in the range from 28 to 40 dB. These are in good agreement with the expected knee points, observed in other studies (e.g., Ruggero *et al.*, 1997; Plack and Oxenham, 1998).

Estimates of the complete BM I/O function were derived from the results from Experiment 1 and 2. Fig. 3.5 shows the individual I/O functions for the seven NH listeners. The solid and dashed curves show I/O functions derived at 1 and 4 kHz,

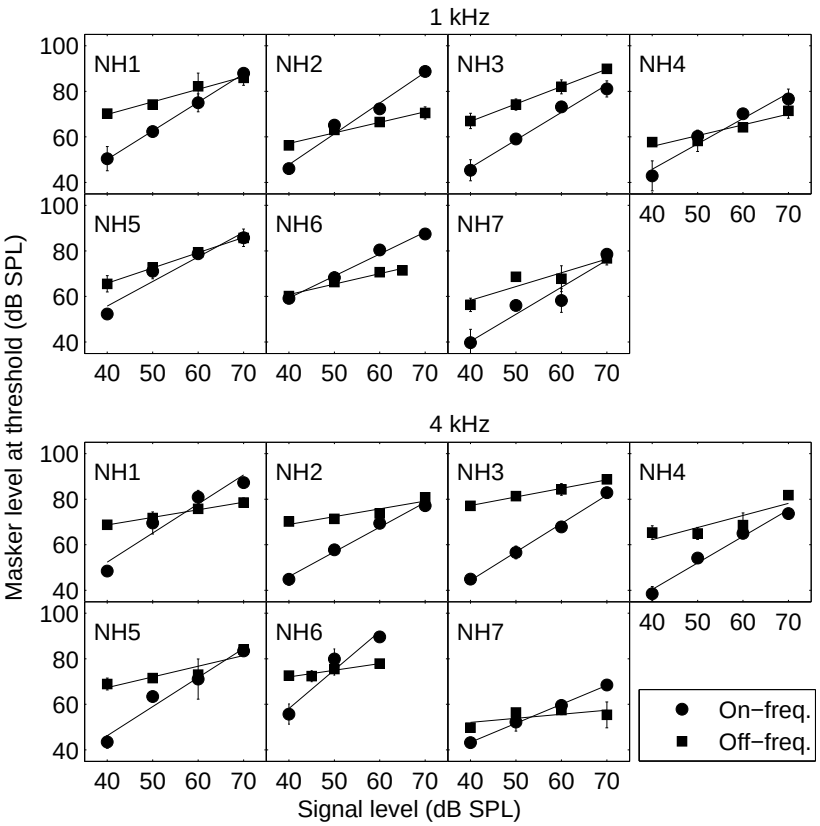

Figure 3.3: GOM functions for the NH listeners, experiment 1. Masker level at thresholds is plotted as a function of the signal input level. Circles indicate results using the on-frequency masker, while squares indicate results using the off-frequency masker. The first two rows show data measured at a signal frequency at 1 kHz, while the two bottom rows show data measured at 4 kHz.

respectively. In the few cases where no knee-point estimates could be obtained, only the compressive part of the I/O function is shown (e.g., NH4 at 1 kHz). These I/O functions are plotted such that an input level of 100 dB SPL has a 100 dB BM response, correspondingly, although this output level reference has been chosen arbitrarily for illustrative purposes.

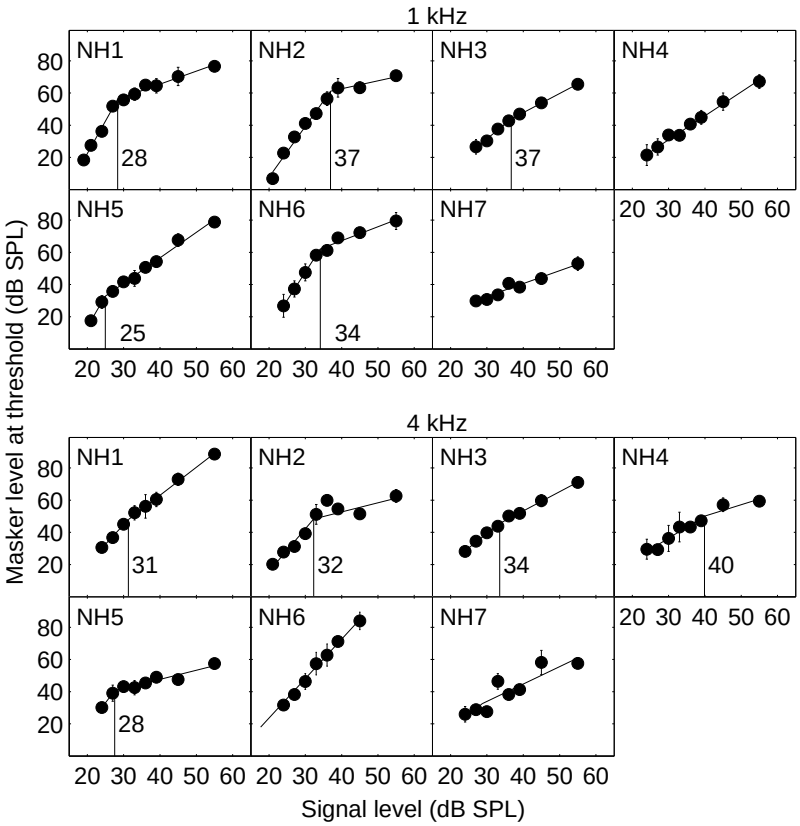

Figure 3.4: GOM functions for the NH listeners, experiment 2. Only on-frequency masking was measured. The fitted linear functions are plotted on top of the data, and if a knee point was obtained it is indicated in the corresponding panel by a vertical line.

3.3.2 BM I/O functions in HI listeners

Figure 3.6 shows the results of experiment 1 for the HI listeners. The same symbols as in Fig. 3.3 were chosen. It can be seen that, in some listeners, signal thresholds could only be measured in a limited dynamic range of levels. The signal levels were typically higher than for the NH listeners. The thresholds produced by the off-frequency masker

	NH1	NH2	NH3	NH4	NH5	NH6	NH7	mean	SD
Compression, 1 kHz	0.44	0.34	0.63	0.42	0.62	0.47	0.51	0.48	0.09
Knee point, 1 kHz	28	37	37	-	25	34	-	32	5.4
Compression, 4 kHz	0.26	0.32	0.30	0.45	0.36	0.17	0.22	0.30	0.09
Knee point, 4 kHz	31	32	34	40	28	-	-	33	4.5

Table 3.1: Overview of the estimated BM I/O parameters for the NH listeners: BM compression in dB/dB and knee point in terms of the input level in dB. The means and standard deviations (SD) are also listed

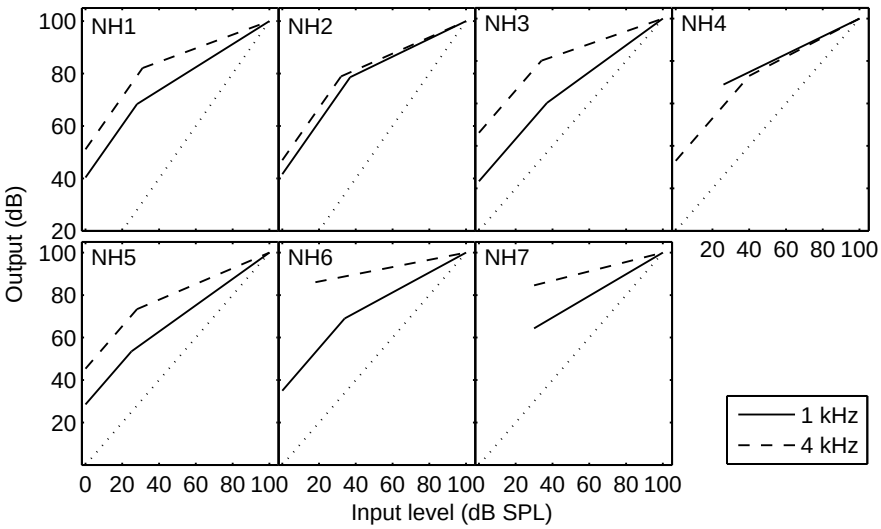

Figure 3.5: Estimated BM I/O functions for the NH listeners obtained from combining the data of the two experiments. I/O functions are plotted such that an input level at 100 dB SPL produces a corresponding output at 100 dB. The solid and dashed curves indicate I/O functions at 1 and 4 kHz, respectively. The dashed-dotted curves indicate the slope of 1.0 (linear relation).

were generally above those found with the on-frequency masker. In several cases, the slopes of the on- and off-frequency masking GOM functions were more similar than found in the NH listeners. This is consistent with recent findings by, e.g., Rosengard *et al.* (2005). The estimated compression was calculated and is listed in Table 3.2.

The compression ratios range from being close to normal (0.31 dB/dB) to about one indicating linear BM processing.

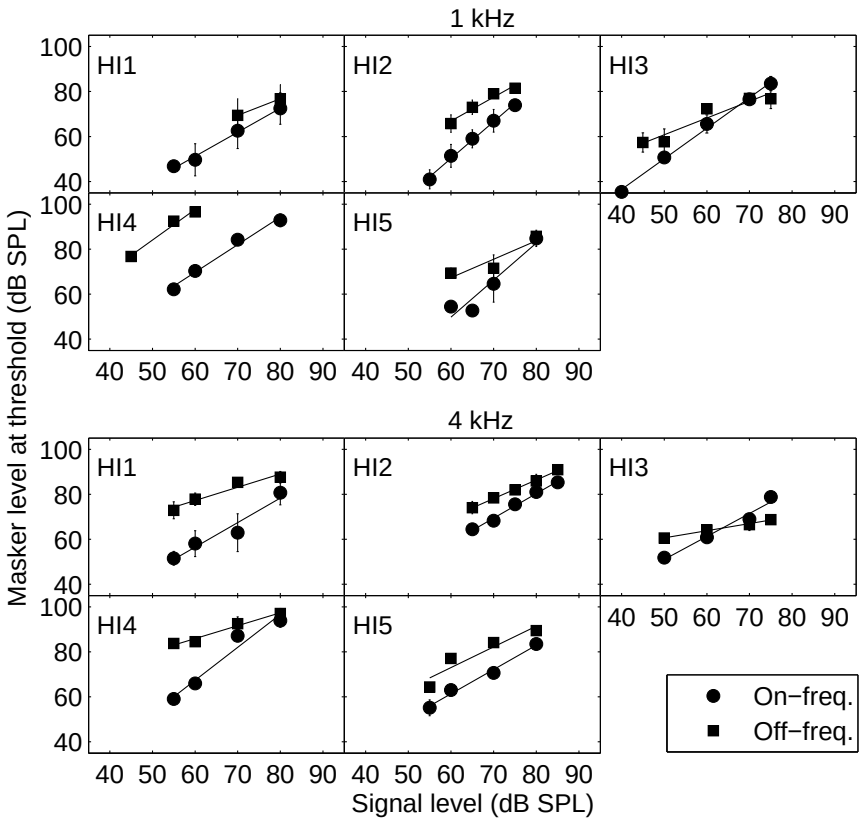

Figure 3.6: Results of experiment 1, as in Fig. 3.3, but for the five HI listeners.

Knee points were estimated from the data in Fig. 3.7. Multi-phase regression lines were calculated as described earlier, and the fitted linear curves are represented by the solid curves. In four cases (e.g., HI2 and HI4 at 1 kHz), where the knee-point estimates are in the normal range (39 to 45 dB), the results reflect the scenario in

	HI1	HI2	HI3	HI4	HI5
Compression, 1 kHz	0.69	0.65	0.55	1.11	0.50
Knee point, 1 kHz	(70)	40	-	39	(50)
Compression, 4 kHz	0.54	0.76	0.31	0.39	0.85
Knee point, 4 kHz	(59)	-	-	40	45

Table 3.2: As Table 3.1, but for the HI listeners. Knee points in brackets indicate particular cases, as described in Fig 1, panels B1 and B2.

A1/A2 in Fig. 3.1. In three other cases cases (HI1 and HI5 at 1 kHz; and HI1 at 4 kHz), the results reflect the B1/B2 scenario, and in these cases the knee-point estimates are at higher-than-normal levels (70, 50 and 59 dB, respectively). In the remaining three cases, no reliable estimate of the knee point could be obtained. For the HI listeners, there are several conditions where one of the two lines in the regression-line fits were based on only few data-points.

As for the NH listeners, the estimates of the complete BM I/O functions were derived from the results from the two experiments. Fig. 3.8 shows the individual I/O functions for the five HI listeners.It is clear that these I/O functions are very different across the five listeners, and depend on frequency within each listener. When no knee-point estimates were obtained, only the compressive part of the I/O function is shown (e.g., HI3 at 1 kHz). Fig. 3.9 shows estimated BM compression as a function of pure-tone sensitivity (left panel) and the knee-point estimates as a function of sensitivity (right panel). No significant correlation was observed in either case. The correlation coefficients (ρ) for the data in the left and right panels were 0.0018 and 0.26, respectively.

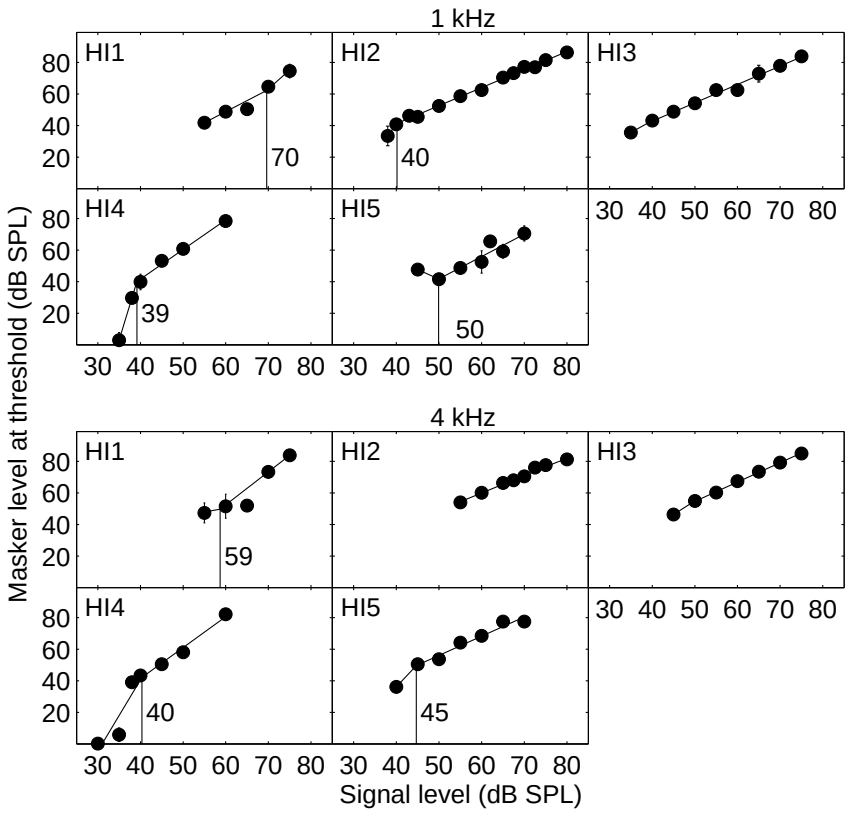

Figure 3.7: Results of experiment 2, as in Fig. 3.4, but for the five HI listeners.

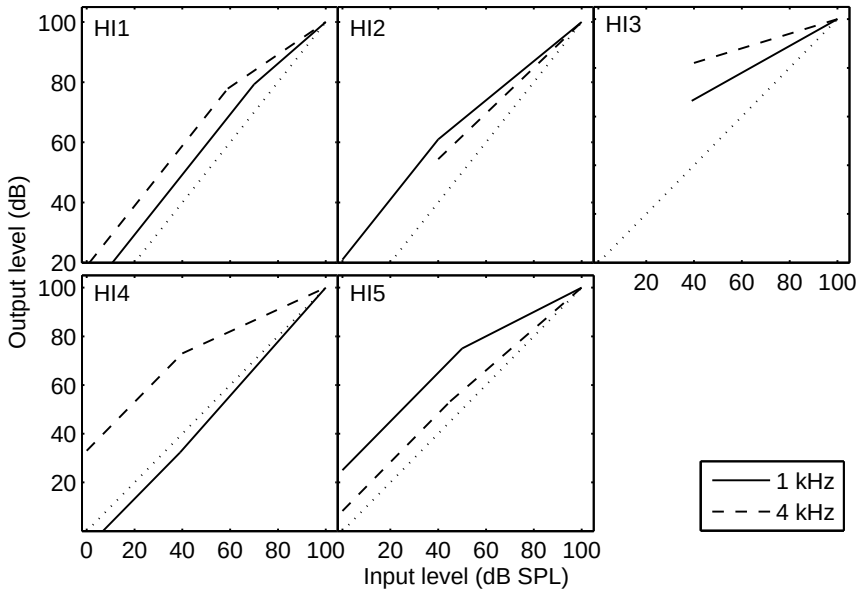

Figure 3.8: As in Fig. 3.5, but for the five HI listeners.

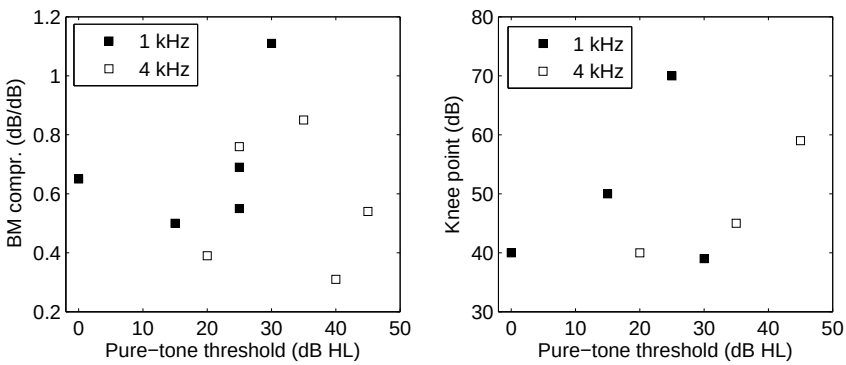

Figure 3.9: Scatter-plots of the relations between the pure-tone thresholds (sensitivity) and estimated compression (left panel) and knee points (right panel)

3.4 Discussion

The measured thresholds in both experiment 1 and 2 showed low within-listener variability. This was earlier emphasized as being one of the major advantages of the GOM method over the TMC method (Rosengard *et al.*, 2005). Estimates of compression were found to be similar across NH listeners, with estimated compression exponents at 1 kHz being slightly higher than at 4 kHz. This is consistent with the observation in Moore *et al.* (1999); Rosengard *et al.* (2005). The estimated compression in the HI listeners varied substantially, as expected from earlier investigations. No correlation between the loss of sensitivity and the estimated amount of compression was found ($\rho = 0.0018$). Moore *et al.* (1999) collected data in six HI listeners with moderate to severe hearing loss. They found a slight correlation between sensitivity and compression estimates for cases where the loss was larger than 35 dB. The listeners from the present study typically had losses less than 35 dB at the tested frequencies which might be the reason for why no correlation was found.

The main contribution of this study was that estimates of both compression exponents and knee point levels were obtained. This was achieved by adding an extra forward masking condition with a longer masker-signal interval. This allows characterization of the BM I/O function for a wider range of input levels. Presently, this is the first behavioral study that use an experimental condition designed to explicitly determine the BM I/O function knee point. It was shown that this can be done reliably. For all NH listeners, except NH7, clear significant knee-point estimates could be obtained. An advantage was that the only change from experiment 2 to experiment 1 was the changed MSI. Thus, the additional experiment requires additional testing time, but no further training. The experiment was sensitive to the choice of the MSI, since the number of measured thresholds above and below the knee-point need to be sufficient. However, it seems the the MSI chosen here (12 ms) was appropriate for all NH listeners. For the HI listeners, knee points were obtained in 7 of the 10 I/O-functions estimates. Some of these estimates relied on few data-points. This could be avoided by choosing the MSI of experiment 2 to be listener specific, based on a pilot run testing a range of MSIs. If the MSI is too short, the levels of the masker and the signal are too similar, and both stimuli are processed

in the same, either linear or compressive, region, such that no transition point could be identified. This could be the reason why no knee points could be found for HI3 (at both frequencies) and HI2 (at 4 kHz). If the MSI is too long, the level of the masker approaches the maximally allowed presentation level of 100 dB SPL, which in turn, reduced the dynamic range of tested input levels in the data reflecting condition A1. Three of the estimated I/O functions showed support of the idea that the knee point is shifted towards higher levels (Plack *et al.*, 2004). However, only one of these (HI5 at 1 kHz) approached a near-normal compression exponent. Four other I/O-function estimates showed a trend where the knee point was close to normal while less compression was found. It was also tested whether there was a relation between the HI listener sensitivity and corresponding estimated knee points. No significant correlation was found ($\rho = 0.26$).

Recently, Wojtczak and Oxenham (2009) discussed that the assumption underlying the GOM method may not be appropriate, since on- and off-frequency maskers show a different recovery from masking at a particular place on the BM, even when the amount of excitation was adjusted to be the same at that place. This means that the amount of compression may be overestimated (lower compression exponents) using forward masking methods to estimate BM compression. Wojtczak and Oxenham (2009) concluded that results obtained with the GOM method are less likely to overestimate compression compared to the TMC method. The mean estimates of compression for the NH listeners of the present study were 0.48 at 1 kHz and 0.30 at 4 kHz. This was slightly higher than, although consistent with, results from other studies (e.g., Rosengard *et al.*, 2005). The results of Plack *et al.* (2004) were obtained with the TMC method, and they found near-normal compression above the knee point. This was only observed in 2 out of 10 conditions in the HI listeners from the present study. For the remaining conditions the compression exponents were higher. The disadvantage of using the GOM method over the TMC method is the requirement of ipsi-lateral masking noise to avoid off-frequency listening, and contra-lateral masking noise to prevent across ear listening. It is not clear how to choose the levels of these noises appropriately for HI listeners. Here, these masker noise levels were chosen relatively lower than those used for NH listeners. The HI listeners may not have the off-frequency cues available due to their reduced sensitivity, and furthermore, the

noise masker levels used for the NH listeners were too high, such that they would be distractive to the HI listeners. The finding of large individual differences in BM I/O functions motivate the importance of characterizing hearing loss on an individual basis, e.g. in terms of BM compression and BM tuning in addition to the audiogram. The valuable contribution from the present study is that the suggested experiment provides reliable estimates of the I/O-function knee point, which is an important parameters when nonlinear I/O-functions of the BM stage in a model is fitted to individual hearing loss. Such model allows to investigate the underlying mechanisms of cochlear hearing loss. This was investigated in Jepsen and Dau (2010) (chapter 4 of this thesis).

3.5 Conclusions

- In experiment 1, forward masking using on- and off-frequency was measured, and the results were used to obtain an estimate of basilar-membrane compression. In experiment 2 a different forward masking condition was used and the results were used to obtain estimates of the knee point of the basilar-membrane input-output function. By combining the results of experiment 1 and 2 an estimate in the complete BM I/O function was obtained in seven normal-hearing and five hearing impaired listeners.

- The method extends the input level range in which I/O functions can be estimated compared to other forward masking paradigms. However, the suggested method requires additional testing time.

- For the NH listeners the choice of masker-signal intervals in experiment 2 was constant and provided reasonable knee-point estimates. However, for the HI listeners an individual-specific choice of masker-signal interval is necessary to obtain reliable knee-point estimates.

3.6 Appendix: Additional information about the listeners

This appendix describes additional information about the hearing-impaired listeners that were used in Chapter 3 and is listed in Table 3.3. The etiologies of the hearing losses are listed, and they are based on clinical diagnoses if available. It is also listed whether the listeners were hearing-aid users or not. Finally, results from a speech intelligibility test are listed. These results were not used or analyzed in the chapter, but are reported here to make these data available to possible future studies.

Speech reception thresholds (SRTs) were measured for Danish Dantale II sentences in two noise conditions. It is a closed-set word recognition test using Hagerman sentences (Wagener *et al.*, 2003). The noise conditions were: (1) stationary speech-shaped noise (SSN) with the long-term spectrum of the Dantale II sentences; (2) sinusoidally amplitude modulated (SAM) noise with a constant modulation rate at 8 Hz and a modulation depths of 1. The SRT was defined as the SNR at which 50% words were identified correctly. The noise level was constant wihle the level of the sentences was varied adaptively. Listeners were trained on a single run with 20 sentences before measurements were made. The reported SRTs are avereages of two measurements. The mean SRT results of the seven NH listeners are also given in the table.

Listener	Etiology	Hearing-aid user	SSN	SAM
HI1	Presbycusis	No	-2.6	-4.8
HI2	Noise induced	Yes	-5.6	-6.3
HI3	Presbycusis	Yes	-6.6	-8.7
HI4	Unknown	No	-6.5	-9.2
HI5	Presbycusis	Yes	-7.1	-8.5
Mean NH			-7.6	-16.7

Table 3.3: Additional information about the five HI listeners used in Chapter 3. The table lists their hearing loss etiology, hearing aid use and SRTs (in dB) in noise condition of stationary speech-shaped noise (SSN) and Sinusoidally amplitude modulated (SAM) noise at a modulation rate of 8 Hz.

4

Characterizing auditory processing and perception in individual listeners with sensorineural hearing loss[5]

This study considered consequences of sensorineural hearing loss in ten listeners. The characterization of individual hearing loss was based on psychoacoustic data addressing audiometric pure-tone sensitivity, cochlear compression, frequency selectivity, temporal resolution and intensity discrimination. In the experiments it was found that listeners with comparable audiograms can show very different results in the supra-threshold measures. In an attempt to account for the observed individual data, a model of auditory signal processing and perception [Jepsen *et al.*, J. Acoust. Soc. Am. **124**, 422-438 (2008)] was used as a framework. The parameters of the cochlear processing stage of the model were adjusted to account for behaviorally estimated individual basilar-membrane input-output functions and the audiogram, from which the amounts of inner hair-cell and outer hair-cell losses were estimated as a function of frequency. All other model parameters were left unchanged. The predictions showed a good agreement with the measured individual data in the frequency selectivity and forward masking conditions while the variation of intensity discrimination thresholds across listeners was underestimated by the model. The model and the associated parameters for individual hearing-impaired listeners might be useful for investigating effects of individual hearing impairment in more complex conditions, such as speech intelligibility in noise.

[5] This chapter was submitted as Jepsen and Dau (2010). Parts of this work were presented at the International Hearing Aid Research Conference (IHCON), Lake Tahoe, CA, USA, 2008

4.1 Introduction

Hearing impairment is a communicative handicap: hearing-impaired (HI) people often experience great difficulty with speech communication. These difficulties are typically most pronounced when background noise is present, in reverberant environments or in situations with multiple interfering sound sources. The most common form of hearing loss can be attributed to damage to the inner ear, or cochlea, where the most obvious symptom is a loss of ability to detect weak sounds. This is accompanied by a variety of other changes in the way that sound is perceived. Even if sounds are amplified by a hearing aid such that reduced audibility is compensated for, many listeners still experience problems in every-day life situations. There can be enormous differences in performance between individual listeners to whom a hearing aid has been fitted (Lunner, 2003). Some listeners might be satisfied with their aids while others continue to experience difficulties when listening to speech in noise or competing speech. In order to choose the right compensation strategy for the individual hearing-impaired listener, one needs to understand where the sources of this variability among the listeners are. It is important to clarify what the limitations besides audibility are and how they can be characterized. Furthermore, if the performance of individual listeners could be predicted through auditory modeling, this would be particularly useful to help design the best compensation strategy for the individuals.

The present study had two major goals. One goal was to experimentally characterize individual hearing impairment, using a set of measures of auditory function. The second goal was to quantitatively account for individual hearing impairment using a model of auditory signal processing and perception. The study focused on perceptual consequences of sensorineural hearing loss (SNHL). Typical consequences of this type of hearing loss are reduced sensitivity, loudness recruitment, reduced temporal resolution and reduced frequency selectivity (e.g., Moore, 1995). While reduced sensitivity explains part of the communication difficulties in HI listeners, some of the reported variability in performance among listeners may be due to supra-threshold deficits. Loudness recruitment as well as reduced frequency selectivity and reduced temporal resolution are examples of "supra-threshold" consequences. In the present study, basic functions of auditory

processing in HI listeners were investigated, using psychoacoustic masking and discrimination experiments. These measures included the sensitivity to pure tones in terms of the audiogram; temporal masking curves (TMC; Nelson *et al.*, 2001) to estimate individual basilar-membrane (BM) input-output (I/O) functions; notched-noise masking to estimate individual auditory filter bandwidths (Patterson and Moore, 1986); simultaneous and forward masking with noise maskers (Glasberg *et al.*, 1987) to estimate temporal resolution; and intensity discrimination for tones to estimate intensity resolution. This approach was similar in Moore *et al.* (1999) where measures of sensitivity and frequency selectivity and their relations to hair-cell loss and changes in BM compression were investigated. However, in contrast to Moore *et al.* (1999) who focused on correlations between measures, the goal here was to characterize individual hearing impairment using a "critical" set of outcome measures. Furthermore, several conditions of non-simultaneous and simultaneous masking were considered which were not studied in Moore *et al.* (1999). The results of the experiments served as the basis for the subsequent modeling efforts described further below.

In the normally functioning system, the BM I/O function has an approximately linear region at low input sound pressure levels (< 30-40 dB) and a compressive region at medium and high sound pressure levels (< 90 dB) (Ruggero *et al.*, 1997). The transition point between the linear and the compressive region reflects the knee point. Some studies observed a return to linear processing for levels above about 90 dB SPL (e.g., Nelson *et al.*, 2001). Several studies have suggested methods to behaviorally estimate the BM I/O function and, thus, the amount of BM compression in humans (e.g., Oxenham and Plack, 1997; Nelson *et al.*, 2001). Nelson *et al.* used forward masking with pure-tone signals and maskers and measured TMCs where the signal level was fixed and the temporal separation between the masker and the signal varied. Based on this, an estimate of the shape of the BM I/O function was obtained, including estimates of the amount of compression and the knee point. This method has since been used in several studies with normal-hearing and hearing-impaired listeners (Nelson *et al.*, 2001; Lopez-Poveda *et al.*, 2003, 2005; Plack *et al.*, 2004; Stainsby and Moore, 2006). In these studies, a reduced or loss of compression was found in HI listeners with severe loss, resulting in a linear or close to linear I/O

function (Nelson *et al.*, 2001; Stainsby and Moore, 2006) which is in line with the assumed effect of a loss of OHCs in such listeners. Other studies dealt with mild-to-moderate losses (Plack *et al.*, 2004; Lopez-Poveda *et al.*, 2005; Dubno *et al.*, 2007; Jepsen and Dau, 2008) where it was found that the estimated I/O functions strongly depended on the individual listener. Some listeners showed an increased compression exponent, i.e. less compression, while others also indicated a shift in the knee point between the linear and compressive region.

In a SNHL, the number of hair cells in the cochlea is typically reduced due to age, hereditary disease, noise trauma or exposure to drugs from medical treatment (e.g., Moore, 2007). The hair cells are divided into outer hair cells (OHCs) and inner hair cells (IHCs). The OHCs are commonly associated with nonlinear gain in the cochlea (e.g., Ruggero *et al.*, 1997). At low stimulation levels, the OHCs amplify the basilar-membrane (BM) response. The amount of gain provided by the OHCs is level dependent; with increasing input level, the OHC gain decreases. This is equivalent to the BM input-output (I/O) function being non-linear and compressive. It is an important property of the normally-functioning inner ear that a wide dynamic range of input levels is transformed into a narrower dynamic range at its output. The OHCs are also responsible for the sharp tuning of the BM at low stimulation levels, a feature which is important for the ability to spectrally resolve complex sounds. The IHCs are responsible for the transduction of the BM motion into electrical potentials that are further processed by the subsequent neural system along the auditory pathway (e.g., Pickles, 2008). In listeners with SNHL, just noticeable differences (JNDs) in intensity are typically similar as or higher than in NH listeners when the stimuli are presented at the same SL, whereby thresholds can vary considerably among individual listeners (Florentine *et al.*, 1993).

It is still unclear how the loss of OHCs and IHCs can be estimated. showed that The degree of OHC- and IHC loss has been shown to strongly depend on the individual listener or animal preparation (e.g., Liberman and Dodds, 1984; Moore *et al.*, 1999; Heinz and Young, 2004). The variability may arise from differences in the cause of the loss, e.g., due to differences in the intensity and duration of noise exposure (Borg and Engström, 1989). Important effects are reduced OHC gain and, in consequence, reduced BM compression and frequency selectivity. Loss of IHCs primarily has an

influence on sensitivity. It has also been hypothesized that IHC loss may affect the temporal acuity of the neural coding, or phase locking (e.g., Moore, 2007); however, clear physiological evidence has not been provided yet (e.g., Heinz *et al.*, 2002). IHC loss has been observed to affect the temporal acuity of the neural coding, or phase locking, but this is not necessarily always the case (see e.g., Moore, 2007). These aspects of a cochlear hearing loss cannot be characterized or predicted from the audiogram alone. Estimates of the degree of impairments and the relation between OHC- and IHC loss in the impaired listeners would be important for characterizing consequences of individual impairment. Moore *et al.* (1999) observed a reduced sensitivity to pure tones in their HI listeners, referred to here as "total hearing loss" (HL_{TOT}). They further used a loudness matching experiment to obtain an estimate of the contribution of OHC loss to the reduced audibility (HL_{OHC}). They estimated IHC loss (HL_{IHC}) from HL_{TOT} and HL_{OHC}, assuming that $HL_{TOT} = HL_{OHC} + HL_{IHC}$. Heinz and Young (2004) measured the growth of auditory-nerve responses as a function of level in cats after acoustic trauma. They observed different impaired response functions, some of which were primarily based on OHC loss, some were primarily resulting from IHC loss and others were based on a more equal distribution of OHC and IHC losses. The observations from these studies demonstrated the importance of characterizing individual SNHL.

To address the second main goal of this study, which was to simulate individual hearing impairment, the computational auditory signal processing and perception (CASP) model of Jepsen *et al.* (2008) was used as a framework. The model consists of various processing stages including, outer- and middle-ear filtering, nonlinear cochlear processing, effects of adaptation, a modulation filterbank and an optimal detector as the decision stage. This model which is based on the original model of Dau *et al.* (1997a) but includes a nonlinear cochlea stage instead of the linear gammatone filterbank, was shown to account for a large variety of detection and masking data in normal-hearing listeners (Jepsen *et al.*, 2008). In the present study, modifications of the model were undertaken in the cochlear stage of the model. These modifications were exclusively based on the individual estimates of the BM I/O functions derived from the TMC data and the audiogram from this study. Even though the model contains numerous parameters in the different processing stages, only very few (five)

frequency-dependent parameters were considered for modification to account for the individual losses. The model was used to predict the measured thresholds obtained in the NH and individual HI listeners. Some of the parameters of the cochlear stage of the model were adjusted to fit estimates of BM compression derived from the psychophysical data, and measured loss of sensitivity. This approach has the principal limitation that such behavioral estimates are themselves based on assumptions and concepts which might not be fully justified and valid.

The CASP model represents only one example of an auditory processing model. In fact, explaining basic auditory masking phenomena in terms of physiological mechanisms has a long tradition. There have been systematic attempts at predicting psychophysical performance limits (both in the NH and HI system) from the activity of auditory nerve (AN) fibers (e.g., Siebert, 1965, 1970; Heinz *et al.*, 2001a,b,c; Colburn *et al.*, 2003; Bruce *et al.*, 2003; Zilany and Bruce, 2006, 2007), combining analytical and computational population models of the AN with statistical decision theory. Different approaches to simulate effects of SNHL have been suggested (e.g., Kates, 1991; Bruce *et al.*, 2003; Zilany and Bruce, 2006). A general result has been that those models that make optimal use of all available information from the AN (e.g., average rate, synchrony, and nonlinear phase information) typically predict performance that is one to two orders of magnitude better than human performance, while the trends often match well human performance (e.g., Heinz *et al.*, 2001a). Other types of auditory models are to a lesser extent inspired by neurophysiological findings and make simplifying assumptions about the auditory processing stages. Such an "effective" modeling strategy does not allow conclusions about the details of signal processing at the neuronal level; on the other hand, if the model accounts for a variety of data, this suggests certain processing principles. For example, the temporal window model (e.g., Oxenham and Moore, 1994; Oxenham *et al.*, 1997; Plack and Oxenham, 1998; Plack *et al.*, 2002) has been shown to account for forward and backward masking data in NH and sensorineural HI listeners as well as for other phenomena associated with temporal resolution such as gap detection. The temporal window model includes an initial stage of bandpass filtering (reflecting a simplified action of BM filtering), followed by a nonlinear device, a smoothing device (implemented as a lowpass filter or a sliding temporal integrator) and finally a decision device. The CASP

model, chosen here, lies conceptually between the two approaches described above. It reflects a perception model designed to account for perceptual data, as the temporal-window model, and is thus less accurate than the AN models in terms of details of peripheral processing. However, it makes several additional assumptions about the processing at and subsequent to the cochlear stage, such as effects of adaptation, modulation filterbank and template-based optimal detection. Since this framework has led to successful predictions of a large variety of perceptual masking data in NH listeners it was chosen here to consider consequences of cochlear hearing impairment.

4.2 Auditory processing model

The structure of the CASP model (Jepsen *et al.*, 2008) is shown in Fig. 4.1. The processing stages comprise outer- and middle-ear filters, nonlinear BM processing, inner hair-cell transduction, expansion, adaptation and a modulation filterbank. Finally, the model includes an optimal detector designed to deal with n-interval alternative forced choice paradigms.

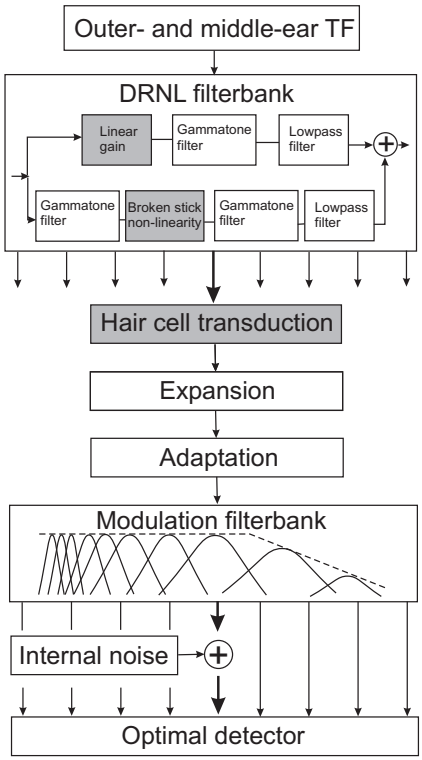

Figure 4.1: Schematic structure of the CASP model. The model comprises: outer- and middle ear filtering, the DRNL filterbank, inner hair-cell transduction, expansion, adaptation, a modulation filterbank and an optimal detector. The gray blocks indicate the stages in which adjustments are made to fit individual hearing loss. In the DRNL filterbank, the gain in the linear path and parameters controlling the broken-stick nonlinearity are fitted. IHC loss is implemented in the IHC transduction stage.

4.2.1 Stages of the auditory processing

The first stage is an outer- and middle-ear stage implemented as two finite impulse response filters as in Lopez-Poveda and Meddis (2001). The second stage is the dual-resonance nonlinear (DRNL) filterbank as in Lopez-Poveda and Meddis (2001). The model uses parallel processing in two independent paths. The linear path comprises linear gain, g, a cascade of gammatone filters and a subsequent lowpass filter, and can be regarded as describing the "passive" BM response. The nonlinear path comprises cascaded gammatone filters, a broken stick nonlinearity (Eq. 4.1), another cascade of gammatone filters and a lowpass filter and can be associated with the "active" part of the BM response. The summed signal of the two paths describes the nonlinear BM processing and accounts for level-dependent compression and tuning. The broken-stick nonlinearity is defined as follows:

$$y[i] = \text{sign}(x[i]) \cdot \min(a|x[i]|, b|x[i]|^c) \tag{4.1}$$

whereby y represents the output signal and x is the input signal, i refers to the ith sample and a, b and c are parameters. After this stage, the signal analysis is performed separately in different frequency channels.

Inner hair-cell transduction is modeled as a half-wave rectification followed by a first-order lowpass filter with a cut-off frequency at 1 kHz. Effectively, it preserves phase information (fine-structure) at low frequencies while the signal envelope is extracted at higher frequencies. The expansion stage transforms the output of the IHC stage into an intensity-like representation by applying a squaring expansion. Effects of adaptation are simulated by a chain of five simple nonlinear circuits, or feedback loops, which include different time constants in the individual loops (Dau *et al.*, 1996a). For stationary input signals, the output of the series of five loops approaches a logarithmic compression. For input variations that are rapid compared to the time constants (τ) of the lowpass filters (with τ in the range from 5 to 500 ms), the transformation through the adaptation loops is more linear, leading to an enhancement of fast temporal variations at the output of the adaptation stage. For example, in response to signal onsets, the output of the adaptation loops is characterized by a pronounced overshoot. In order to simulate absolute threshold, the lower limit of the

input to the adaptation loops, and thus the size of the dynamic range in the model, was chosen here to be different for different frequency channels such that the model for normal hearing predicts the 0 dB hearing level (HL) line in the simulation of the audiogram (see gray squares in the top left panel in Fig. 4.3). This lower limit used to be frequency independent in Dau *et al.* (1996a, 1997a,b) and Jepsen *et al.* (2008) where the focus was on signal in noise detection while pure-tone sensitivity in quiet was not considered in detail.

The output of the adaptation stage is processed by a first-order lowpass filter with a cut-off frequency at 150 Hz. The lowpass filter is followed by the modulation filterbank which is a bank of bandpass filters tuned to different modulation frequencies. The decision device is realized as an optimal detector. It derives a template of the model's internal representation, using a supra-threshold representation of the signal in the target interval, and a representation of the reference intervals (Dau *et al.*, 1996a,b). The internal representation of the stimuli after the modulation filterbank is a three-dimensional pattern with axes time, center frequency and modulation frequency. In the present study, the templates were derived from the model fitted to the individual listener; thus, the templates used to simulate the effects of hearing impairment were based on the impaired, i.e. the not normal, auditory processing. Internal noise is added to the internal representation in order to limit the model's resolution and match human performance. The variance of this noise was adjusted such that the model follows Weber's law in intensity discrimination with pure tones, at a reference level of 60 dB SPL (Dau *et al.*, 1996a). The variance was kept constant in all simulations. It was determined in the model of normal hearing and assumed to be the same in listeners with SNHL. The effect of the internal noise depends on the experimental conditions. For example, if a masking experiment is simulated and stochastic maskers are used, then the *external* variability of the stimuli typically dominates, whereas performance is limited by the internal noise in experiments using deterministic maskers. For further details, the reader is referred to Dau *et al.* (1996a, 1997a,b) and Jepsen *et al.* (2008).

4.2.2 Parameter changes to account for SNHL

To simulate consequences of sensorineural hearing loss, the stages associated with hair-cell loss were modified. The changes were thus included in the DRNL filterbank and the IHC transduction stage. The input-output behavior of the DRNL filter is determined by the interaction of the linear and the nonlinear path. The resulting knee point and compression exponent are therefore not solely defined by the broken-stick nonlinearity. The linear path has more dominance when the linear gain, g, is increased, leading to a linear response at high input levels. Parameters a and b in the broken-stick nonlinearity (Eq. 4.1) can be adjusted to fit the target knee point. The relation between the values of a and b determines the level at which the transition from linear to compressive processing (the knee point) occurs. By decreasing a, the low-level linear part will be extended, thus shifting the knee point towards higher levels. A decrease of b extends the compressive region towards lower levels, thus shifting the knee point towards lower levels. Parameter c is the compression exponent and will resemble the effective compression of the complete input-output function where the term $b|x[i]|^c$ in Eq. 4.1 is smallest. The interaction between a, b, c and g determines the resulting compression exponent of the complete DRNL I/O function.

In the present study, these four parameters were adjusted to fit the BM I/O functions of the individual listeners. This was done manually. The first step was to adjust a and b in parallel according to the estimated knee, or to the lowest measurable point in the TMC data. The DRNL I/O function was assumed to be linear for levels below this level or the knee point. It was further assumed that the compression exponent (parameter c) of the fitted DRNL I/O functions cannot be below that of the DRNL I/O functions simulating normal hearing. Parameter c was only in few cases adjusted, since the adjusted a and b already influenced the effective compression in the compressive region. Finally, parameter g was adjusted such that the extent of the compressive region was matching the estimated I/O function. The DRNL I/O function was assumed to be linear for levels below the lowest measurable point in the TMC data. It was further assumed that the compression exponent (parameter c) of the fitted DRNL I/O functions cannot be below that of the DRNL I/O functions simulating normal hearing. The parameters were determined at 1 and 4 kHz. For other filter center frequencies (from 0.05 to 10 kHz in 25 Hz steps), the corresponding

parameters were obtained using a linear interpolation and extrapolation procedure. This procedure was the same as the one used in the regression analysis in Lopez-Poveda and Meddis (2001) to derive the DRNL parameters at arbitrary filterbank frequencies. Linear interpolation was performed such that the parameters followed the form $\log_{10}(\text{parameter}) = p_0 + m \cdot \log_{10}(BF)$, where p_0 and m describe the offset and slope of the linear relation, respectively, and BF denotes the filter's center frequency in Hz.

An estimate of OHC loss in terms of sensitivity loss was obtained from the fitted DRNL I/O function. It was assumed that the output magnitude of the "normal" DRNL I/O function for an input level of 0 dB SPL reflects absolute sensitivity of this stage. Figure 4.2 shows the I/O functions of the DRNL model for normal hearing at different frequencies. The filters centered at 250 (open squares) and 500 Hz (open circles) have their knee points shifted towards at higher input levels and their low-level linear parts are extended compared to the functions shown for the higher frequencies. One consequence is that the maximum amount of OHC loss that can be simulated is lower than at higher center frequencies, since the I/O functions for these low-frequency filters reflect less nonlinear gain. Similar frequency-dependent knee points were observed in the pulsation threshold data ofPlack and Oxenham (2000), to which the original version of the human DRNL filterbank was fitted (Lopez-Poveda and Meddis, 2001). The previoulsy proposed animal filterbank (Meddis *et al.*, 2001) also simulated limited compression at low center frequencies based on data of Rhode and Cooper (1996). It is now commonly assumed that on-frequency BM compression is frequency independent (Lopez-Poveda *et al.*, 2003). However, a modification of the DRNL to comply with these findings has been outside the scope of the present study. Table 4.1 shows the frequency-dependent maximum amount of OHC loss as predicted by the DRNL model.

The amount of IHC loss (HL_{IHC}) was estimated as the difference between HL_{TOT} (as measured in the audiogram) and HL_{OHC} (estimated from the fitted DRNL I/O functions). Liberman and Dodds (1984) found that noise-induced damage to the IHCs, mainly causes elevated tuning curves. Here, it was assumed that HLIHC can be simulated as a linear attenuation at the output of the hair-cell transduction stage. Other studies involving simulation of IHC loss use similar and simple forms of attenuation,

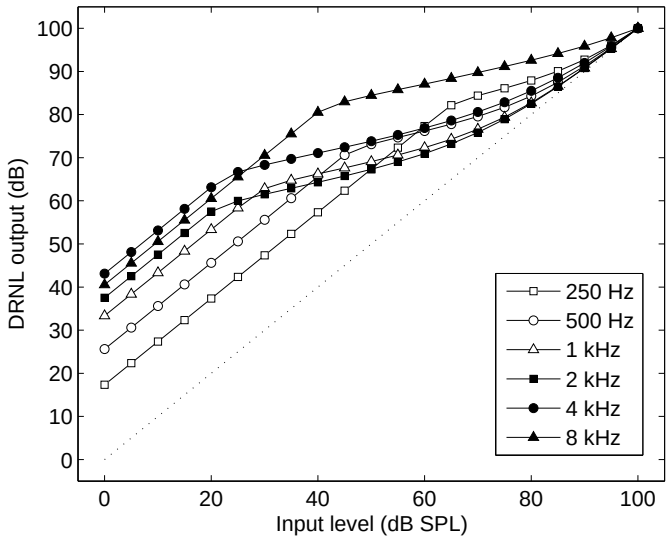

Figure 4.2: DRNL input-output functions at different center frequencies ranging from 0.25 to 8 kHz. The functions are aligned such that an input level of 100 dB SPL produces a model output of 100 dB. The dotted line indicates linear processing.

Center frequency (kHz)	0.25	0.5	1	2	4	8
Max HL_{OHC} (dB)	17	25	34	38	43	45
Knee point (dB)	65	45	30	20	30	40
Compression (dB/dB)	0.35	0.35	0.25	0.25	0.25	0.25

Table 4.1: Maximum HL_{OHC} that can be simulated by the DRNL filterbank at different center frequencies as well as the values for the simulated knee point and compression of the DRNL simulating normal hearing.

although implemented in different ways (e.g., Kates, 1991; Bruce *et al.*, 2003; Zilany and Bruce, 2006). It was assumed that HL_{IHC} can be simulated as a linear attenuation at the output of the hair-cell transduction stage. Linear interpolation was used to obtain attenuation factors for frequencies from 0.05 to 10 kHz with a resolution of 25 Hz. This was done for each individual listener.

4.3 Experimental method

4.3.1 Test subjects

Ten hearing-impaired (HI) and three normal-hearing (NH) listeners participated in this study. All HI listeners had a SNHL indicated by air-bone gaps of less than 10 dB in their pure-tone audiograms. Only one ear of each subject was measured. The measured audiograms of all ten listeners are shown in Fig. 4.3 and indicated as open symbols. Additional information, e.g., listener's age and gender, can be found in Table 4.2 and in Sec. 4.7. The filled symbols indicate simulated thresholds which will be described in section 4.4.2. The listeners consisted of six males and four females, aged between 48 and 73 years. Seven of the ten listeners were using hearing aids regularly. The measurements in this study were carried out without hearing-aid amplification. Two of the HI listeners had previous experience in listening experiments. The three NH listeners (two males and one female, aged between 20 and 27 years) were included as a control group. All had audiometric pure-tone thresholds below 10 dB HL. One of the NH listeners was the first author who had experience in listening tests. All listeners (except the first author) were paid for their participation. Measurement sessions were between 30 to 45 minutes long depending on the listener's self-reported ability to focus on the task. No appointment lasted for longer than two hours. The amount of training depended on the experiment. Training was performed until no systematic improvements in thresholds were observed. The TMC experiment was the most demanding task and required two to four hours of training to reach stable results. In all measurements except the audiogram, the subjects completed at least three runs per condition. The total testing time for each subject, including training, was 14 to 20 hours.

4.3.2 Apparatus and procedure

The pure-tone audiograms were measured manually with a PC-based clinical setting, using the Interacoustics Affinity and Sennheiser HDA200 headphones. The same system was used to perform the bone-conduction measurements. All other measurements were carried out in a double-walled sound insulated booth with a computer monitor

to provide instructions and visual feedback. The computer keyboard was used to obtain the responses. The stimuli were presented monaurally via Sennheiser HD580 headphones. They were generated in MATLAB on a personal computer and converted to analogue signals by a 24-bit soundcard (RME DIGI 96/8). The notched-noise masking stimuli were generated at a sampling rate of 48 kHz. In the other experiments, the sampling rate was at 44.1 kHz. FIR equalization filters were applied to obtain a flat frequency response at the headphone output. A three-interval three-alternative forced choice paradigm combined with a 1-up-2-down tracking rule was used, except for the TMC experiment where a 2-up-1-down rule was applied. The reported thresholds thus reflect the 70.7% point on the psychometric function and represent the mean of at least three measurements. The step size was varied adaptively and thresholds represent an average of the levels at the last eight reversals at the final step size. The listeners received immediate feedback on whether a response was correct or not.

4.3.3 Stimuli

Temporal masking curves (TMC)

In the TMC experiment, forward masking of a fixed-level brief tone was measured as a function of the signal-masker interval. The probe signal was a pure tone with a duration of 20 ms, which was Hanning windowed over its entire duration. The frequency (f_{sig}) was either 1 or 4 kHz. The signal was presented at 10 dB sensation level (SL). The masker was also a pure tone with a duration of 200 ms and 5-ms raised-cosine on- and off ramps were applied. The masker frequency (f_m) was equal to f_{sig} (on-frequency condition) or $0.6 \cdot f_{sig}$ (off-frequency condition). The masker-signal interval was 2, 5, 10 ms and additional 10-ms increments until the subject reported (in pilot runs) that the masker level became uncomfortably loud, or reached the maximum level of 102 dB SPL. The masker level was adjusted to reach masked signal threshold. The initial step size was 8 dB and the final step size was 1 dB.

Notched-noise masking

In order to estimate the shape and bandwidth of the auditory filters, the notched-noise masking method was used (Patterson and Nimmo-Smith, 1980; Patterson and Moore,

1986). The signal was a pure tone at frequency f_0 (1 or 4 kHz) with a duration of 440 ms. Maskers were generated as band-limited Gaussian noise and had a duration of 550 ms. Both signal and masker were gated with 50-ms raised-cosine ramps. The outside edges of the noise were fixed at $\pm 0.8 \cdot f_0$. Five symmetric (δf / f_0 : 0.0; 0.1; 0.2; 0.3; 0.4) and two asymmetric notch conditions (δf / f_0: 0.2|0.4; 0.4|0.2) were tested, where δf was the spacing between the inner noise edges and f_0. The constant signal paradigm was used, i.e., the signal level was kept constant while the masker level was varied.. For the NH listeners, the signal level was 40 dB SPL. For the HI listeners, the signal level was at least 50 dB SPL, and the specific levels used for the individuals (given in Table 4.2) were typically between 15 and 25 dB SL and were based on pilot runs of the experiment, such that the signal was clearly audible and data could be obtained for the widest notch conditions.

Simultaneous- and forward masking with noise maskers

In order to measure temporal processing, the transition from simultaneous to forward masking was measured using a noise masker as in Glasberg *et al.* (1987). The same short signal as in the TMC experiment was used. The masker had a duration of 220 ms. Raised-cosine ramps were applied. The duration of the onset ramp was 10 ms and 5 ms for the offset ramp. The masker was generated as a Gaussian noise and was band-limited to frequencies ranging from 0.75 to 1.25 times the signal frequency. The masker level was fixed at 85 dB SPL. The measured masker-signal intervals were -219, -120, -20, 0, 20 and 60 ms, defined relative to the masker offset. Thus, negative values reflect simultaneous masking while intervals at and above 0 ms reflect forward masking. The initial and final step sizes were 8 dB and 1 dB, respectively.

Intensity discrimination with pure tones

Intensity discrimination was measured to investigate potential individual differences in intensity resolution, which may, at least partly, be associated with cochlear processing. In listeners with SNHL, just noticeable differences (JNDs) in intensity are typically similar as or higher than in NH listeners when the stimuli are presented at the same sensation level. For equal SPL conditions the impaired listeners generally show higher

JNDs. Depending on the shape of the audiogram the JNDs can vary considerably among individual listeners, but a general observation has been that, for listeners with a sloping audiogram, the JND increased strongly (e.g., Florentine *et al.*, 1993). Here, the signal was a pure tone at 1 or 4 kHz. In the signal interval, the level of the tone was higher than in the reference intervals. The difference between the measured threshold and the reference level denoted the JND in intensity. The signal duration was 600 ms and had 125-ms raised cosine ramps. JNDs were measured for reference levels of 60 and 80 dB SPL. In a few cases, where audibility was an issue, the JNDs were measured at 70 and 90 dB SPL. The silent interval between intervals was 500 ms. The initial and final step sizes were 1 and 0.1 dB, respectively.

General simulation parameters

Pure-tone thresholds, off-frequency temporal masking curves, simultaneous and forward masking thresholds, notched-noise masking and intensity discrimination data were predicted using the models that had been fitted to account for the BM I/O functions in the individual listeners. The range of peripheral filters considered in the simulations was chosen to be within $\pm$ one octave from the signal frequency in these experiments. Another model parameter was the level at which the supra-threshold target was presented in the template generation (the detector level). In the audiogram simulations, this level was generally 15 dB above expected threshold. In the intensity discrimination experiment, the detector level was chosen to be 5 dB above the reference level. In the simultaneous- and forward masking experiments, the detector level was fixed at 90 dB SPL. The detector level needs to be above the expected threshold level, otherwise the model has difficulties t derive a "stable" representation of the target signal. For example, if the detector level I s very low, the (normalized) template typically gets a structure which strongly differ from the signal representation at the current signal level.

Listener	NH	HI1	HI2	HI3	HI4	HI5	HI6	HI7	HI8	HI9	HI10
Tested ear: Left/Right		R	L	L	L	L	L	R	R	R	L
Age (years)	21/20/27	67	63	61	73	50	48	62	71	63	51
Gender (Male/Female)	F/M/M	F	M	M	F	M	F	M	M	M	F
Pure-tone thr. 1/4 kHz (dB HL)	0/0	20/45	35/50	30/30	20/35	30/25	40/55	30/60	50/65	10/60	25/50
Probe-signal thr. 1/4 kHz (dB SPL)	12/12	25/36	37/48	29/37	28/32	23/30	43/56	33/60	55/62	21/54	28/53
BM compression, 1 kHz (dB/dB)	0.29	0.30	0.52	0.34	0.13	0.51	0.17	0.84	0.51	0.17	0.63
BM compression, 4 kHz (dB/dB)	0.26	0.29	0.42	0.18	0.29	0.17	-	0.44	0.97	0.43	1.28
I/O knee-point 1/4 kHz (dB SPL)	-/-	-/59	-/-	-/55	-/69	-/-	-/-	51/-	81/-	-/-	-/-
Knee point of fitted DRNL	30/30	40/55	55/65	40/55	30/65	40/55	75/-	50/75	80/-	30/70	35/-
Signal level, NN 1 kHz (dB SPL)	40	50	60	50	50	50	55	50	60	50	60
Signal level, NN 4 kHz (dB SPL)	40	60	65	50	50	50	-	-	75	-	75
ERB of 1 kHz roex filter	155	156	220	206	143	162	153	210	365	142	166
ERB of 4 kHz roex filter	494[a]	840	541	714	472	384	-	-	2232	-	-
Intensity JND, 1 kHz 60/80 dB ref.	1.4/1.1	2.0/2.1	3.1/2.6	2.0/1.4	2.8/1.4	2.7/1.5	5.0/5.3	2.3/1.4	-/1.8[b]	3.1/3.1	4.1/3.1
Intensity JND, 4 kHz 60/80 dB ref.	1.4/0.9	-/1.7	2.8/1.7[b]	3.1/1.2	3.0/2.8	3.5/1.1	7.3/7.3[b]	2.2/1.8[b]	-/1.7[b]	-/2.1	3.4/1.7[b]

Table 4.2: Detailed information about listeners and results of audiogram, estimated BM compression, knee point, as well as results from the notched-noise (NN) and intensity discrimination (JND) experiments. NH refers to the average NH listener. (a): Average of NH1 and NH3. (b): The reference level was increased by 10 dB.

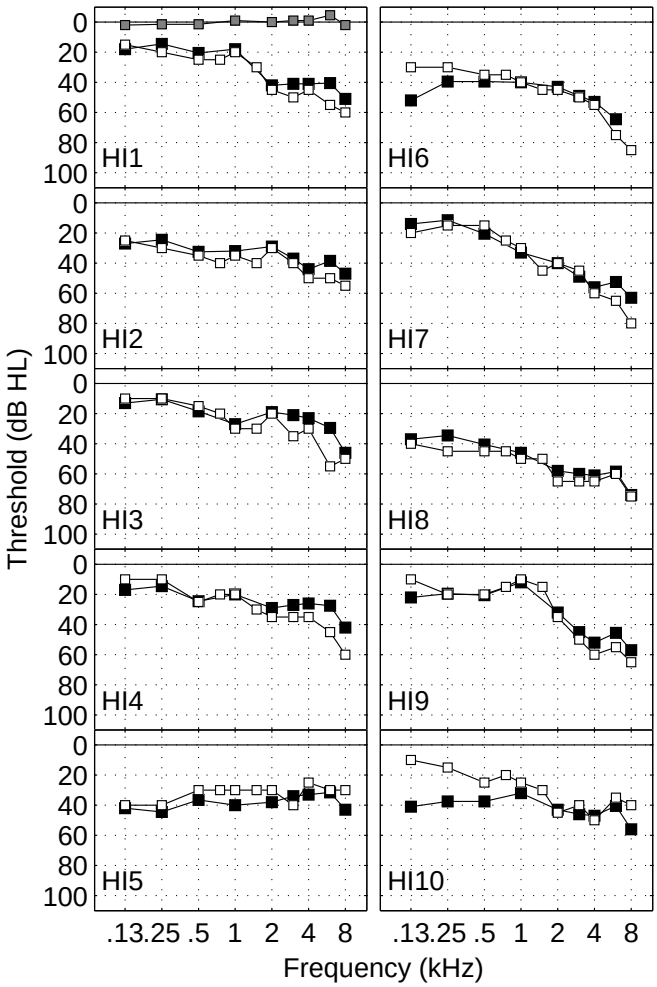

Figure 4.3: The open symbols indicate pure-tone thresholds in dB hearing level (HL) for the different hearing-impaired listeners. Listeners in the left column (HI1 to HI5) had mild-to-moderate losses while the right column indicates listeners (HI6 to HI10) with severe high-frequency losses. The black filled symbols show the corresponding simulated thresholds using the CASP model fitted to the individual listeners. The gray filled symbols in the upper left panel show the simulated thresholds obtained with the CASP model for normal hearing.

4.4 Results

4.4.1 BM input-output functions

Temporal masking curves

The results from the TMC experiment are shown in Fig. 4.4. The first two columns show the results for 1 kHz. The third and fourth columns show the results for 4 kHz. The circles represent the measured data obtained in the on-frequency masking condition. The open squares show the corresponding data obtained in the off-frequency condition. The horizontal dashed lines indicate the signal thresholds without any masker. The error bars, indicating $\pm$ one standard deviation, are typically smaller than the data symbol. The results for the NH listeners are shown in the two top panels. The other panels represent the results for the individual hearing-impaired listeners HI1 to HI10.

Generally, the off-frequency TMC thresholds (squares) lie above the on-frequency thresholds (circles) since an off-frequency masker produces less masking than an on-frequency masker at the signal frequency. The off-frequency TMCs typically have a constant slope whereas the on-frequency TMCs often show a change in the slope with changing masker-signal interval. In some listeners (e.g., HI1, HI4, HI6, HI9 at 1 kHz), the on-frequency TMC has a steeper slope than the off-frequency TMC. This is consistent with previous studies (Nelson *et al.*, 2001; Nelson and Schroder, 2004) and indicates BM compression. For some listeners (e.g., HI1 and HI4 at 1 kHz), the off-frequency TMC converges with the on-frequency curve. For other listeners (e.g. HI7, HI8 and HI9), no thresholds could be obtained for the largest masker-signal intervals since the masker levels became uncomfortably loud or exceeded the maximal presentation level allowed (102 dB SPL). No data were obtained for HI6 at 4 kHz because the shortest masker-signal interval already required uncomfortably loud maskers.

In a few cases (e.g., HI1, HI3 and HI5 at 4 kHz), the on-frequency masker produced higher thresholds than the off-frequency masker. This was also observed in earlier studies with impaired listeners (e.g., Moore *et al.*, 1999; Nelson and Schroder, 2004) and was explained by possible level differences originating from the

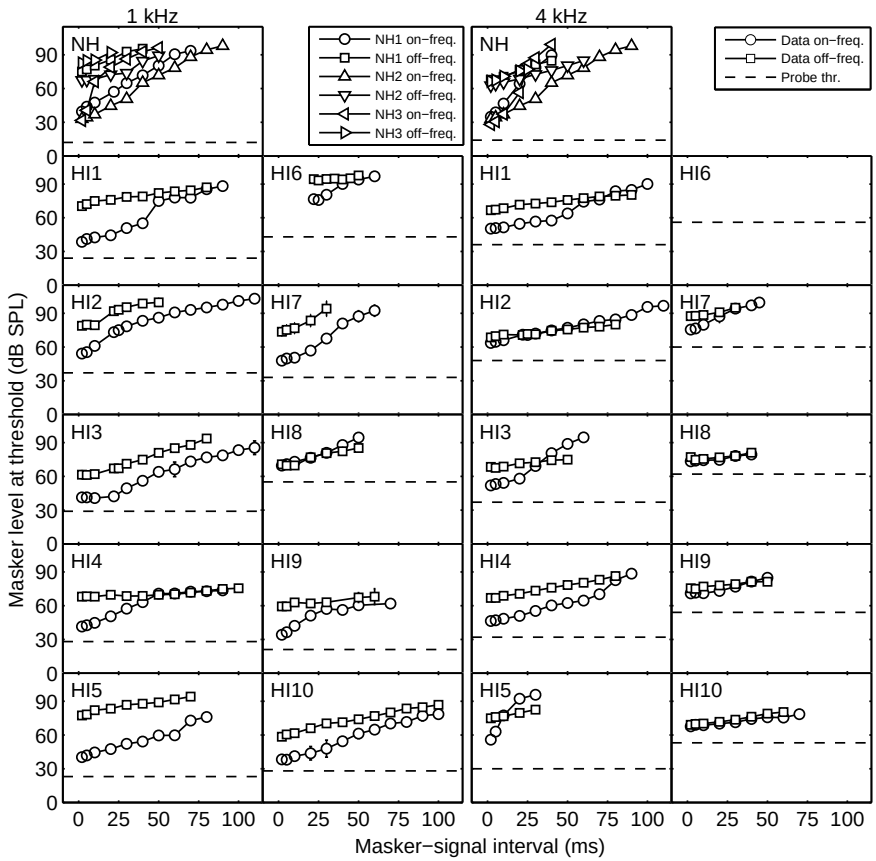

Figure 4.4: Results from the TMC experiment for the HI listeners and one NH listener (top panels). The first two columns show the results for the signal frequency at 1 kHz. The third and fourth columns show the corresponding results at 4 kHz. The circles and squares represent thresholds in the on- and off-frequency masking conditions, respectively. Error bars of one standard deviation are generally smaller than the symbol size. The horizontal dashed lines show the absolute threshold of the probe signal for each listener.

headphones. This explanation can be excluded here since equalized headphones were used and the effect was not generally observed in the data. In a sloping SNHL, OHC damage has presumably mostly affected the cochlear sites at high frequencies. If the OHC gain at the off-frequency masker frequency is closer to normal than at the on-frequency site, it is likely that the off-frequency masker produces more masking at the signal frequency than the on-frequency masker. In these cases, the off-frequency data were shifted vertically to compensate for such effects, as indicated by the filled squares in Fig. 4.4. The shift was applied such that the on- and off-frequency TMC converge at long masker-signal intervals. This was done in order to obtain BM I/O functions where an input level of 100 dB produces an output level of 100 dB. However, the shift of the off-frequency data did not affect the level of the knee point and the compression exponent which were the key parameters estimated from the data.

For some listeners, there were several conditions (e.g., HI8, HI9 and HI10 at 4 kHz) where on- and off-frequency masking curves were essentially on top of each other. According to the TMC paradigm, BM compression is absent at that site if the slopes of the two curves are the same. The slopes of the TMCs produced by the off-frequency masker, referred to as off-frequency TMCs, are listed in Tab. 4.3 for the ten HI listeners together with the mean slope of the three NH listeners. The values of the slopes of the NH listeners, 0.503 and 0.448 (dB/ms) at 1 and 4 kHz, respectively, are consistent with earlier findings of Rosengard *et al.* (2005), where the corresponding slopes were 0.53 and 0.39. The slopes for the ten HI listeners are generally shallower (mean slope = 0.303 and 0.189 at 1 and 4 kHz, respectively) than those for the NH listeners, except for a few conditions (HI2, HI3 and HI7 at 1 kHz) where they are close to the normal values. Shallower slopes of off-frequency TMCs were also generally observed in the studies of Plack *et al.* (2004); Rosengard *et al.* (2005).

Estimated BM input-output functions

BM input-output functions were derived from the TMC data (in Fig. 4.4) following the procedure suggested by Nelson *et al.* (2001). Figure 4.5 shows two examples of estimated BM I/O functions. The circles indicate the I/O function for HI4 at 4 kHz and the squares show the I/O function obtained for listener NH1. A straight line was in each case fitted to the off-frequency masking data (in Fig. 4.4), which reflects the

masker level at signal threshold as a function of the masker-signal separation. These output levels were then plotted as a function of the input level corresponding to the masker-signal intervals measured with on-frequency masking. The short vertical line close to the abscissa indicates the threshold in quiet for the probe signal for HI4. The dotted line in Fig. 4.5 has a slope of one indicating a linear I/O function. As in Lopez-Poveda *et al.* (2003) and Plack *et al.* (2004), a multi-segment regression fit was used. Here, one-, two- or three-line fits were permitted by the procedure and the number of lines fitted were chosen based on the best least-squares fit to the data.. Three-line fits were required where the data showed a return to linearity at high input levels. The solid gray curves in Fig. 4.5 show the two-line regression fit to the data of HI4. The intersection indicates the estimate of the knee point.

Figure 4.6 shows the obtained BM I/O functions (circles) for all HI listeners. Estimates of maximum compression and knee points for all test subjects are listed in Table 4.5. In a few cases (HI1, HI3 and HI5 at 4 kHz), the derived I/O function fell below the I/O function indicating linear processing. In these cases, the complete I/O function was shifted horizontally. This shift helped adjusting the DRNL parameters, but did not affect the knee point or compression values. BM compression was found in all listeners with mild-to-moderate loss (HI1 to HI5), both at 1 and 4 kHz. The slopes ranged from 0.13 to 0.64 dB/dB. In about 30% of the conditions, a knee point could be estimated and was in the range from 55 to 69 dB SPL. In the other conditions, it was not possible to obtain data at low levels to estimate the knee point between linear and compressive processing, and linear processing was assumed for levels below the lowest measurable data point. The lowest measurable points on the I/O functions were at 10 - 25 dB above the absolute threshold of the signal. At high input levels, the I/O functions indicated a return to linearity in 50% of the conditions. For seven of the ten I/O functions for the listeners with mild-to-moderate loss in this study, the amount of compression was close to that for the NH listeners. This was also observed in Plack *et al.* (2004). The data in Fig. 4.6 show a remarkable variation of the I/O functions across listeners, indicating the importance of estimating individual BM processing in the HI listeners. For example, HI9 at 1 kHz shows a near-to-normal I/O function, HI6 at 1 kHz and HI7 at 4 kHz show near-to-normal compression but an elevated knee point and HI7, HI8 and HI10 at 1 kHz as well as HI9 at 4 kHz show some residual

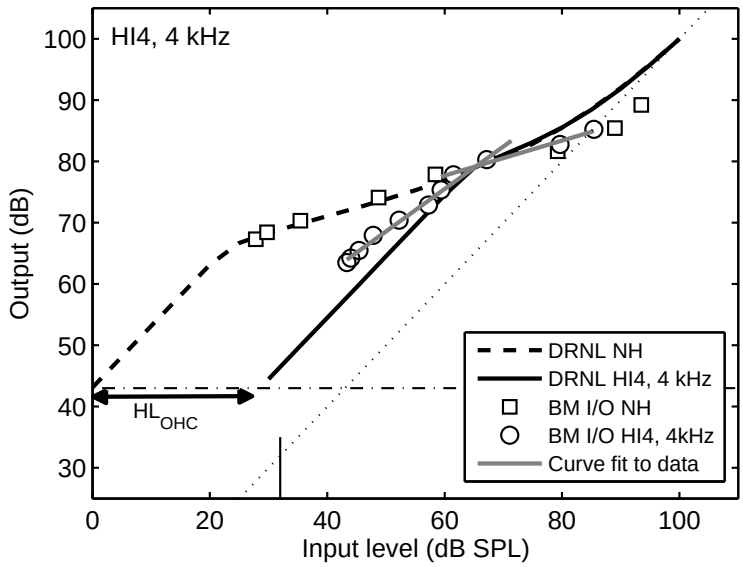

Figure 4.5: Example of measured and simulated BM I/O functions. The squares and circles indicate the measured I/O function for the listeners NH1 and HI4 at 4 kHz, respectively, derived from the TMC data. The two gray straight lines represent linear fits to the HI4 data. The dashed curve shows the simulated I/O function for the corresponding DRNL filter for NH. The black solid curve indicates the simulated DRNL I/O function adjusted to fit the data of HI4 at 4 kHz. The horizontal dash-dotted line indicates the output level of the model in response to a 0 dB SPL input level. The dotted line indicates a linear I/O function. The vertical black represents HI4's absolute threshold for the forward masking signal at 4 kHz. The double arrow indicates the estimated loss of sensitivity due to OHC loss ($\mathrm{HL_{OHC}}$).

compression which is smaller than that observed in the NH listeners. HI8 and HI10 at 4 kHz show no compression. A similar variation in the individual patterns was found in Nelson *et al.* (2001) and Stainsby and Moore (2006). Thus, the general observation was that I/O functions can be very different across listeners even though their audiograms are relatively similar.

Simulated BM input-output functions

The thin dashed-dotted horizontal line in Fig. 4.5 represents the output level of the model for a 0 dB SPL input level. The dashed curve shows the DRNL model's I/O

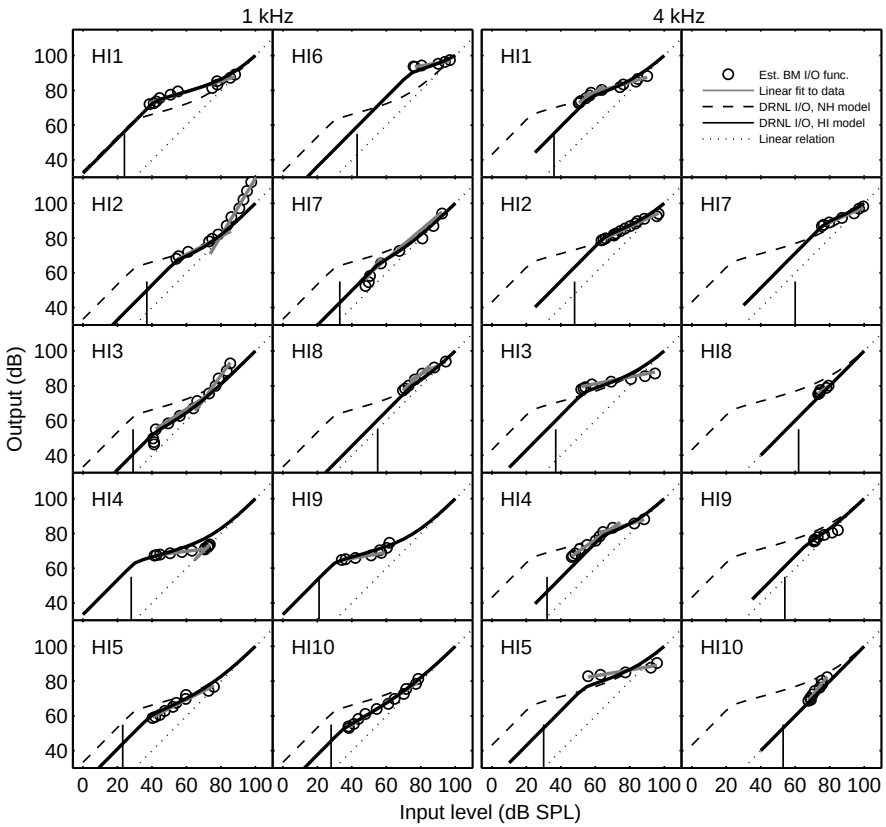

Figure 4.6: Derived BM I/O functions for the HI listeners and their corresponding DRNL I/O functions. The first two columns show the results for the 1 kHz signal. The third and fourth columns show the corresponding results at 4 kHz. The circles indicate the estimated BM I/O functions, derived from the data. They gray lines indicate straight-line fits to the data. The black solid curves indicate the DRNL I/O function fitted to the data. The dashed curve represent the I/O function of the DRNL simulating normal hearing. The dotted line indicate a linear relation and the vertical line indicate the absolute threshold of the signal in the TMC experiment.

function for normal hearing at the corresponding signal frequency (4 kHz). A set of DRNL parameters (a, b, c and g) was determined, such that the DRNL I/O function

fitted the BM I/O data. The solid black curve represents the DRNL I/O function fitted to listener HI4. The same method was used to obtain corresponding parameter sets for each individual HI listener. The values for the adjusted DRNL parameters are listed in Tab. 4.4. For listeners HI2, HI4 and HI9, the estimated BM I/O functions were close to normal. The solid black curves in Fig. 4.6 show the fitted DRNL I/O functions for the individual listeners at 1 and 4 kHz. In few cases where the measured I/O functions indicated return to linearity (e.g., HI4 at 4 kHz in Fig. 4.5), the DRNL I/O functions could not be fitted exactly to the measured functions, due to the way the DRNL parameters interact. In these cases, output levels produced by high input levels (above 70 dB SPL) might be slightly higher than the corresponding measured output levels.If a near-to-normal I/O function at 1 kHz was observed in a listener, then the DRNL parameters for the filters below 1 kHz were not changed relative to those for normal hearing, assuming normal BM behavior at low frequencies. This was done for listeners with a flat hearing loss below 1 kHz, HI2 HI4 and HI9. Other listeners with a flat low frequency loss (e.g., HI1 and HI3) did not show near-to-normal BM I/O functions, such that their parameters for the low-frequency DRNL filters were changed accordingly.

Measured and simulated off-frequency TMCs

The slopes of the off-frequency TMCs were calculated from the data in Fig. 4.4 and listed in Tab. 4.3. Furthermore, off-frequency TMCs were simulated using the models of the individual listeners (not shown explicitly), and the slopes of the simulated TMCs were calculated and listed in Tab. 4.3. The TMCs were qualitatively accounted for in the sense that if compression was simulated for a particular listener, then the slopes of the on- and off-frequency TMC were different. However, the simulated on-frequency TMC only rarely represented a good quantitative account, since the masker-signal interval at which the steepness of the TMC changed was not matched. Predictions of the slopes of the off-frequency TMCs is interesting since it may help understanding the observed shallower slopes in HI listeners in this and earlier studies. The slopes produced by the model of normal hearing were comparable to the measured slopes at 1 kHz, while it was slightly shallower at 4 kHz. Shallower slopes at higher frequencies was observed in Lopez-Poveda *et al.* (2003), but not in the present study.

The predicted slopes for the HI listeners were generally shallower than for the NH model, and this effect is broadly consistent with the results of several studies using the TMC method in HI listeners (e.g., Plack *et al.*, 2004; Lopez-Poveda *et al.*, 2005; Rosengard *et al.*, 2005).

4.4.2 Predicted pure-tone audiograms

The sensitivity loss due to OHC loss (HL_{OHC}) was estimated on the basis of derived DRNL I/O functions at 0.25, 0.5, 1, 2, 4 and 8 kHz. The values of HL_{OHC} for the individual listeners at 1 and 4 kHz, and the interpolated range of HL_{OHC} across all frequencies are listed in Table 4.5. HL_{OHC} ranged from 0 dB, where the data indicate normal I/O behavior, up to 46 dB (depending on the frequency) where the data indicate a complete loss of compression. As expected, the largest HL_{OHC}-values were found in the listeners in which no compression was observed (HI8 and HI10) at the higher frequencies. The IHC loss component (HL_{IHC}) was assumed to represent the difference between the total sensitivity loss reflected in the audiogram (HL_{TOT}) and the estimated sensitivity loss due to outer hair-cell loss, i.e., $HL_{IHC} = HL_{TOT} - HL_{OHC}$. The values of HL_{IHC} for each listener at 1 and 4 kHz as well as the range of the interpolated values across all frequencies are listed in Table 4.5. The individual HL_{IHC} estimates are in the range from 0 to 40 dB and are similar across frequencies.

Predicted pure-tone thresholds are shown by the black symbols in Fig. 4.3. The quantitative estimates of the thresholds as well as the curve shapes are predicted well, and deviations are within 10 dB with a few exceptions. This was expected since the audiogram data were used to estimate HL_{IHC} for frequencies from 0.25 to 8 kHz. The results show that the simulated HL_{OHC} and HL_{IHC} in the cochlear stage have the desired effect on the actual threshold prediction obtained with the overall perception model (CASP).

4.4.3 Relation between pure-tone threshold and estimates of compression, HL_{OHC} and HL_{IHC}

Figure 4.7 shows the relation between the measured audiometric threshold and the different quantities derived in the present study, namely BM compression, HL_{OHC},

HL_{IHC}. The calculated correlations also include the individual data for the NH listeners. Panel A shows that there is a clear correlation between pure-tone threshold and HL_{OHC} ($r = 0.927$, $n = 26$, $p < 0.001$) indicating that higher loss of sensitivity is associated with higher OHC loss. Panel B shows that there is a weaker, although still significant correlation between the pure-tone threshold and HL_{IHC} ($r = 0.771$, $n = 26$, $p < 0.001$). Panel C shows only a weak correlation between the pure-tone threshold and the estimated compression values ($r = 0.518$, $n = 25$, $p = 0.008$). This means that BM compression cannot be predicted from the measured audiogram. Moore *et al.* (1999) found a similar correlation between threshold and BM compression estimate ($r = 0.56$). The relation between HL_{OHC} and compression, shown in Panel D, was weak but significant ($r = 0.5062$, $n = 25$, $p = 0.010$), where Moore *et al.* (1999) found a stronger correlation between the corresponding measures ($r = 0.68$). The correlation here between HL_{IHC} and compression, as shown in Panel E, was weak ($r = 0.4179$, $n = 25$, $p = 0.038$) but stronger than the corresponding correlation found in Moore *et al.* (1999) ($r = 0.26$, not significant).

4.4.4 Frequency selectivity

Data from the notched-noise masking experiment

Figure 4.8 shows the data from the experiment, indicated by open symbols connected by solid lines. No data could be obtained in the 4-kHz condition for listeners HI6 and HI9, due to uncomfortably loud masker levels. As expected, the masker level generally increases with increasing notch width. However, the rate of increase was different across HI listeners and frequencies.

Predicted notched-noise data

Simulated thresholds are indicated by the filled black symbols in Fig. 4.8, connected by dashed lines. The simulations agree well with the mean data of the NH listeners in the 1-kHz condition. However, in the 4 kHz condition the model overestimates the masker level at particular notch conditions (0.1|0.1, 0.2|0.2, 0.3|0.3), indicating a too narrow tuning within the model. At both frequencies, the asymmetric conditions are fairly well predicted. The models of the HI listeners generally predict acceptable

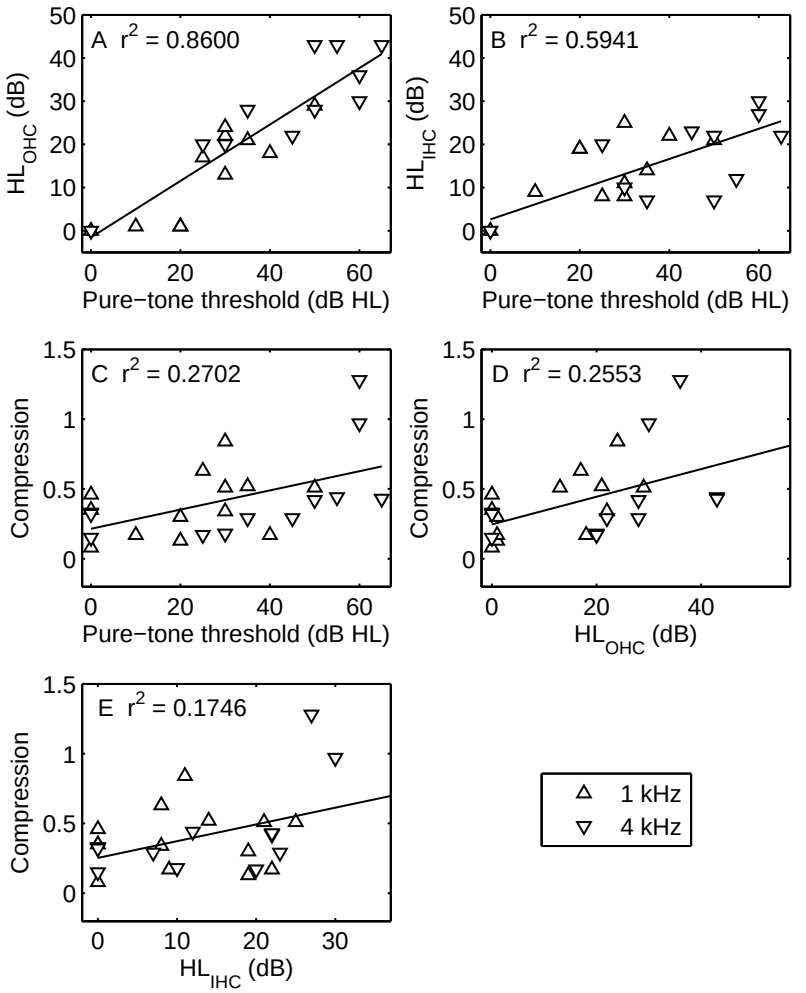

Figure 4.7: The relation between measures of the pure-tone threshold in quiet (from the audiogram), estimated HL_{OHC}, HL_{IHC}, BM compression (in dB/dB). Upward- and downward pointing triangles indicate data and estimates at 1 and 4 kHz, respectively.

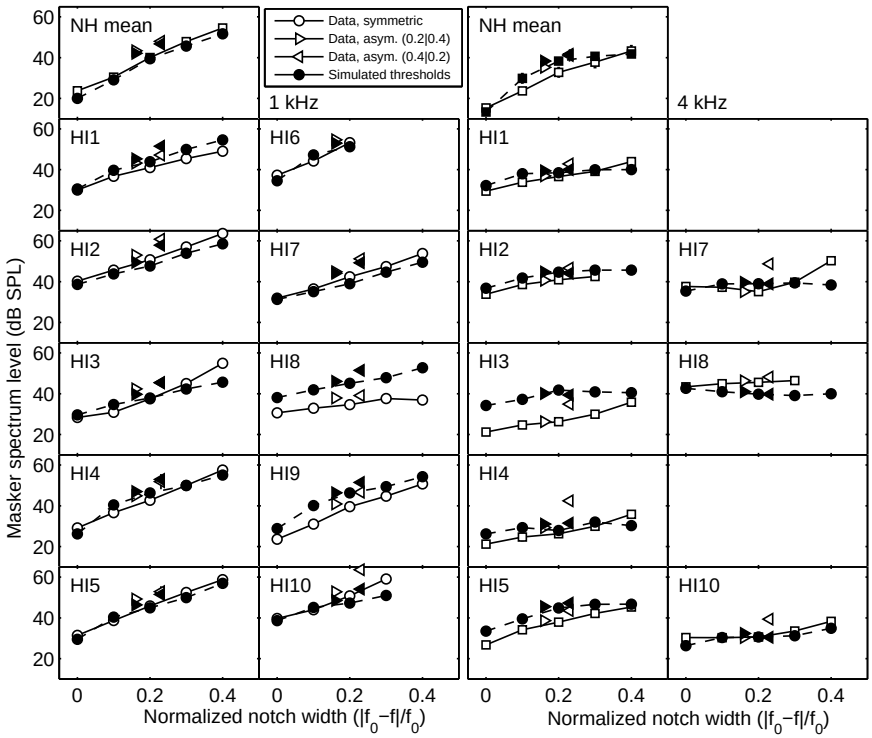

Figure 4.8: Results from the notched-noise masking experiment. The open symbols indicate the measured thresholds. Circles indicate symmetric-notch condition, and triangles represent the asymmetric conditions. The first two columns show the results for the 1 kHz signal. The third and fourth columns show the corresponding results at 4 kHz. The filled symbols indicate the simulated thresholds.

matches to the data at 1 kHz, except for the models simulating listener HI8 and HI9 where the masker level is overestimated. The predictions are generally worse at the 4-kHz conditions, where the predictions in several cases are poor both in terms of the absolute levels and in the slope of the masking functions. Only the model simulating listeners HI1, HI2 and HI10 produced fair matches to the data.

Measured auditory filter shapes

The measured notched-noise masking paradigm was used to estimate the shape and bandwidth of the auditory filters in the individual listeners. The actual masking data are not shown explicitly here. Rounded-exponential (roex) filters were fitted to the masking data, using the paradigm suggested in Rosen *et al.* (1998). The fitted roex filters for each listener are presented in Fig. 4.9 and indicated by the thin curves. The lower left panel shows the roex filters for the three NH listeners. It is important to note that the data were collected using different signal levels (see Table 4.2); the filter bandwidth might therefore not be directly comparable across listeners. There were not enough data available at 4 kHz to obtain reliable roex filter estimates for listeners HI6, HI7, HI9 and HI10, since the maskers at the widest notch condition became uncomfortably loud or exceeded 102 dB SPL. The equivalent rectangular bandwidths (ERBs) of the fitted filters were calculated and are listed in Table 4.2.

Simulated filter shapes based on individual BM I/O functions

Figure 4.9 also shows DRNL iso-intensity response curves for the filters (thick solid curves) using the same parameters as determined above to account for the individual BM I/O functions. This was done in order to evaluate how well the corresponding DRNL filters actually match the estimated auditory filters derived from the "independent" notched-noise masking experiment. A quantitative comparison was made in terms of the difference between the -10-dB bandwidths in percent. These are listed in Table 4.6. Here, DRNL filter tuning was considered to be a fair match if this difference was less than 20%. Roex and DRNL filters matched well for the three NH listeners, except for one listener at 4 kHz. For the majority (8 out of 10) of the 1-kHz filters, the roex- and fitted DRNL filters agree well, especially with respect to the bandwidth at the filter's tip. It appears that the DRNL filters are generally too sharply tuned at 4 kHz compared to the roex filters for the listeners HI1 to HI5. The measured asymmetry of the filters were, overall, not well captured. It was not possible to obtain -10-dB bandwidths for the roex-filters of listeners HI6 to HI10 at 4 kHz since there were either no data or the filter slope was too shallow on the low-frequency side. Bandwidths of the corresponding DRNL filters were not specified due to the shallow

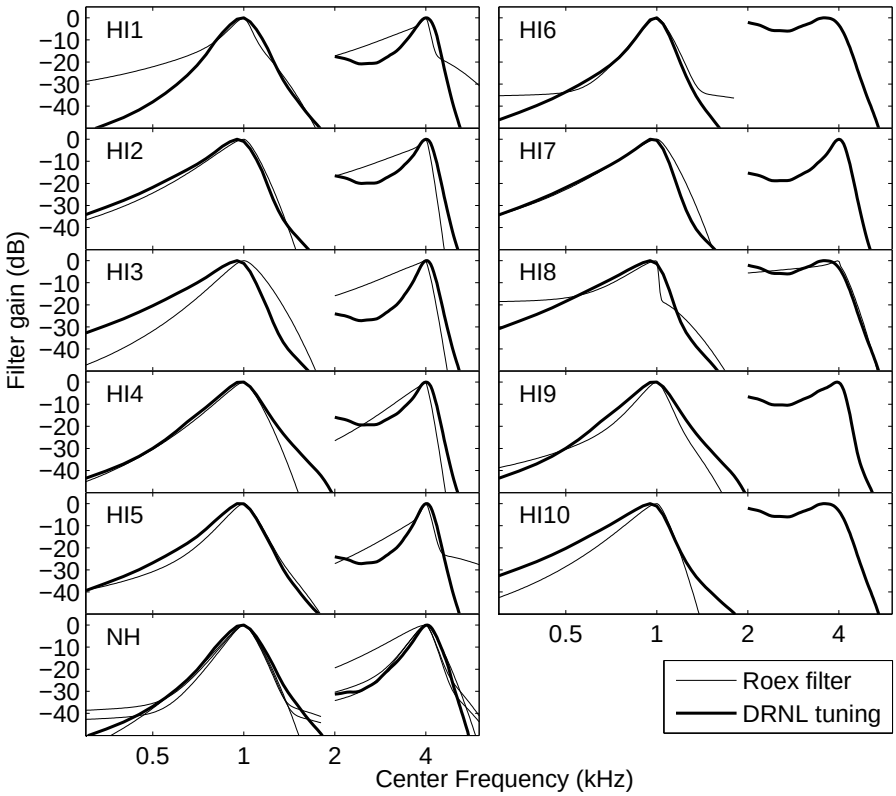

Figure 4.9: Estimated auditory filter shapes for the ten HI and three NH listeners (bottom left panel). The thin curves show roex filters derived from the notched-noise masking data. The thick curves show simulated filter shapes obtained with DRNL filters (iso-intensity response curves) that were earlier fitted to the individual BM I/O functions.

slopes of the low-frequency side. The varying bandwidths of the DRNL filters are directly resulting from the differences in compression. These results indicate that individual BM tuning at 1 kHz was estimated reasonably well by the DRNL filters fitted to the individuals. An example, where listeners with equal sensitivity show a different amount of tuning can be seen in the data of HI1 and HI4 at 1 kHz. The

pure-tone thresholds of the two listeners was 20 dB HL and the -10-dB bandwidths of the roex filter were 290 Hz for HI1 and 330 Hz for HI4. The -10-dB bandwidths of the simulated filters were 350 and 390 Hz, correspondingly. In both conditions the simulated tuning was slightly broader than the estimated tuning (17 and 15%, respectively). Another example shows that higher HL_{OHC} leads to broader simulated filters. HI1 and HI3 had estimated HL_{OHC} of 1 and 22 dB, respectively. The simulated tuning was based on the same signal (50 dB SPL) and was 350 and 390 Hz for the same two listeners, respectively.

The relation between ERB, BM compression, HL_{OHC} and HL_{IHC}

Figure 4.10 shows the relationships between the derived ERBs and the four quantities: absolute threshold, compression, HL_{OHC} and HL_{IHC}. Panel A shows a weak correlation between absolute threshold and the ERB given as the proportion of the corresponding center frequency (r = 0.5812, n = 19, p = 0.005). Moore *et al.* (1999) found a correlation of r = 0.58 for condition where the absolute threshold was higher than 25 dB HL. Panel B shows the relation between the HL_{OHC} and the ERB with a weak correlation (r = 0.592, n = 19, p = 0.004). For the corresponding measures, Moore *et al.* (1999) found a correlation of r = 0.75. Relating BM compression and ERB in Panel C reveals a correlation of r = 0.662 (n = 19, p = 0.008). The corresponding data in Moore *et al.* (1999) showed a strong correlation of r = 0.92. In Panel D the relation between HL_{IHC} and the ERB is shown. Here, there is a weak correlation, but this was not significant (r = 0.3076, n = 19, p = 0.164). Moore et al. found also a weak correlation of r = 0.38.

4.4.5 Simultaneous- and forward masking

The data from the simultaneous and forward masking experiment are shown in Fig. 4.11. The first two columns show results for the signal frequency at 1 kHz. The third and fourth columns show the corresponding results at 4 kHz. The measured data are indicated by the open squares whereby error bars indicate one standard deviation. The dashed horizontal lines indicate the absolute threshold for the signal when presented in quiet. The results obtained by NH3 (top panels) and the HI listeners

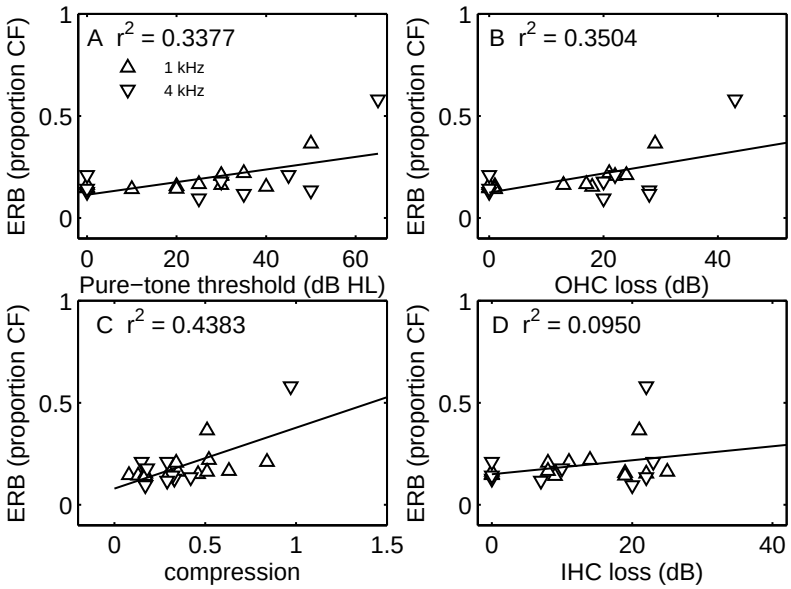

Figure 4.10: The relation between the estimated ERB, given as a proportion of the CF, and measured pure-tone threshold, as well as derived measures HL_{OHC}, HL_{IHC} and BM compression Upward- and downward pointing triangles indicate data and estimates at 1 and 4 kHz, respectively.

are in good agreement with the results of Glasberg *et al.* (1987). The forward masking conditions, indicated by the masker-signal intervals 0, 20 and 60 ms, show a decay of thresholds with increasing masker-signal interval. The rate of recovery from forward masking is slower than normal in cases where the absolute signal threshold is higher. This is also in line with the results of Glasberg *et al.* (1987).

The model predictions are indicated by the filled symbols. To quantify the match between data and predictions, a goodness-of-fit was defined as their *rms* difference. The results are provided in Table 4.6. Predictions were considered to be good matches if this measure was below 8 dB, averaged across the six masker-signal intervals. The model of normal hearing describes the masking data reasonably well at both frequencies. This was expected since the experimental conditions considered here were similar to the forward masking conditions in Jepsen *et al.* (2008) using the

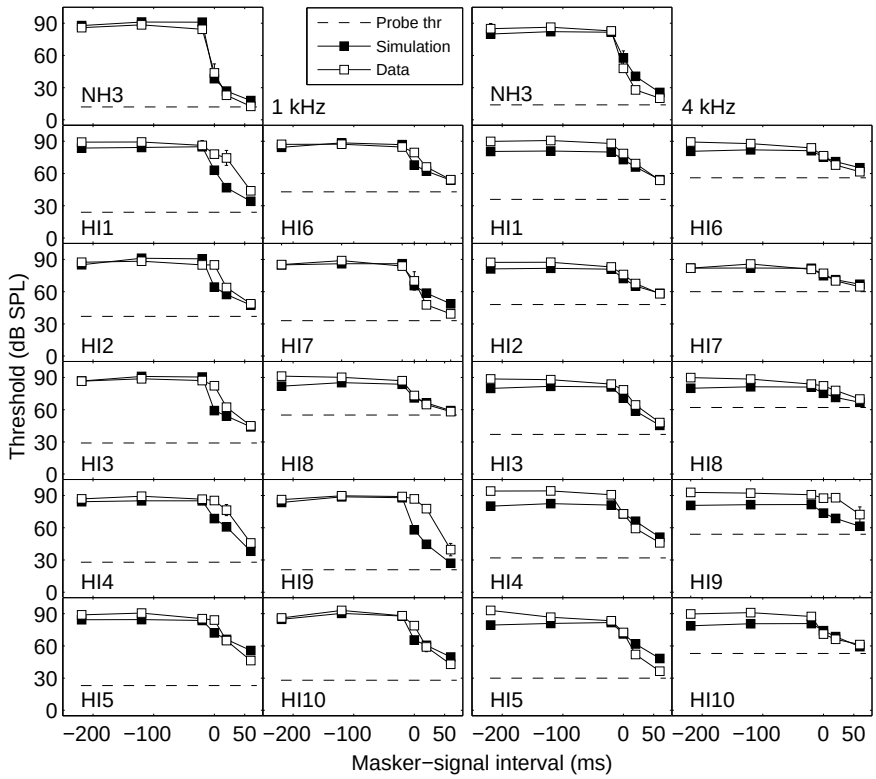

Figure 4.11: Measured (open symbols) and simulated (filled symbols) simultaneous- and forward masking thresholds. The two left columns show results for the 1-kHz signal. The two right columns show the corresponding results at 4 kHz. Negative masker-signal intervals (-219, -120 and -20 ms) indicate simultaneous masking conditions and positive intervals (0, 20 and 60 ms) reflect forward masking conditions. The dashed horizontal lines indicate the absolute threshold for the signal.

same model. For the HI listeners, the predicted simultaneous and forward masking thresholds were predicted within this limit for 16 of the 20 experimental conditions. For the remaining four conditions (HI1, HI4, HI9 at 1 kHz and HI9 at 4 kHz), the

predicted thresholds underestimate the measured thresholds by up to 33 dB. In terms of forward masking at 1 kHz the model predicts a too fast decay in five of the ten cases, and for HI7 at 1 kHz the predicted rate of decay is too shallow. At 4 kHz, the forward-masked thresholds are fairly well predicted, except for listener HI9. In the simultaneous masking conditions at 4 kHz, the model underestimated the thresholds in most cases, while for 1 kHz the predictions were fairly good.

4.4.6 Intensity discrimination

The results from the intensity discrimination experiment are presented in Table 4.2. For the NH listeners, the mean just noticeable differences (JND) in intensity at 1 kHz. were 1.4 and 1.1 dB at reference intensities of 60 and 80 dB SPL, respectively. At 4 kHz, the corresponding JNDs were 1.4 and 0.9 dB. These values are slightly higher than those of Florentine *et al.* (1993) in terms of equal SPL. For subjects HI2, HI6, HI7, HI8 and HI10, JNDs could not be measured at 60 dB SPL. Therefore, a 10 dB higher reference level was used here. The JNDs were generally higher for the HI listeners than for the NH listeners and were typically in the range from 1 to 3 dB, consistent with the findings of Florentine *et al.* (1993). HI6 had untypically high JNDs at both frequencies and levels (5.0 to 7.3 dB) where audibility cannot have been a limiting factor.

The simulated intensity JNDs are not reported individually, since they were roughly constant and deviated by less than 0.2 dB from the value simulated for normal hearing. Thus, within the model, the simulated JNDs were not affected by the simulated cochlear hearing loss. The higher JNDs observed in the data of some of the HI listeners could thus not be accounted for. A better fit could, in principle, be realized by increasing the variance of the internal noise in the model accordingly, but such an attempt was not undertaken in this study since it would imply a "central" source of hearing impairment which was outside the focus here, as discussed further below.

	NH mean	HI1	HI2	HI3	HI4	HI5	HI6	HI7	HI8	HI9	HI10	HI mean
Measured slope												
1 kHz	0.503	0.194	0.501	0.431	0.073	0.230	0.103	0.719	0.347	0.146	0.288	0.303
4 kHz	0.448	0.159	0.142	0.158	0.247	0.269	-	0.263	0.126	0.136	0.200	0.189
Predicted slope	NH											
1 kHz	0.426	0.272	0.312	0.114	0.279	0.200	0.198	0.284	0.235	0.326	0.271	0.249
4 kHz	0.312	0.178	0.281	0.293	0.278	.264	-	0.293	0.266	0.275	0.275	0.267

Table 4.3: Measured and predicted values of the slopes of the off-frequency TMCs in units of (dB/ms). The NH mean represent the mean of the three NH subjects. The dashes indicate that no TMC data were obtained for HI6 at 4 kHz.

Listener	NH	HI1	HI2	HI3	HI4	HI5	HI6	HI7	HI8	HI9	HI10
1 kHz											
a	7250	7250	600	500	7250	1200	1000	400	200	7250	600
b	0.15	0.4	0.1	0.2	0.15	0.4	0.9	0.4	0.2	0.15	0.6
c	0.25	0.25	0.25	0.40	0.25	0.40	0.25	0.40	0.25	0.25	0.50
g	585	585	585	585	585	400	300	585	600	585	300
4 kHz											
a	1500	1500	800	3000	1500	3000	0	500	0	300	0
b	0.06	0.1	0.12	0.15	0.06	0.15	-	0.2	-	0.05	-
c	0.25	0.25	0.25	0.25	0.25	0.25	-	0.25	-	0.25	-
g	300	500	400	600	1000	600	300	300	300	700	300
NH values < 1 kHz		-	+	-	+	-	-	-	-	+	-

Table 4.4: DRNL parameters that were adjusted to account for the BM I/O behavior of the individual listeners. The dashes indicate conditions were the parameter value was irrelevant due to zero contribution of the nonlinear path. In the bottom row (NH values) the (+) indicates that the parameter-values for DRNL filters below 1 kHz were not modified, since it was assumed that BM processing at these low frequencies was normal.

HL_{OHC}	HI1	HI2	HI3	HI4	HI5	HI6	HI7	HI8	HI9	HI10
0.25 kHz	16	14	10	10	1	4	15	17	13	0
0.5 kHz	11	22	7	8	10	10	15	23	8	8
1.0 kHz	1	21	22	1	13	18	24	29	1	17
2.0 kHz	11	28	10	15	15	38	25	38	18	38
4.0 kHz	22	28	20	28	20	43	30	43	36	43
8.0 kHz	37	43	25	46	20	46	46	46	46	40
HL_{IHC}	HI1	HI2	HI3	HI4	HI5	HI6	HI7	HI8	HI9	HI10
0.25 kHz	4	16	0	0	39	26	0	28	7	15
0.5 kHz	14	13	8	17	20	25	0	22	12	17
1.0 kHz	19	14	8	19	17	22	6	21	9	8
2.0 kHz	34	2	10	20	15	7	15	27	17	7
4.0 kHz	23	22	10	7	5	12	30	22	24	7
8.0 kHz	23	12	25	14	10	39	34	29	19	0

Table 4.5: Values of HL_{OHC} and HL_{IHC} at different frequencies derived from the models fitted to the individual listeners.

Listener	NH	HI1	HI2	HI3	HI4	HI5	HI6	HI7	HI8	HI9	HI10
−10-dB BW, roex, 1kHz (Hz)	300	290	380	410	330	320	300	410	300	280	330
−10-dB BW, DRNL, 1kHz (Hz)	350	350	380	390	390	370	270	360	410	380	400
Difference, 1 kHz (in %)	14	17	0	-5	15	14	-11	-14	28	26	18
−10-dB BW, roex, 4kHz (Hz)	940	1330	1380	1550	1520	790	-	-	-	-	-
−10-dB BW, DRNL, 4kHz (Hz)	990	940	850	730	850	740	-	-	-	-	-
Difference, 4 kHz (in %)	5	-42	-62	-112	-78	7	-	-	-	-	-
SFM rms diff., 1 kHz (dB)	4.2	10.7	6.5	6.3	8.1	5.7	3.6	4.9	3.7	13.2	4.3
SFM rms diff., 4 kHz (dB)	6.3	6.1	3.4	5.6	7.9	7.3	4.2	1.7	6.0	12.7	5.9

Table 4.6: Results of the model evaluation: -10 dB bandwidths for the roex-filters and DRNL iso-intensity responses and the difference between the bandwidths in percent; and rms difference between measured and simulated thresholds for the simultaneous- and forward masking (SFM) experiment. The dashes indicate conditions were the -10-dB BW could not be obtained. For the BWs a difference below 20% was considered reasonable, while for the SFM experiment rms difference values lower than 8 dB were considered fair matches.

4.5 Discussion

4.5.1 Behavioral estimates of human BM input/output functions

In the present study, the TMC method was used to behaviorally estimate individual BM I/O functions. The results showed a large variability of knee-point position and amount of compression among the HI listeners, even in the cases of similar pure-tone sensitivity at the corresponding frequencies. These findings are consistent with other studies (e.g., Plack *et al.*, 2004; Lopez-Poveda *et al.*, 2005; Rosengard *et al.*, 2005) which also found compression ratios for the HI listeners that ranged between values of 0.15-0.25 dB/dB, as typically found in NH listeners, and values of one (i.e., linear processing), with considerable variation across the individual listeners. The estimated parameters of the I/O functions found in the present study were consistent with the measured frequency selectivity in the same individual listeners, i.e., losses of compression were generally associated with a decreased frequency selectivity and a shallower decay of forward masking curves, which agrees with earlier studies (e.g., Oxenham *et al.*, 1997; Moore *et al.*, 1999). For some of the listeners of the present study, it was not possible to obtain an estimate of the knee-point of the I/O function. In these cases, only an estimate of the amount of compression could be derived from the data and linear processing was assumed below the lowest measurable data point. However, in other listeners and conditions, the knee-point could be estimated and provided valuable additional information thus increasing the confidence in the I/O function estimates. On the basis of the estimated I/O functions, the amount of sensitivity loss due to OHC loss could be estimated in the individual listeners. However, in the conditions were the knee-point estimate could not be obtained the amount of OHC loss may be overestimated. If a knee point existed and was different from the assumed value, then the difference would result in an overestimation of OHC loss by an equal amount in dB. This, in turn, would lead to underestimated IHC loss by the same amount, since this quantity was derived based on the OHC loss estimate. It may be useful to have more robust psychophysical measures of the BM knee point as e.g., suggested in Jepsen and Dau (2008) to overcome the present issue. An earlier suggested method to obtain estimates of HL_{OHC} was using a loudness-model (Moore *et al.*, 1999). In their study, it appeared that the estimated ERB only

increased with increasing HL_{OHC} when HL_{OHC} was above 25 dB. This could reflect that their loudness-based estimate of HLOHC is less reliable at the mild losses. In the present study the listeners generally had less hearing loss than those of the Moore et al. study, and the presented correlation between HLOHC and ERB is compromised, since very few ERB estimates was obtained for the severe losses.

As discussed in related recent studies (e.g., Rosengard *et al.*, 2005; Wojtczak and Oxenham, 2009), the TMC method has several limitations. Rosengard *et al.* (2005) found that the TMC data generally exhibit a larger variability than data obtained with an alternative paradigm also based on forward masking, the growth of masking (GOM) method (Oxenham and Plack, 1997). The GOM method varies the signal level and keeps the masker-signal interval constant, which might provide a more stable cue for the listeners of "when to listen" for the signal. Furthermore, the reliability of the compression estimate has been found to be affected by the choice of the "linear" (off-frequency) reference condition. Rosengard *et al.* (2005) further concluded that the TMC method was less effective, since it was necessary to test a large range of masker-signal intervals to measure in dynamic range of input levels of interest. However, if the original assumption on the off-frequency TMC representing a linear reference (Nelson *et al.*, 2001) is valid, then it is expected that the slope does not change due to reduced or lost BM compression. The related earlier studies (Nelson and Carney, 2004; Plack *et al.*, 2004; Lopez-Poveda *et al.*, 2005; Rosengard *et al.*, 2005; Wojtczak and Oxenham, 2009) discuss the origin of the observed shallower slope of the off-frequency TMC in HI listeners. It could be due to reduced temporal resolution in the HI listeners, since the HI listeners were generally older than the NH listeners in these studies. It would be expected that reduced temporal resolution would affect on- and off-frequency masking by an equal amount. It is more likely that shallower off-frequency TMC are reflecting that the necessary masker levels generally are higher for the HI listeners, and therefore influence sources of forward masking other than BM processing, such as adaptation and therefore lead to different rates of recovery from forward masking. Furthermore, Wojtczak and Oxenham (2009) showed that the recovery from forward masking, with on- versus off-frequency maskers adjusted to produce the same amount of masking at a particular masker-signal interval, was different, especially at high masker levels. This violates the basic assumption of the TMC paradigm which assumes a frequency and

level-independent recovery. As a consequence, compression might be overestimated by the TMC method by a factor of two (Wojtczak and Oxenham, 2009). This would of course have an impact on the results from this study, since an overestimated compression would imply an underestimated amount of OHC loss (derived from the estimated I/O function) and would lead to too narrow tuning of the simulated BM filters (discussed further below). However, also the alternative attempts to estimate BM I/O function have their clear drawbacks and limitations (Wojtczak and Oxenham, 2009). For example, the GOM method does not provide reliable information about the knee-point of the I/O functions, and might be influenced by off-frequency listening due to the varying signal levels, and is also based on the assumption of a frequency independent recovery from forward masking. Thus, the TMC method can still be regarded as a reliable tool to behaviorally estimate BM I/O functions in humans.

The predicted slope of the off-frequency TMC mainly depended on the nonlinear processing of the DRNL and adaptation stage within the model. The match between the slope values at 1 kHz for the model of normal hearing reflects that the interaction between these two can account for tone on tone forward masking which was expected from the results of Jepsen *et al.* (2008). At 4 kHz, the predicted slope for NH was slightly shallower than the data of this study, and consistent with slope estimates of, e.g., Lopez-Poveda *et al.* (2003). The model fitted to the individual HI listeners generally produced a shallower and roughly constant slope of the off-frequency TMC. These shallower slopes are primarily due to the processing of the adaptation stage. The adaptation stage acts in a nonlinear way and higher input levels would lead to a faster recovery of masking (Dau *et al.*, 1996a,b; Jepsen *et al.*, 2008). Faster recovery of masking is expected to produce steeper TMCs. Within the presented model the output of the early stages of the model, prior to the adaptation stage, is reduced due to the simulation of OHC and IHC loss. Consequently, the adaptation stage effectively processes the stimulus as if it was at a lower level and this leads to a prediction of shallower slopes of the TMCs and differently for the on- and off frequency conditions in the cases where residual BM compression is simulated. In other studies, the shallower TMCs were discussed as being due to the general use of higher masker levels for HI listeners (e.g., Lopez-Poveda *et al.*, 2005). The present modeling efforts show that shallower slopes may not be due to the use of high external

masker levels, but due to a lower internal representation of the masker in models of HI.

From a clinical and application-oriented perspective, though, the TMC method might be unattractive because it is very time consuming. It would therefore be interesting to investigate alternative behavioral methods such as, for example, loudness scaling (with narrowband stimuli) in connection with predictions from loudness models to estimate BM compression. While loudness growth functions are relatively easy to assess, it is not clear to what extent such measures can actually estimate peripheral compression and estimates of OHC and IHC losses. Alternatively, objective methods have been suggested to estimate BM properties, such as distortion-product otoacoustic emissions (Williams and Bacon, 2005; Lopez-Poveda *et al.*, 2009). So far, however, this has only been tested in NH listeners and it is unclear how reliable such measures are in HI listeners.

It remains unclear why this crossing of on- and off-frequency TMCs was observed for particular listeners at some frequencies. One possibility could be related to the tuning of the auditory nerve associated with SNHL. Liberman and Dodds (1984) measured AN tuning in animals after noise trauma. They observed that the tails of the AN tuning functions were hypersensitive at sites basal to the site of the trauma. However, these observations were made in animals were the noise trauma were induced locally by narrowband noise, and the hair cells at the relevant sites were mainly intact. It is therefore questionable that this effect is a primary explanation for the crossing TMCs, since the human listeners in the present study are unlikely to have SNHL in very distinct region in the cochlea.

4.5.2 Evaluation of the models fitted to individuals

The models fitted to the individuals were evaluated in terms of predictions of data from the experiments, as well as psychophysical measures derived from these data. Models of auditory perception are most appropriately evaluated in terms of its ability to predict measured data. Additionally, measures derived from the data can be compared to the processing of individual stages in the model. In the present study, the model was employed to predict the psychophysical data in terms of pure-tone sensitivity, off-frequency TMCs, notched-noise masking and conditions of simultaneous and forward

masking using broadband maskers. Overall, these data were well accounted for. However, the off-frequency TMCs were accounted for in terms of the slope of the masking curve, and to a less degree the actual masker levels. In the notched-noise masking experiment there was a general problem in simulating the masked thresholds produced by the 4-kHz signal. Regarding the evaluation against derived measures, the tuning of the DRNL stage fitted to the listeners was evaluated against roex filters derived from the notched noise data. These results confirmed that the tuning of the model at 4 kHz was not well simulated.

4.5.3 Relationships between different measures in individual listeners

The relationships between several quantities (absolute threshold, compression, HL_{OHC}, HL_{IHC}, ERB) derived from the data showed a broad agreement with the literature. Strong correlations were found between absolute threshold and HLOHC. The correlation between absolute threshold and HL_{IHC} was slightly weaker. The relationship between compression and the three measures: absolute threshold, HL_{OHC}, HL_{IHC} showed only weak correlations. Broadly the data indicates that several of these quantities are not predictable from the absolute threshold and strengthens the point that further individual characterization of cochlear hearing loss is relevant. The relationships between the tested quantities and the ERB the picture was in good agreement with the findings of Moore *et al.* (1999), except that the present data showed a weaker correlation between compression and the ERB. The two studies share approximately the same amount of data points. The discrepancy between the correlations may reflect that the Moore et al. study had more listeners with severe hearing loss and estimates of compression higher than 0.7.

4.5.4 Capabilities and limitations of the modeling approach

The model framework has earlier been successfully applied to NH data in various experimental detection and masking conditions (e.g., Dau *et al.*, 1996b, 1997a,b; Verhey *et al.*, 1999; Derleth and Dau, 2000; Piechowiak *et al.*, 2007). Recently, nonlinear effects associated with BM processing were included in this model (Jepsen

et al., 2008) using the DRNL filterbank (Lopez-Poveda and Meddis, 2001). This model was also considered here to predict effects of SNHL. However, in principle, other cochlear front-ends could have been chosen alternatively, such as the auditory nerve (AN) model of Heinz *et al.* (2001a,c) and more recent implementations of it (e.g., Bruce *et al.*, 2003). One focus of their modeling has been to account for IHC and OHC losses. For example, Bruce *et al.* (2003) assumed that OHC function is responsible for the active gain mechanism and for BM tuning while the function of the IHCs is primarily a transduction of information to the AN. They simulated a more linear BM response, less gain and broadened tuning with increasing OHC loss. The maximum OHC gain in their model was 46 dB which also reflects the largest possible effect of OHC loss in their model in terms of sensitivity loss. Their model used a single parameter to simulate the effect of OHC loss, and allowing only one parameter to control the I/O behavior due to OHC damage may be too restrictive, and may not provide the necessary flexibility to capture individual BM I/O behavior in listeners with SNHL. In the present study, four parameters were adjusted and this leads to more flexibility in term of fitting I/O function to data in terms of, e.g., knee point and compression, with the cost of a more complex and less straight-forward procedure. In Bruce *et al.* (2003); Zilany and Bruce (2006) their simulated IHC loss leads to reduced sensitivity and does not affect the model's tuning and compression. This approach is thus conceptually similar to the one used in the present study. The dynamic compressive gammachirp filter, suggested by Irino and Patterson (2006), provides another peripheral filtering simulation stage, but it is not clear how the model can be modified to implement changes in the I/O function to account for hearing loss. The multi-bandpass nonlinear filter of Goldstein (1990) has a very similar structure as the DRNL filter, but it is unclear if the model's I/O behavior can be modified without disrupting other important properties of that particular model. Overall, the DRNL filterbank was chosen here because of its computational efficiency and the possibility to relatively easily modify the BM filters' input-output characteristic to account for hearing loss (Lopez-Poveda and Meddis, 2001).

While the earlier studies (e.g., Dau *et al.*, 1997a; Verhey *et al.*, 1999; Jepsen *et al.*, 2008) were focused on the simulation of average NH data, one important aspect of the present work was to provide a tool that allows to quantitatively account for the

variability in the HI data (whereas NH listeners typically show much less variability). Specifically, the present study tried to evaluate and quantitatively predict the relations between the results obtained in the TMC experiment, the frequency and temporal resolution tasks and the audibility test in more detail than earlier studies. The current model provided a good overall description of the NH and HI data. Based on the fitted I/O functions and the audiograms, OHC and IHC losses were estimated, and the simulations showed how absolute sensitivity loss is related to supra-threshold deficits within the framework of the model. The modeling results support the importance of individual characterization of SNHL based on separate estimates of OHC and IHC losses. However, the adjusted parameters were based on data collected at only 1 and 4 kHz. Similar data could be obtained at more frequencies to gain more confidence in the used cochlear model parameters. The use of interpolation and extrapolation of the parameters at other DRNL filterbank frequencies may prove to be a too crude assumption. It should be noted that to simulate the estimated BM I/O function, there may exist another set of DRNL parameters (a, b, c and g) providing a similar DRNL I/O function, since their interaction is nonlinear. The parameter-sets presented here are thus not unique, but they reflect a suggestion following the manual fitting procedure. The estimated values of HL_{IHC} was derived from the measured audiogram and the estimated HL_{OHC}. This was done at discrete frequencies. In Fig.4.3 it was observed that the predicted audiogram were not exactly fitting the measured audiograms. The value of HL_{IHC} could alternatively have been adjusted to fit the measured audiograms. The predictions are, however, depending on the processing in neighboring channels, such that the adjustment procedure would become less straightforward.

Regarding intensity resolution, the model predicted an essentially constant JND across the simulated hearing-impaired listeners, which was not consistent with the results for some of the HI listeners who clearly showed increased JNDs. The finding of a constant intensity JND in the model, independent of the amount of peripheral compression, is a consequence of the roughly logarithmic overall compression in the (perception) model, as discussed in detail in Jepsen *et al.* (2008). Thus, in this framework, no effects of SNHL were expected in terms of intensity JNDs. This means that either the assumptions regarding intensity coding in the model are inappropriate,

or other sources of variability, potentially of retro-cochlear origin, need to be assumed in order to explain the increased JNDs in some of the listeners. The model of normal hearing could not predict the near miss to Weber's Law (Jepsen *et al.*, 2008). This effect (observed in data) may be due to the integration of information across peripheral channels, and may not be accounted for in the current modeling framework. If the elevated JNDs observed in the present data for HI listeners reflect a lack of account for the near miss to Weber's Law, then this modeling framework was again not expected to predict the observed data. In the framework of this model, an increased JND could effectively be simulated by increasing the variance of the internal noise. However, more specific hypotheses about potential sources for the limitations would be needed as well as more knowledge about how such limitations might be accounted for in an auditory model.

The presented model in its current form has several limitations. First of all, it was observed that the tuning of the DRNL filters fitted to listeners with mild-to-moderate losses at 4 kHz was generally too sharp,both in relation to the prediction of notched noise data, and evaluating the DRNL tuning to roex filters fitted to the data. The tuning was determined by the simulated BM compression at the corresponding levels. For these listeners, residual compression was found at mid-to-high frequencies and, consequently, a near-normal DRNL filter tuning was simulated. The reason could indeed be that the amount of compression was overestimated by the TMC method, as discussed above. Less compression in the DRNL filters would lead to a broader tuning. It is, however, unclear why this problem was only observed at 4 kHz and not at 1 kHz. The discrepancy in the matches at 4 kHz could potentially affect future applications of the model of SNHL. If the model generally simulate a too good frequency resolution at high frequencies, then the subjective performance in complex tasks might be overestimated if the task reflects an influence of reduced frequency selectivity. The results might also suggest that auditory filter widths, as estimated by notched-noise masking, may not be solely determined by the BM compression. Peripheral suppression has also been shown to affect frequency selectivity in simultaneous notched-noise masking (e.g., Shera *et al.*, 2002; Oxenham and Shera, 2003) and suppression appears to be reduced with SNHL (e.g., Heinz *et al.*, 2002). Two-tone suppression is included in the DRNL model but its effects on

frequency selectivity in a notched-noise masking paradigm have not been investigated explicitly yet. The results might also suggest that auditory filter widths, as estimated by notched-noise masking, may not be solely determined by the BM compression. Additional contributors could be the shape of the assumed middle-ear transfer function and/or changes at later stages of processing in the HI listeners.

Second, no temporal processing deficits in terms of the coding of temporal fine structure (TFS) have been considered. Recently, the processing of TFS information has been discussed intensively, particularly in connection with speech reception in noise (e.g., Lorenzi *et al.*, 2006; Strelcyk and Dau, 2009). TFS information typically refers to the temporal fine structure at the output of the cochlear filters and this fine structure evokes phase-locked activity, i.e. synchronized timing of action potentials in the subsequent stages of neural processing (e.g., Ruggero, 1992). Evidence for TFS processing deficits in HI listeners has been found in previous studies of monaural as well as binaural auditory functions. Several factors might contribute to the deficits in TFS processing. A loss of OHCs could lead to a reduced precision of phase locking (Woolf *et al.*, 1981) even though this is controversial since other studies have not found any physiological of SNHL on TFS coding (e.g., Harrison and Evans, 1979; Miller *et al.*, 1997). Alternatively, TFS deficits might also be attributable to damage to or loss of auditory nerve fibers or the innervated IHCs (e.g., Schuknecht and Woellner, 1953). In terms of modeling, several studies have suggested that the extraction of spatiotemporal information, i.e. the combination of phase-locked responses and systematic frequency-dependent delays along the cochlea (associated with the traveling wave), is important in the context of pitch perception (e.g., Loeb *et al.*, 1983), localization (e.g., Shamma, 2001), speech formant detection (e.g., Deng and Geisler, 1987) and tone-in-noise detection (Carney *et al.*, 2002). It has been proposed that a distorted spatiotemporal response might be, at least partly, responsible for the problems of HI listeners to process TFS information across frequencies (e.g., Moore, 1996; Heinz and Swaminathan, 2009). In the present study, OHC and IHC losses have only been considered in terms of associated sensitivity losses but not in terms of temporal coding. Thus, consequences of TFS loss cannot be accounted for by this model.

4.5.5 Perspectives

Reed *et al.* (2009) reviewed a number of studies where SNHL was simulated by adding threshold-shaped noise to the stimuli presented to NH listeners. Some of these studies demonstrated that data on temporal processing, such as gap detection, can be accounted for by adding noise masking (e.g., Florentine and Buus, 1984). In other experiments, such as temporal integration, this relation was not found (e.g., Florentine *et al.*, 1988). It is not fully understood how additive external noise affects the processing in the cochlea. The noise might linearize the BM response since higher input levels are used such that the system operates similarly as in the case of a (severe) SNHL. This could be tested by adding low-to-moderate level background noise while estimating BM compression in comparison to a quiet condition. It may also be found that the BM response does not change significantly with additive external noise. The model presented here might be useful to explicitly investigate the effect of the additional noise in the various experimental conditions and could help relating the different findings to each other.

It would also be interesting to investigate more complex tasks, such as speech perception in noise, which also depend on spectral and temporal resolution of the auditory system. Models of speech intelligibility, e.g., the speech intelligibility index (SII; ANSI, 1997), typically consider only aspects of reduced sensitivity; thus, individual differences resulting from supra-threshold deficits are not accounted for. Using the present model as a front-end in speech intelligibility predictions might thus provide further insights into how HI listeners process speech sounds.

4.6 Conclusions

- Audiometric pure-tone sensitivity, cochlear compression, frequency selectivity, intensity discrimination and temporal resolution were measured in ten sensorineural hearing-impaired listeners. Considerable differences of the results across the listeners were observed even for those listeners with similar audiograms.

- The cochlear processing stage of the considered model framework was adjusted to account for the individual behaviorally estimated BM input/output functions and the audiograms. The model was evaluated in the experiments of frequency selectivity, forward masking and intensity discrimination. The predictions of the experimental data reflected the variability observed in the experimental data across listeners, as well as for the results obtained in the normal-hearing listeners. However, the model generally overestimated the amount of frequency selectivity at 4 kHz for the listeners with mild-to-moderate hearing loss which might be resulting from an overestimation of cochlear compression via the temporal masking curve paradigm. Furthermore, the model predicted a roughly constant intensity discrimination threshold across all listeners whereas the data showed increased thresholds in some of the HI listeners.

- Overall, the results support the importance of an individual characterization of (sensorineural) hearing impairment. The presented modeling framework might also be useful for future investigations of effects of individual hearing impairment on speech intelligibility in various experimental conditions and could further be beneficial for the evaluation of compensation strategies and signal-processing algorithms in hearing instruments, where listening tests are time consuming and expensive.

4.7 Appendix: Additional information about the listeners

This appendix describes additional information about the hearing-impaired listeners that were used in Chapter 4 and is listed in Table 4.7. The etiologies of the hearing losses are listed, and they are based on clinical diagnoses. It is also listed whether the listeners were hearing-aid users or not. Finally, results from a speech intelligibility test are listed. These results were not used or analyzed in the chapter, but are reported here to make these data available to possible future studies.

Speech reception thresholds (SRTs) were measured for Danish Dantale II sentences in three noise conditions. It is a closed-set word recognition test using Hagerman sentences (Wagener *et al.*, 2003). The noise conditions were: (1) stationary speech-shaped noise (SSN) with the long-term spectrum of the Dantale II sentences; (2) sinusoidally amplitude modulated (SAM) noise with a constant modulation rate at 8 Hz and a modulation depths of 1; (3) randomly amplitude modulated (RAM) noise was randomly modulated with the Hilbert envelope of a bandpass-noise (4 to 12 Hz) as modulator, which reflect typical modulation rates in running speech. The modulation depth was 1. The SRT was defined as the SNR at which 50% words were identified correctly. The noise level was constant while the level of the sentences was varied adaptively. Listeners were trained on a single run with 20 sentences before measurements were made. The reported SRTs are averages of two measurements. The mean SRT results of the seven NH listeners used in Chapter 3 are also given in the table.

Listener	Etiology	Hearing-aid user	SSN	SAM	RAM
HI1	Presbycusis	No	-4.5	-7.7	-6.1
HI2	Noise induced	Yes	-5.6	-6.4	-4.8
HI3	Presbycusis	Yes	-4.2	-10.5	-6.1
HI4	Presbycusis	No	-6.7	-9.2	-7.7
HI5	Unknown	No	-5.8	-9.4	-6.9
HI6	Unknown	Yes	-6.5	-9.3	-7.5
HI7	Presbycusis	Yes	-4.8	-10.0	-6.9
HI8	Presbycusis	Yes	2.2	1.8	2.0
HI9	Presbycusis	Yes	-3.2	-5.8	-4.2
HI10	Unknown	Yes	-4.6	-7.0	-6.1
Mean NH			-7.6	-16.7	-10.7

Table 4.7: Additional information about the ten HI listeners used in Chapter 4. The table lists their hearing loss etiology, hearing aid use and SRTs (in dB) in noise condition of stationary speech-shaped noise (SSN), Sinusoidally amplitude modulated (SAM) noise and an amplitude modulated noise with a random modulation rate (RAM).

5

Relating individual consonant confusions to auditory processing in listeners with cochlear damage [6]

Reduced sensitivity to sounds represents only one typical consequence of hearing impairment. Additional factors such as spectral and temporal resolution have been considered to characterize (individual) hearing loss. The present study investigated consequences of deficits in auditory signal processing and the perception of speech sounds in individual listeners. First, psychophysical forward-masking data were obtained and the parameters of a peripheral auditory model were adjusted accordingly to simulate the individual listeners' cochlear processing. Second, the same individuals were tested in a Diagnostic Rhyme Test (DRT). These stimuli were processed by the peripheral model obtained in the first phase. The resulting internal auditory representation was analyzed by a detector and error patterns were predicted along the acoustic-phonetic dimensions of the DRT. An important feature of the DRT framework using synthesized diphones was the separation of errors originating from the periphery and detector, respectively. Most error patterns were accounted for by the model, providing a link between the speech and non-speech data in hearing-impaired listeners. Error patterns were further predicted by a model which simulated reduced sensitivity only. It was found that this model produced too few errors and indicated that supra-threshold deficits have an influence on consonant confusions in hearing-impaired listeners.

[5] This chapter represents a journal article manuscript in preparation. The data and preliminary modeling results were presented at the International Symposium on Auditory and Audiological Research (ISAAR), Helsingør, Denmark, 2009.

5.1 Introduction

A major concern of hearing-impaired (HI) people is their reduced ability to reliably communicate through speech. Some are more handicapped in their communication than others, depending on the type and salience of their hearing impairment. Even people with similar a hearing loss, in terms of audibility, can differ greatly in their ability to understand speech, particularly in complex acoustic environments with background noise, reverberation or multiple sound sources. Hearing aids can restore audibility by amplifying speech signals and can improve the speech-to-noise ratio (SNR) by different techniques, such as directional microphones and noise reduction schemes. However, the benefit from the available technical solutions differ in individual hearing-aid users. For some people, the hearing aids restore the ability to function almost normally in every-day communication, while others report only limited or no benefit from hearing aids, particularly in challenging situations. It is of great importance to obtain a better understanding of how the processing of speech sounds is affected by the individual hearing impairment in order to identify the sources of the variability in the speech-in-noise perception data across listeners.

spects of hearing impairment which are not accounted for by sensitivity loss are referred to as supra-threshold deficits, such as loudness recruitment, reduced frequency selectivity and reduced temporal resolution which also are typical consequences of a sensorineural hearing loss. Moore *et al.* (1999) and Jepsen and Dau (2010) showed that even hearing-impaired listeners with comparable audiograms can show large differences in their performance in tasks related to supra-threshold deficits. The differences may be associated with individual patterns of outer hair-cell (OHC) and inner hair-cell (IHC) damages (Jepsen and Dau, 2010; Lopez-Poveda *et al.*, 2009). Frequency selectivity, temporal resolution and intensity resolution are usually measured by psychoacoustic experiments using synthetic non-speech stimuli such as tones presented in noise maskers. It is unclear how these deficits are reflected in psychoacoustic tasks with more natural stimuli such as speech. Linking speech and non-speech psychophysics might provide a step towards a better understanding of the variability observed, particularly in the speech data of HI listeners.

Jepsen and Dau (2010) modified some of the parameters of computational

auditory signal-processing and perception (CASP) model (Jepsen *et al.*, 2008) on the basis of estimated basilar-membrane (BM) input-output (I/O) function and the audiogram. This was done on an individual basis for ten listeners with cochlear hearing loss, and individual differences were associated with differences in the estimates of OHC and IHC loss. Their model accounted for supra-thresholds deficits such as broader auditory filters and reduced temporal resolution as well as reduced sensitivity. An earlier version of the CASP model has earlier been used as a front end in studies involving speech stimuli. Holube and Kollmeier (1996) considered the model of auditory perception from Dau *et al.* (1996a) as the front end and derived an intelligibility index. They accounted for the reduced intelligibility of speech in noise for NH and HI listeners. Holube and Kollmeier (1996) simulated effects of hearing loss due to audibility and frequency selectivity, however, these aspects were not simulated as a direct consequence of cochlear compression as suggested in Jepsen and Dau (2010). The same perception model front-end was used in an automatic speech recognizer system in Tchorz and Kollmeier (1999) with a Hidden-Markov Model (HMM) back end, where it was shown that higher robustness to noise was obtained using the auditory processing front end compared to the commonly used mel-scale cepstral coefficient feature extraction. However, due to the HMM back end it cannot be concluded whether the robustness is obtained due to the front-end processing alone.

Models of the auditory periphery attempt to appropriately describe a perceptually relevant "internal representation" (IR) of the incoming sounds. To investigate whether the simulated IR provides a good match to the “real” IR, it is crucial that front-end and back-end processing, for example in a speech recognition system, are clearly separated (Ghitza, 1993). The ultimate goal is not to obtain perfect speech recognition but to match human performance, and thereby to contribute to a better understanding of how speech is processed in the auditory system. Ghitza (1993) suggested that the cognitive component involved in consonant recognition (both for humans and machines) could be minimized by using the diagnostic rhyme test (DRT; Voiers, 1983), because this test represents a simple binary discrimination task. However, their back-end stage was found to be a source of errors since a HMM was used as a recognizer, even after attempts were made to keep its errors at a minimum. Messing *et al.* (2009) proposed

a modeling framework to predict confusion patterns from DRT in NH listeners, where they further separated the peripheral model (front end) and the detector stage (back end) by using synthesized DRT diphones. These allowed them to use of a simple back end which measures a perceptual distance to templates in order to keep the back-end errors at a minimum. Their framework and data was used to measure inaccuracies in the front-end model's internal representation of speech.

The goal of the present study was to investigate how degraded auditory processing, due to cochlear damage, affects speech perception in individual listeners. This was done in the framwork of the synthesized DRT, using the CASP model (Jepsen *et al.*, 2008; Jepsen and Dau, 2010) as the front end and a detector similar to that of Messing *et al.* (2009) as the back end. The separation of front-end and back-end processing was of conceptual importance here, since predicted errors could thus be uniquely associated with the front-end processing and could provide a measure of how well the CASP model, including the simulation of cochlear hearing loss, can describe the actual IR of speech sounds in individual hearing-impaired listeners. For the simulation of hearing impairment, the front end was fitted to the individual listeners due to non-speech psychophysics, based on behavioral estimates of BM I/O functions and the audiogram following the method suggested in Jepsen and Dau (2010). The peripheral model then remained unchanged for the simulations of DRT error patterns. If the model was able to predict individual error patterns in the DRT task based on individual fits to the non-speech tasks, then degraded performance in the speech tasks could be associated with limitations in basic auditory processing in the individuals. In order to resolve whether simulated DRT errors were accounted for due to reduced sensitivity (audibility) alone, individual error patterns were simulated using a configuration of the CASP model which only simulated reduced sensitivity without changing the BM processing stage.

A common measure of speech intelligibility is the speech reception threshold (SRT), which is a single value typically defined as the SNR at which 50% of a sentence is correctly understood. HI listeners commonly have higher SRTs than NH listeners, i.e., they need a larger SNR to recognize speech. The SRT depends critically on experiment-specific factors, such as speech material, background-noise characteristics as well as specific characteristics of the hearing loss. SRT measurements provide a

useful tool to study the influence of a specific noise-type or a transmission channel on speech intelligibility or to roughly quantify the communication difficulties of hearing-impaired listeners. However, a SRT value does not reveal information about which elements of the speech that were received incorrectly and what the source of the errors was, for example in terms of specific hearing impairment factors.

Other experiments using speech stimuli have been designed to obtain more detailed information about speech perception. One example is the DRT (Voiers, 1983), used in the present study, where consonant confusions can be measured by consonant discrimination along a number of acoustic-phonetic features. Another example is the approach described in Miller and Nicely (1955) where consonant recognition is measured (at different SNRs) and consonant confusion patterns can be derived from the data. This allows categorizing typical confusions in terms of perceptual features. Phatak and Allen (2007) and Phatak *et al.* (2008) extended the analysis of consonant confusion patterns and provided a detailed analysis in terms of perceptual consonant groups.

Speech perception models have been useful, for example for evaluating the effect of room acoustics on speech intelligibility. The articulation index (e.g., Kryter, 1962; ANSI, 1969) and later the speech intelligibility index (SII; ANSI, 1997) provide estimates of the expected average speech intelligibility of a signal that has been distorted by a transmission-line. The SII also includes a component that addresses hearing impairment, but only the loss of sensitivity is considered. The speech transmission index (STI; Steeneken and Houtgast, 1980), is based on the distortion of the modulation depth through a transmission channel, such as a reverberant room. There are no standardized procedures to account for hearing loss in the STI method, but some attempts have been made to address this issue (Humes *et al.*, 1986). More recently, Elhilali *et al.* (2003) presented a model that analyzes (joint) spectra-temporal modulations in the signal to predict speech intelligibility. They introduced the measure of the spectro-temporal modulation index (STMI) which could account for effects of degraded temporal modulations in a similar way as the STI, but could further describe effects of nonlinear distortions on speech intelligibility which degraded the pattern of spectral periodicities (spectral modulation).

In this study, the representation of speech sounds in the CASP model was used to

predict the DRT error patterns of listeners with cochlear hearing loss. The hypothesis was that an appropriate simulation of sensitivity loss and supra-threshold deficits is required to account for individual differences in the error patterns measured in the same individuals.

5.2 Experimental methods

5.2.1 Listeners

Three listeners with mild-to-moderate sensorineural hearing loss participated in this study. Listeners S1, S2 and S3 were 21, 45 and 27 years old, respectively. All these have had a hearing loss since their early childhood. S1 and S2 were regular users of hearing aids while S3 did not use hearing aids. Only one ear of each listener was measured in the speech and non-speech tasks. The audiograms of the measured ears are shown in Fig. 5.1 (open symbols). The listeners were selected to have hearing losses less than 55 dB HL at frequencies from 0.25 to 4 kHz. The rationale behind this choice was to be able to measure performance in the speech task without compensating for audibility and thereby potentially introducing undesired distortion. The listeners were paid for their participation on an hourly basis. Measurement appointments lasted two hours and sessions had durations of about 30 to 45 minutes. Training sessions in the forward masking task were run until no systematic improvements were observed, usually after two to four hours. For the DRT, three hours of training were provided. The total testing time for each subject was about 16 to 20 hours, including training.

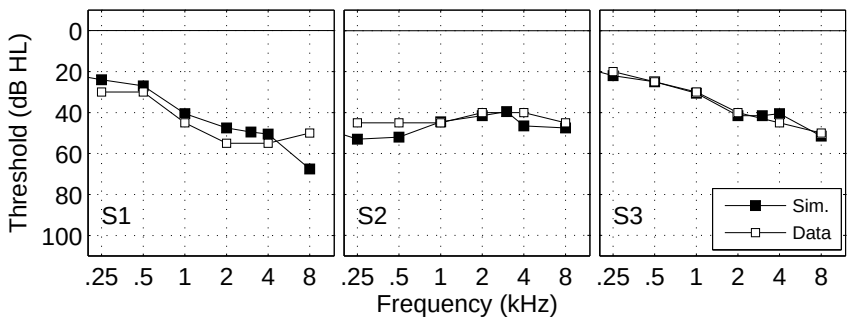

Figure 5.1: Audiograms of the measured ears of the three HI listeners. Pure-tone thresholds are plotted in dB hearing level (HL). Open symbols indicate measured thresholds, while filled symbols indicate simulated thresholds by the corresponding models (described in Sec. 5.4).

5.2.2 Apparatus

Audiograms were provided by audiological clinics while all other data were collected in the laboratory of the Biomedical Engineering department at Boston University. The stimuli were presented monaurally to the subject via headphones (Sennheiser HD265) in a sound-insulated listening booth. Listeners responded on a computer keyboard, following the instructions on a computer monitor located in the booth. The experiments were run on a personal computer with a 16-bit high-quality soundcard.

5.2.3 Temporal masking curves (TMC)

In the TMC experiment, forward masking of a fixed-level brief tone was measured as a function of signal-masker interval. The probe signal was a pure tone with a duration of 20 ms, which was Hanning windowed over its entire duration. The frequency (f_{sig}) was either 1 or 4 kHz. The signal was presented at 10 dB sensation level (SL). The masker was also a pure tone with a duration of 200 ms including 5-ms raised-cosine on- and off ramps. The masker frequency (f_m) was equal to f_{sig} (on-frequency condition) or $0.6 \cdot f_{sig}$ (off-frequency condition). The masker-signal interval was 2, 5, 10 ms and additional 10-ms increments until the subject reported (in pilot runs) that the masker level became uncomfortably loud, or reached the maximum level of 95 dB SPL. Stimuli were generated in Matlab at a sampling rate of 44.1 kHz. The masker level was adjusted by the adaptive procedure to reach masked signal threshold. A three-interval tree-alternative forced choice paradigm in connection with a two-up-one-down rule were applied. The reported thresholds reflect the 70.7% point on the psychometric function and represent the mean of at least three measured thresholds. The step size was varied adaptively, starting at 8 and ending at 1 dB, and thresholds were an average of the levels at the last eight reversals with the final step size. The listener received immediate feedback on whether a response was correct or not.

5.2.4 The diagnostic rhyme test (DRT)

The DRT of Voiers (1983) uses 192 minimal pair diphones and was designed to cover six acoustic-phonetic dimensions: voicing (VC), nasality (NS), sustention (ST), sibilation (SI), graveness (GV) and compactness (CM). The diphones were

synthesized by a text-to-speech system, such that the acoustic waveforms only differed in the initial consonant. The test stimuli had a sampling rate of 16 kHz and were identical to those used in Messing *et al.* (2009). The noise was a Gaussian noise which was spectrally shaped to have a long-term spectrum similar to speech. Different noise tokens were realized in the generation of the noisy stimuli. The speech had a constant *rms* level of 70 dB SPL and was presented in background noise at SNRs of 0 and 10 dB. Eight repetitions of the 192 diphones were presented in blocks of 128 in random order. The DRT is a binary consonant discrimination task realized in a one-interval two-alternative forced-choice method. The listeners were not given feedback on their responses. The performance of the listeners was evaluated by the error rate along the six acoustic-phonetic dimensions. Examples of minimal pairs are given in Table 5.1 (see also, Voiers, 1983; Ghitza, 1993).

Voicing (VC)	**Nasality (NS)**	**Sustention (ST)**
Voiced - Unvoiced	*Nasal - Oral*	*Sustained - Interrupted*
veal - feel	meat - beat	vee - bee
bean - peen	need - deed	sheet - cheat
gin - chin	mitt - bit	vill - bill
dint - tint	nip - dip	thick - tick
zoo - Sue	moot - boot	foo - pooh
dune - tune	news - dues	shoes - choose
vole - foal	moan - bone	those - doze
goat - coat	note - dote	though - dough
zed - said	mend - bend	then - den
dense - tense	neck - deck	fence - pence
vast - fast	mad - bad	than - Dan
gaff - calf	nab - dab	shad - chad
vault - fault	moss - boss	thong - tong
daunt - taunt	gnaw - daw	shaw - chaw
jock - chock	mom - bomb	von - bon
bond - pond	knock - dock	vox - box
Sibilation (SB)	**Graveness (GV)**	**Compactness (CM)**
Sibilated - Assibilated	*Grave - Acuté*	*Compact - Diffuse*
zee - thee	weed - reed	yield - wield
cheep - keep	peak - teak	key - tea
jilt - gilt	bid - did	hit - fit
sing - thing	fin - thin	gill - dill
juice - goose	moon - noon	coop - poop
chew - coo	pool - tool	you - rue
Joe - go	bowl - dole	ghost - boast
sole - thole	fore - thor	show - so
jest - guest	met - net	keg - peg
chair - care	pent - tent	yen - wren
jab - dab	bank - dank	gat - bat
sank - thank	fad - thad	shag - sag
jaws - gauze	fought - thought	yawl - wall
saw - thaw	bong - dong	caught - taught
jot - got	wad - rod	hop - fop
chop - cop	pot - tot	got - dot

Table 5.1: Examples of diphone minimal pairs in the six acoustic-phonetic features. Each feature-block contains 16 minimal pairs, thus there are 192 diphones in total.

5.3 Modeling speech perception

5.3.1 The front end

A schematic structure of the front-end, the CASP model (Jepsen *et al.*, 2008; Jepsen and Dau, 2010), is shown in Fig. 5.2. The acoustic stimuli are first processed by the outer- and middle ear filters, followed by the dual-resonance nonlinear (DRNL) filterbank (Lopez-Poveda and Meddis, 2001) simulating BM processing. The processing of the subsequent stages is carried out in parallel in the frequency channels. Inner hair-cell transduction is modeled roughly by half-wave rectification followed by a first-order lowpass filter with a cut-off frequency at 1 kHz. The expansion stage transforms the output of the IHC stage into an intensity-like representation by applying a squaring expansion. The adaptation stage simulates dynamic changes in the gain of the system in response to changes in the input level. It consists of five feedback loops with time-constants in the range from 5 to 500 ms. For a stationary input signals, the output approaches a logarithmic compression. For rapid input variations the transformation through the adaptation loops is more linear, leading to an enhancement in fast temporal variations, such as onsets. The output of the adaptation stage is processed by a first-order lowpass filter with a cut-off frequency at 150 Hz, followed by the modulation filterbank, which is a bank of bandpass filters tuned to different modulation frequencies (Dau *et al.*, 1997a). For further details on the CASP model stages, the reader is referred to (Jepsen *et al.*, 2008) and (Jepsen and Dau, 2010).

5.3.2 Simulation of individual hearing loss

Jepsen and Dau (2010) described a method to adjust the parameters of the cochlear stages of the model (DRNL filterbank and hair-cell transduction, gray blocks in Fig. 5.2 to simulate degraded processing due to hair-cell loss. The I/O function of the DRNL filters simulating normal hearing has a linear low-level part for input levels below about 30-40 dB SPL, whereas compressive processing is assumed above this level. The transition between the linear and the compressive region is referred to as the knee point. Here, the I/O behavior of the DRNL filterbank was adjusted to correspond to the BM I/O functions estimated behaviorally in the three HI listeners, in terms of the

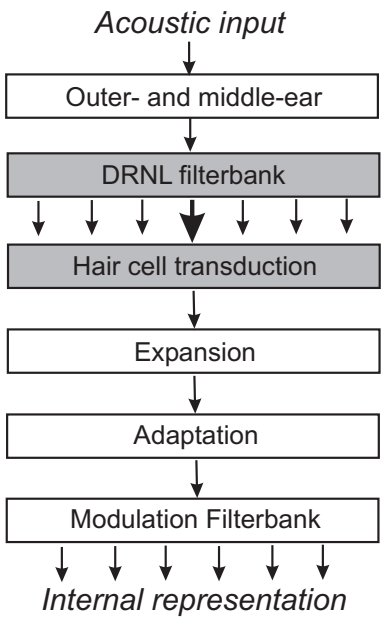

Figure 5.2: Structure of the model's front-end. The acoustic input is processed by several stages of auditory processing to form an internal representation with axes; time, frequency and modulation frequency.

compression exponent and the knee point. The DRNL I/O function was assumed to be linear for levels lower than the lowest measurable point in the data. After parameters were determined at 1 and 4 kHz, linear interpolation and extrapolation were used to obtain parameter-sets for a range of filter center frequencies (0.1 to 8 kHz). The suggested procedure also provided estimates of the effects of OHC and IHC losses with respect to sensitivity. OHC loss was derived from the fitted I/O functions and the loss of sensitivity due to IHC loss was simulated as a linear attenuation at the output of the hair cell transduction stage. The model simulating normal hearing was denoted MNH while models fitteds fitted to listeners S1, S2 and S3 was denoted M1, M2 and M3, respectively.

Model configurations which simulate individual loss of sensitivity only had BM I/O behavior of the normal system, and the signal was attenuated after the DRNL stage to account for reduced sensitivity. These configurations would thus *not* simulate supra-

thresholds deficits due hair-cell loss. These model configuration were denoted A1, A2 and A3, respectively. These are also referred to as the "sensitivity-only" models.

5.3.3 Internal representation of the stimuli after auditory processing

The output of the preprocessing stages, the internal representation (IR) of the respective input stimulus, has the dimensions time (t), frequency (f) and modulation frequency (mf). IRs were generated using DRNL filters in the range from 0.1 to 8 kHz, with 4 filters per equivalent rectangular bandwidth (60 channels in total) and considering the first six modulation filters, with modulation filter center frequencies ranging from 0 to 46 Hz. Including more filters did not change performance; therefore, they were not considered in order to reduce the computational load. In the following, the IRs are defined as the model's response from time 150 to 600 ms. In the first 150 ms, the response to the noise onset dominates, and the diphone onset had not yet occurred. For the present purpose, this noise-onset response was disregarded since it did not influence the diphone recognition. Figure 5.3 shows IRs generated from the voiced/unvoiced minimal pair */daunt/* - */taunt/* at the two tested SNRs 0 and 10 dB. For illustrative purposes, the modulation filterbank was disregarded in this example and replaced by a modulation-lowpass filter with a cut-off frequency at 8 Hz (Dau *et al.*, 1996a). This representation can be regarded as an auditory spectrogram with axes time and frequency. Darker colors reflect a larger internal excitation.

In the top-right panel (*/daunt/*, voiced, SNR = 10 dB) it can be seen that there is a strong response to the onset across frequency at about 250 ms. The strong response reflects a short "voice onset time". Multiple formant trajectories are represented and resolved in frequency. The top-left panel was generated with the same diphone but at the lower SNR (0 dB). Here, the response to the diphone signal is less clear, since there is a stronger overall response to the background noise due to the lower SNR. The lower panels in Fig. 3.3 show corresponding IRs generated from the unvoiced */taunt/*. Recall that a synthesized diphone pair only differs in the initial consonant. The shown responses to the diphones were thus different from about time 200 ms and the following 100-150 ms in this particular case. It can be seen that the onset of taunt

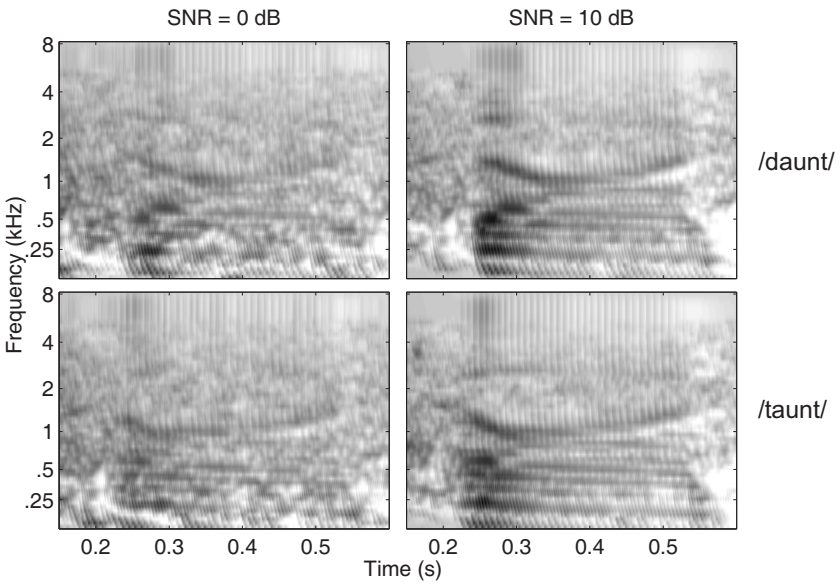

Figure 5.3: Examples of internal representations (IRs) at two SNRs. These are generated by replacing the modulation filterbank with a lowpass filter with a cut-off frequency at 8 Hz. The left and right columns show IRs at SNRs of 0 and 10 dB, respectively. The top row shows IRs of the diphone */daunt/*, while the bottom row of diphone */taunt/*.

occurs earlier which indicates that the */t/* has a longer duration or "voice onset time". One would expect a more pronounced high-frequecy onset response from the transient */t/*, but this is is not visually clear in the figure. Since the preprocessing includes adaptation the responses to the post-consonantal part of the diphone are not identical in a minimal pair, but exhibit small differences. Furthermore, the noise-tokens in a pair were different. However, the post-consonantal part of a noisy diphone-pair, after 400 ms time point, differed by less than 6% of the total mean-squared-error (described later).

The IRs produced at the output of individual modulations filters are represented by a series of auditory spectrograms - one for each modulation channel. Figure 5.4

shows these IRs for the diphone pair */daunt/ - /taunt/* at a SNR of 10 dB. The first channel is a lowpass filter which contains the "direct-current"(DC) energy of the signal after auditory processing. In the other five channels, it can be observed that for */daunt/* (left column), the strongest response has a shorter duration compared to */taunt/*, while the excitation amplitude is higher (darker color). The high modulation frequency channels thus also contributed to a detection of differences in the diphone pairs within the model.

Figure 5.5 shows IRs that reflect hypothetical hearing losses assumed in the model. Consequences of broader auditory filters, IHC loss and a combination of the two are illustrated. In order to isolate the effects, the IRs were generated using a linear BM stage, the gammatone filterbank, which was also used in an earlier version of the processing model (Dau *et al.*, 1997a). The IR of */daunt/* produced by this model (without the modulation filterbank) is shown in the upper left panel. To simulate IHC loss, a constant attenuation of 25 dB was applied at the hair-cell stage across frequencies. The corresponding IR is shown in the upper right panel. Consequently, the amplitude of the response is reduced in the entire IR, but the spectral resolution is unchanged. To simulate broader filters, the bandwidths of the gammatone filters were increased by a factor of 2 in all channels, resulting in the IR shown in the lower left panel. As a consequence, the excitation is smeared across frequency and signal information is reduced due to less resolved spectral components. A combination of broader filters and IHC loss is presented in the lower-right panel. Here, it can be observed that the amount of information is strongly reduced. The CASP model fitted to the three individual listeners (described further below, Fig. 5.10) provides IRs reflecting individual level- and frequency-dependent combinations of reduced sensitivity and reduced spectral and temporal resolution.

5.3.4 The back end

Messing *et al.* (2009) introduced the concept of using synthesized DRT diphones and a detector (back end) based on the L_2-norm. With their method, it can be assumed that the source of model errors must be originating from the front-end processing. Here, the same synthesized diphones and the same detector were used. Templates (Y) were the IRs of each diphone presented in a random realization of the noise, at a SNR of 5

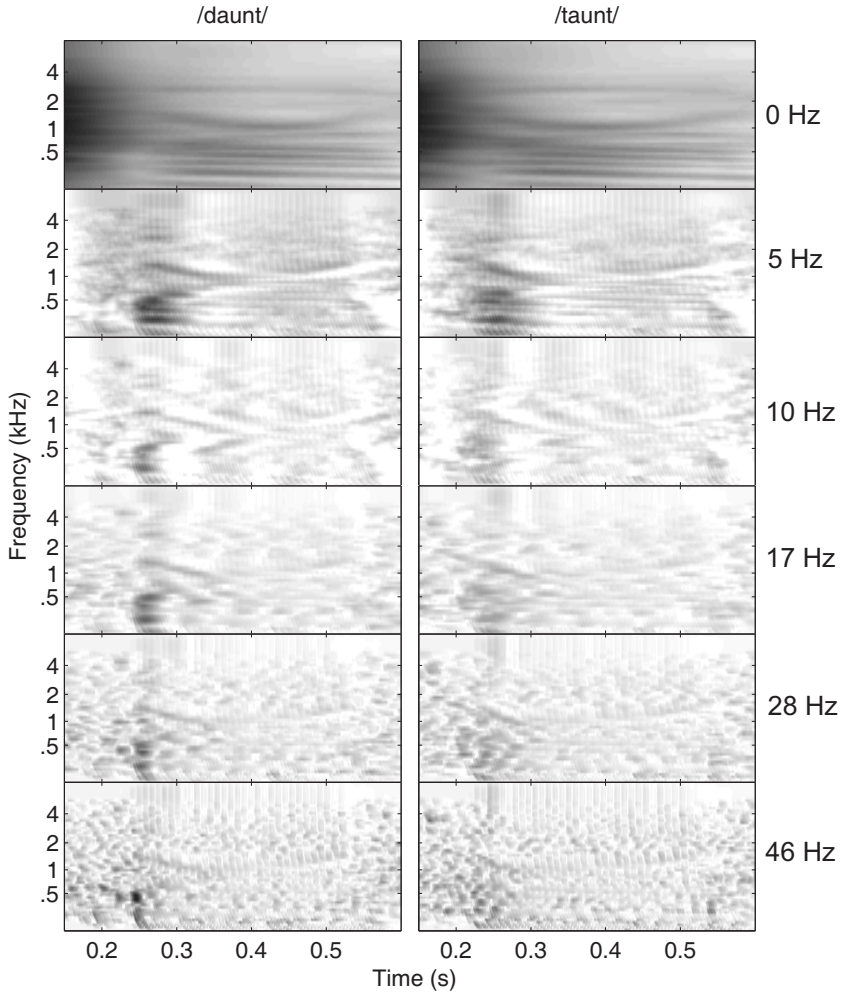

Figure 5.4: Examples of IRs in the six modulation channels tuned to modulations center frequencies at 0, 5, 10, 17, 28 and 43 Hz (top to bottom). The left column shows responses to */daunt/*, while the right column shows the responses to */taunt/*. The SNR was 10 dB.

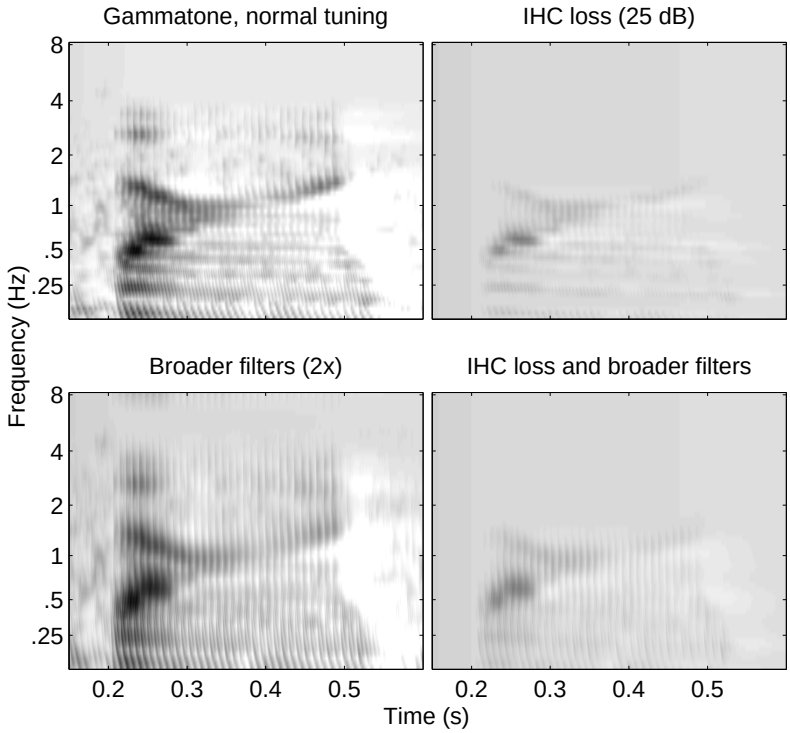

Figure 5.5: Examples of IRs to illustrate front-end processing consequences of simulated hearing loss. They were generated using a lowpass filter instead of the modulation filterbank, as in Fig. 5.3. The upper left panel shows the IR from */daunt/* using the gammatone filterbank as the BM stage. The upper right panel shows the effect of a constant IHC loss of 25 dB. The lower left shows the consequence of using broader gammatone filter, where the ERBs are doubled in all channels. The lower right panel exemplifies a response with both constant IHC loss and broader filters.

dB. For a given test diphone, the IR was calculated at a particular SNR (IR_x), and the mean-squared-errors (MSEs) between IR_x and the two possible templates (e.g., for */daunt/* and */taunt/*) was calculated across time, frequency and modulation frequency. The MSE represents the L_2-norm or Euclidean distance and is considered here as representing the *perceptual* distance between test IR and template. The MSE between

IR_x and the correct template (Y_C) was denoted MSE_C, while the MSE calculated for the corresponding wrong template (Y_W) was denoted MSE_W:

$$\text{MSE}_C(x) = \frac{\sum_{t=1}^{N_T}\sum_{f=1}^{N_F}\sum_{mf=1}^{N_{MF}}[Y_C(t,f,mf) - \text{IR}_x(t,f,mf)]^2}{N_T N_F N_{MF}} \tag{5.1}$$

$$\text{MSE}_W(x) = \frac{\sum_{t=1}^{N_T}\sum_{f=1}^{N_F}\sum_{mf=1}^{N_{MF}}[Y_W(t,f,mf) - \text{IR}_x(t,f,mf)]^2}{N_T N_F N_{MF}} \tag{5.2}$$

whereby t represents the time index, f is frequency index and *mf* is the modulation frequency index. N_T, N_F and N_{MF} represent the total number of time, frequency and modulation frequency indices, respectively. The argument x indicates that this calculation is carried out for each of the 192 diphones. Detection is based on the difference, $\Delta\text{MSE} = \text{MSE}_W - \text{MSE}_C$. Messing *et al.* used a *hard* decision criterion, where the detector chooses the template which produces the smallest MSE as representing the detected diphone. For $\Delta\text{MSE} < 0$, a wrong decision was made, while for $\Delta\text{MSE} > 0$, the correct word was detected. In the present study, a probabilistic decision criterion was introduced which reflects the introduction of internal noise in the model. In a binary task, the probability of being correct when $\Delta\text{MSE} = 0$ is 0.5. In this new approach, the probability of being correct followed a Gaussian cumulative density function (CDF) with $\mu = 0$ and standard deviation σ, thus implying a *soft* decision criterion.

$$\text{CDF}(x) = \int_{-\infty}^{x} \frac{1}{\sqrt{2\pi}\sigma}\exp(-\frac{x^2}{2\sigma^2})dx \tag{5.3}$$

To preserve the argumentation of Messing *et al.* (2009) that the source of model errors reflects front-end processing, it was important that σ was fixed at this stage. Notice that the introduced stochasticity in this detector, unlike the back end in Messing *et al.*, now introduce back-end errors. Therefore, predicted error patterns will be presented as the mean error rates across 5 runs of the simulation.

Figure 5.6 shows examples of the ΔMSE-distribution from actual simulations using MNH, M1, M2 and M3. These show distributions produced while simulating

the detection of voiced consonants (VC+) at the two tested SNRs. The distribution produced by the MNH has most of the ΔMSE-values greater than zero at the higher SNR (10 dB), while there is an increased number of ΔMSEs smaller than zero at 0 dB SNR. In the bottom panels, it can be seen that the HI models generally produce narrower ΔMSE-distributions but no increase in the occurrences of $\Delta\text{MSE} < 0$ relative to the NH model. Consequently, the HI models would not produce more errors compared to the NH model if the hard decision rule was used. However, the values of ΔMSE are generally closer to zero in the HI models than in the NH model. Thus, the use of the proposed probabilistic decision criterion will produce more errors with the HI models.

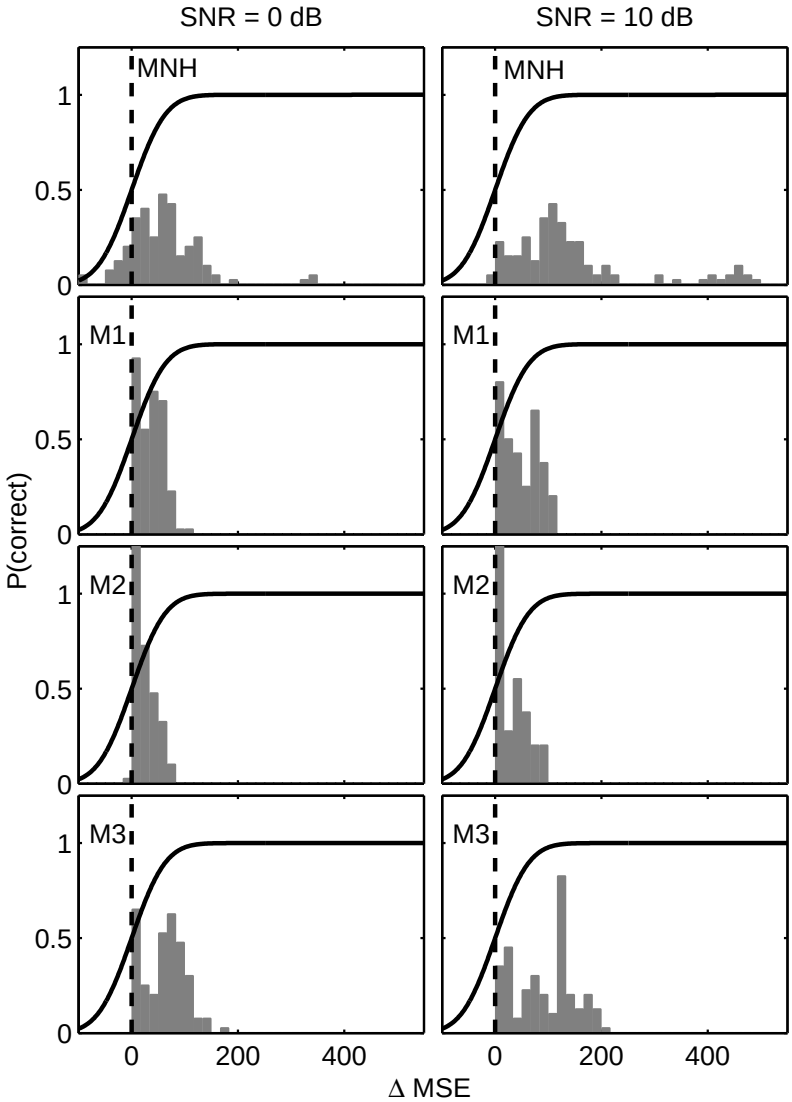

Figure 5.6: Example of ΔMSE-distributions (gray bars in histograms) from the four models (MNH, M1, M2 and M3). These are produced from simulations of the VC+ dimension. Left and right columns show distributions from 0 and 10 dB, respectively. The vertical dashed line indicates the decision boundary at $\Delta\text{MSE} = 0$, where the probability of being correct, P(correct), was 50%. The solid curve shows the CDF which determines P(correct) for detection as a function of ΔMSE. σ of the CDF was constant at 25 in all models.

5.4 Results

5.4.1 Characterizing individual hearing impairment using non-speech stimuli

Estimated BM input-output functions

The results from the TMC experiment are shown in Fig. 5.7. The left and right columns show the results at 1 and 4 kHz, respectively. The circles represent the measured data obtained in the on-frequency masking condition. The open squares show corresponding data obtained in the off-frequency condition. The horizontal dashed lines indicate the thresholds for the signal without any masker. The error bars, indicating $\pm$ one standard deviation, are typically smaller than the data symbol.

The off-frequency thresholds (squares) lie above the on-frequency thresholds (circles), since an off-frequency masker produces less masking than an on-frequency masker at the signal frequency. No data were obtained using the off-frequency masker for S2 at the 4-kHz condition, since the necessary masker levels exceeded the limit of the hardware (95 dB SPL). In order to be able to derive the BM I/O function in this condition, the off-frequency TMC at 600 Hz, indicated by the asterisks, was used. For listener S2 at 1 and 4 kHz, and S3 at 4 kHz the slope of parts of the on-frequency TMC is steeper than the off-frequency TMC. This indicates BM compression, and was also observed, e.g., in Nelson *et al.* (2001) and Jepsen and Dau (2010). In the case of S1 at 1 kHz, the on- and off-frequency TMCs are roughly parallel which indicates no BM compression, i.e. linear processing. However, for S1 at 4 kHz and S3 at 1 kHz, it can be observed that the slope of the on-frequency TMC is shallower than that of the off-frequency TMC. This is not a typical result of this experiment, which has been conducted in several studies using HI listeners. Here, it is assumed that BM processing cannot be expansive, and these data may reflect inappropriate assumptions, for these HI listeners, in the TMC method.

BM I/O functions were derived from the TMC data following the procedure suggested by Nelson *et al.* (2001). No data were obtained using the off-frequency masker for S2 at the 4-kHz condition, since the necessary masker levels exceeded the limit of the hardware (95 dB SPL). In order to be able to derive the BM I/O function

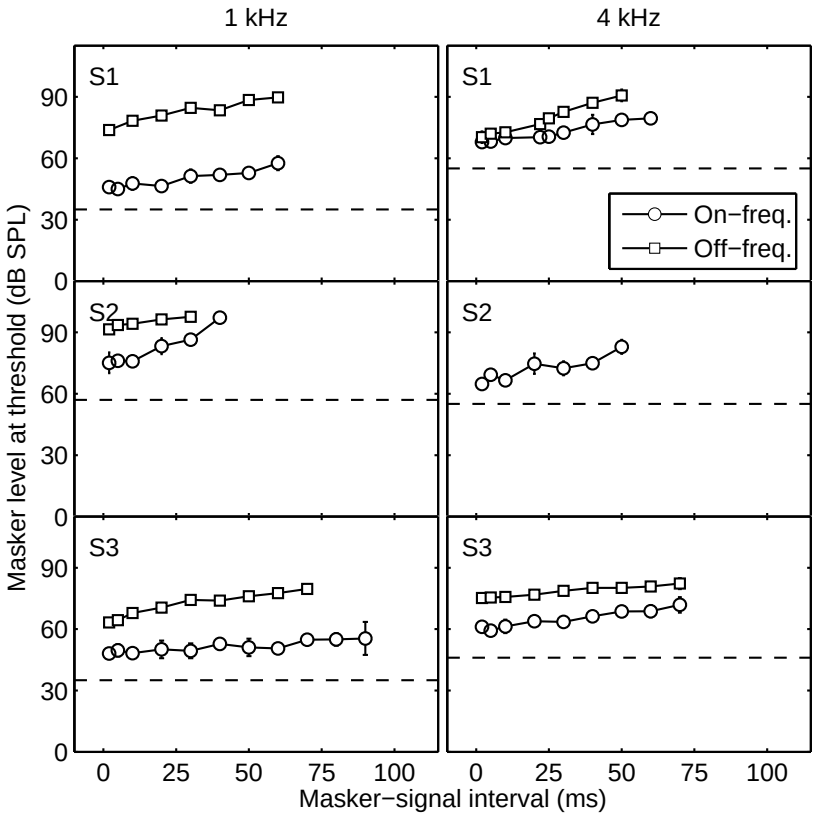

Figure 5.7: Results of the TMC experiment for the HI listeners. The left and right columns show results where the signal frequency was 1 or 4 kHz, respectively. Open circle and square symbols indicate thresholds in the on- and off-frequency masking conditions, respectively. Error bars of one SD are generally smaller than the symbol.

in this condition, the off-frequency TMC at 600 Hz was used. The circles in Fig. 5.8 represent estimated I/O functions for the three listeners. These were obtained by using a method similar to Jepsen and Dau (2010): A straight line was in each case fitted to the off-frequency masking data, which reflects the masker level at signal threshold as a function of the masker-signal separation. These output levels were then plotted as a function of the input level corresponding to the masker-signal intervals measured

with on-frequency masking. The dotted line has a slope of one indicating a linear I/O behavior.

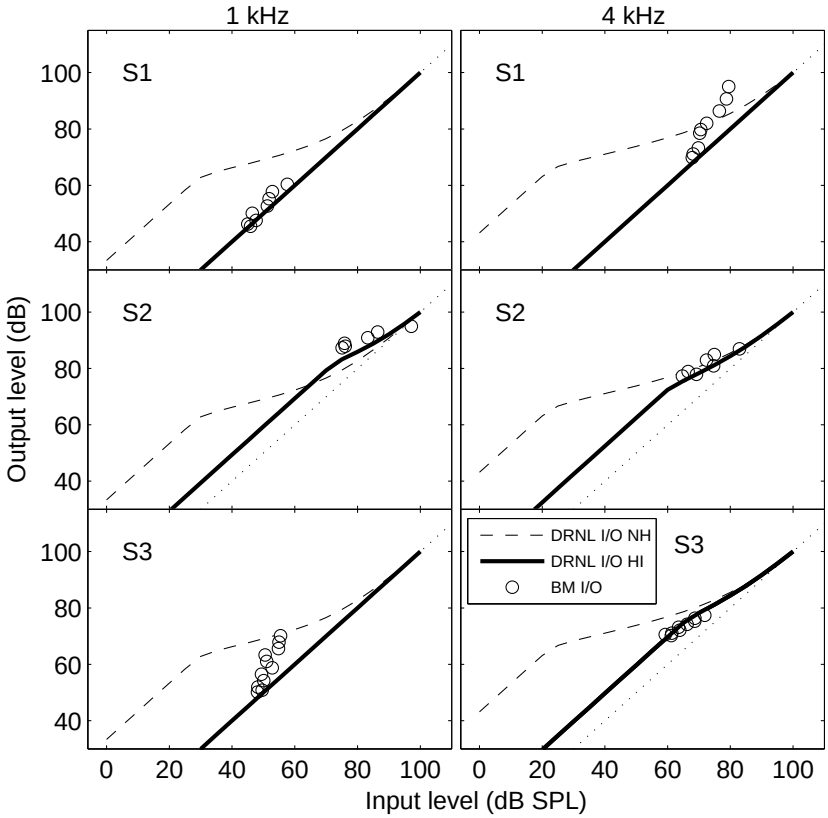

Figure 5.8: Measured and simulated BM I/O functions for the three HI listeners. Left and right columns show the results at 1 and 4 kHz, respectively. The circles indicate the measured I/O functions for listeners. The dashed curve shows the I/O function for the corresponding DRNL filter for MNH. The black curve indicates the DRNL I/O function adjusted to fit the measured I/O function. The dotted line indicates linear I/O behavior.

The slopes of the estimated I/O function were calculated and are shown in Table 5.2. BM compression was found for listeners S2 at both 1 and 4 kHz, and for S3 at 4 kHz, but in all cases slopes were higher than in NH listeners, i.e. above

about 0.25. The three other conditions showed a slight expansion (S1 at 1 kHz) or a substantial expansion (S1 at 4 kHz and S3 at 1 kHz). Indication of expansion is not a typical result of this experiment, which has been conducted in several studies using HI listeners. Here, it is assumed that BM processing cannot be expansive, and these data may reflect inappropriate assumptions, for these HI listeners, in the TMC method. However, some studies reported a few listeners were the slopes were higher than one (up to 1.70 in Rosengard *et al.* (2005) and up to 1.56 in Stainsby and Moore (2006)). It remains unclear why substantial expansion was observed. It was not possible to determine a knee point in any of the estimated I/O functions here. As in Jepsen and Dau (2010), the general observation was that I/O functions were different across listeners even though their sensitivity at the tested frequencies was comparable..

Listener	S1	S2	S3
BM compression, 1 kHz	1.34	0.36	2.88
BM compression, 4 kHz	2.01	0.66	0.64

Table 5.2: Estimated BM compression exponents in units of dB/dB

Simulated BM I/O functions, sensitivity and frequency tuning

The dashed curve in Fig. 5.7 shows the DRNL model's I/O function for normal hearing at the corresponding signal frequencies. Following the procedure suggested in Jepsen and Dau (2010), a set of frequency-dependent DRNL parameters (a, b, c and g) was determined, such that the DRNL I/O function fitted the BM I/O data. In the three cases where the estimated compression exponent was higher than one (expansive). There are no psychophysical or physiological data on the literature that suggest expansive BM I/O behavior, so when the present data suggest expansion, the model processing was assumed to be linear. The solid black curves represent the fitted DRNL I/O functions.

The sensitivity loss due to OHC loss ($\mathrm{HL_{OHC}}$) was estimated on the basis of these derived DRNL I/O functions for 0.25, 0.5, 1, 2, 4 and 8 kHz. The values of $\mathrm{HL_{OHC}}$ for the three listeners at 1 and 4 kHz, and the range of estimated $\mathrm{HL_{OHC}}$ over all frequencies are listed in Table 5.3. Values of $\mathrm{HL_{OHC}}$ of ranged from 10 dB to 45 dB. Less compression was reflected by higher values. The IHC loss component ($\mathrm{HL_{IHC}}$)

was assumed to represent the difference between the total sensitivity loss reflected in the audiogram (HL_{TOT}) and HL_{OHC}, i.e., $HL_{IHC} = HL_{TOT} - HL_{OHC}$. The results for each listener at 1 and 4 kHz as well as the range over all frequencies are listed in Table 5.3. The HL_{IHC} estimates are in the range from 0 to 35 dB. Overall, the data suggest that S1 and S3 primarily had lost sensitivity due to OHC loss, while for S2 the sensitivity loss appears distributed equally between OHC and IHC loss. The models fitted to listeners S1, S2 and S3 were named M1, M2 and M3. Pure-tone thresholds were predicted and are indicated by the black symbols in Fig. 5.1. It can be seen that the frequency dependent sensitivity is appropriately accounted for, typically within 10 dB. This was expected since the audiogram was used to determine the value for HL_{IHC}.

Listener	S1	S2	S3
HL_{OHC} at 1 kHz (dB)	35	25	35
HL_{OHC} at 4 kHz (dB)	45	35	35
HL_{OHC} range in filterbank	17-45	10-35	10-45
HL_{IHC} at 1 kHz (dB)	10	20	0
HL_{IHC} at 4 kHz (dB)	10	10	10
HL_{IHC} range in filterbank	0-15	10-35	0-10

Table 5.3: Estimated loss of sensitivity due to OHC and IHC loss in dB. HL_{OHC}-values were obtained from the model's individually fitted I/O function. HL_{IHC} was estimated from the value of HL_{OHC} and the audiogram

Further individual differences were explored by investigating the tuning of the DRNL filters of M1, M2 and M3. The tuning of the filters was represented by iso-intensity response functions in Fig. 5.9. They are shown for four center frequencies (at 0.5, 1, 2 and 4 kHz) and at two different input levels, 30 (dashed) and 70 dB SPL (solid). Such simulated filter tuning was shown to resemble roex filters measured in individual listeners in Jepsen and Dau (2010). The top panel shows the level-dependent DRNL tuning for MNH. The lower input level produced the most sharply tuned response curves. This is a direct consequence of the compression in the model. The filterbank of M1 had completely linear BM processing; the filters were generally broader and had no dependency on level. The DRNL filters of M2 had residual compression. The tuning was thus close to that of the NH model for the highest

level and level-dependency could only be seen at 2 and 4 kHz (at the levels tested here). The filters of M3 were broad and level-independent at 0.5 and 1 kHz, while their relative sharpness increased for the higher center frequencies. Level-dependent tuning was only observed at 4 kHz.

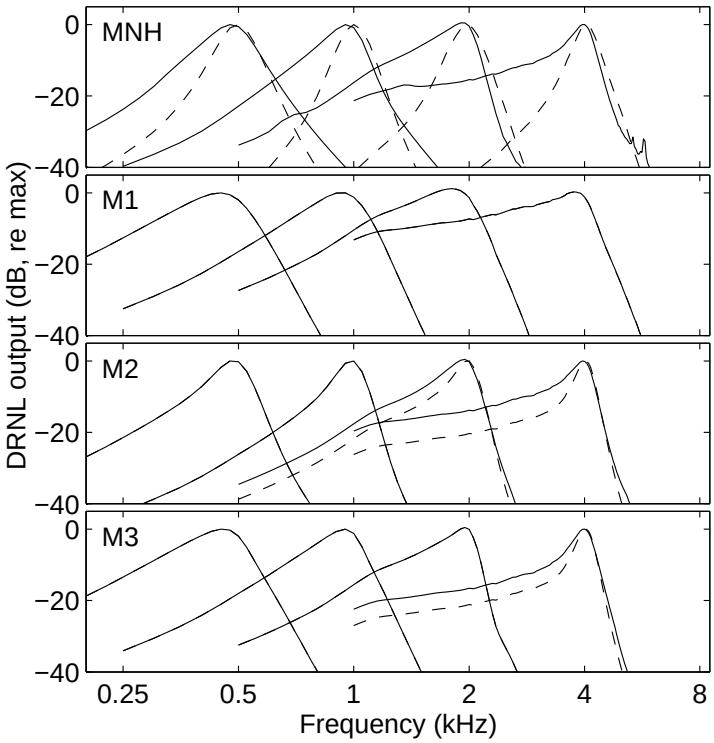

Figure 5.9: Simulated BM tuning for the four models (MNH, M1, M2 and M3). The iso-intensity response functions for DRNL filters are shown for center-frequencies at 0.5, 1, 2 and 4 kHz. The dashed curves were produced from an input level of 30 dB SPL and the solid line from 70 dB SPL. The tip gains are normalized to the corresponding max filter gains.

Simulated internal representations of speech sounds

Figure 5.10 illustrates how the simulated individual BM compression, frequency selectivity and IHC loss affected the processing of the speech signals in the framework of the model. The shown IRs of MNH and three HI models were generated from */daunt/* at a SNR of 10 dB, in a manner similar to those of Fig. 5.5, but here using the individually fitted processing. The IR of MNH is identical to the upper right panel of Fig. 5.3, and was re-plotted here for a better visual comparison. In the IR of M1 it can be observed that the corresponding signal was less resolved in frequency, and the overall amplitude of excitation is reduced (brighter colors). This was expected due to the linear BM processing, and consequently lower sensitivity. For M2 it is clear that most low-frequency (< 500 Hz) information is lost due to the reduced sensitivity in these channels. The frequency resolution for the mid- and high frequencies was higher than for M1. This reflected the simulated residual compression M2. M3 show a stronger excitation compared to M1 and M2, since listener S3 had the mildest hearing loss in terms of sensitivity. The frequency resolution is reduced at least at frequencies below 1 kHz, as expected from Fig. 5.9.

5.4.2 DRT error patterns

Measured error patterns

The human performance in the DRT is presented as the error rate percentage in each of the tested acoustic-phonetic dimensions; VC, NS, ST, SB, GV and CM. They are further resolved in two groups, indicating whether the attribute was present (+) or not (−). The chance level in this task was 50% and is indicated by the dashed horizontal line. The error rates are shown in Fig. 5.11 for the NH listeners and the three HI listeners, represented by the bars. These plots are referred to as DRT error patterns. These error rates also represent the target rates for the model predictions. The data for NH listeners were taken from Messing *et al.* (2009) at the corresponding signal level and SNR (their Fig. 9, panels "70dB SPL 0 dB SNR" and "60dB SPL 10 dB SNR"). They represent mean errors of 6 NH listeners, and the error bars indicate ± one standard deviation (SD) across listeners. For the NH listeners, it can be observed that the dimensions VC−, ST+ and ST− have the highest error rates. The remaining

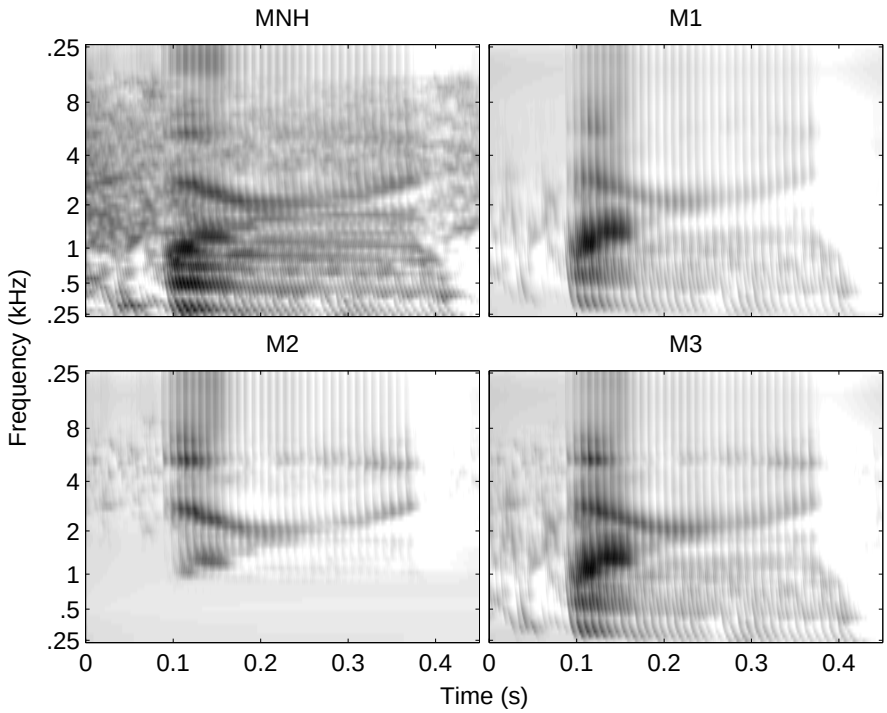

Figure 5.10: Examples of IRs of the four models (MNH, M1, M2 and M3). They were generated from diphone */daunt/* at an SNR of 10 dB.

dimensions typically have error rates below 20% and for NS the error rate is close to zero errors. The general trend was that more errors were produced at the lower SNR (0 dB). According to Messing *et al.* (2009) these error rates are similar to those produced with natural DRT stimuli.

The remaining data were obtained by the three HI listeners of the present study. Here, the error bars indicate $\pm$ one SD across eight diphone repetitions within the listener. Listener S1 clearly produced more errors than the NH listeners at both SNRs. ST+ has the highest amount of errors of about 60%, exceeding chance level.

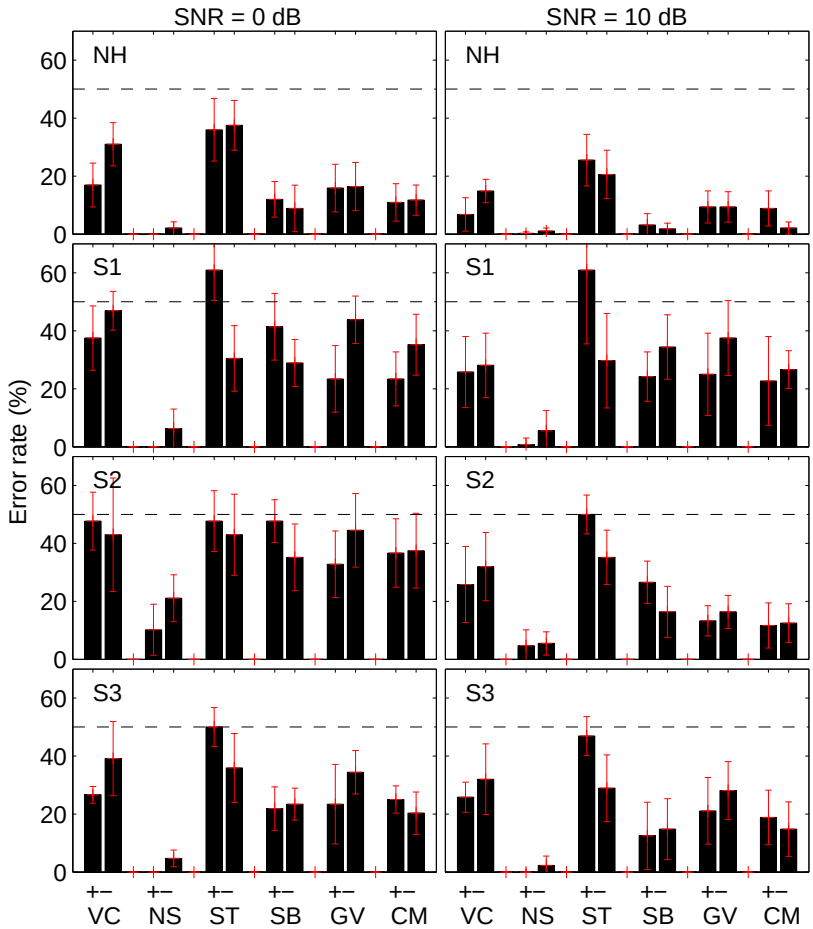

Figure 5.11: Measured error patterns of the DRT at the two SNRs (0 and 10 dB). The bars indicate the error rate in percent in the six acoustic-phonetic dimensions, and $+/-$ indicate if the attribute was present or not. The data in the top row (NH) is re-plotted from Messing *et al.* (2009) in the SNR conditions corresponding to those of the present study. The three remaining rows show data measured in the three HI listeners of the present study. Error bars indicate $\pm$one SD. The horizontal dashed line indicates the chance level at 50%.

For the dimensions VC, SB, GV and CM the amount of errors were about twice of that obtained in the NH listeners or higher. However, this listener showed good

performance in the NS condition. Overall, slightly fewer errors were found at the higher SNR (10 dB). S1 had the worst overall performance among the HI listeners of this study. S2 showed a high error rate (above 30%) in all dimensions at 0 dB SNR, except for NS. At SNR = 10 dB there a substantially fewer errors, so it seems that S2 had a great benefit from the better SNR (except for dimension ST). Interestingly, S2 was the only HI listener producing errors in dimension NS higher than 6%. S3 also shows a benefit from the better SNR, and had the best performance at SNR = 0 dB among the HI listeners.

Simulated error patterns

The predicted error patterns of the models simulating normal hearing (MNH) and individual hearing loss (M1, M2 and M3) are shown in Fig. 5.12. The error bars indicate $\pm$ one SD across three model runs of the DRT. The error rates had a slight variability across runs, since a stochastic decision criterion was used. The SDs were typically within 4%. For MNH at SNR = 0 dB it can be seen that error rates for VC, ST, SB and CM were about 20%. For GV they were about 28%, and for NS the error rates were close to zero. At SNR = 10 dB there were generally about 10% fewer errors with a similar error pattern. Model M1 produced more errors than MNH. At SNR = 0 dB there were about 5-10% more errors for ST, SB and CM, while the other dimensions, VC, NS and GV, had about the same error rate as for MNH. This may indicate that the discrimination cues used in ST, SB and CM are less robust to noise due to supra-thresholds deficits. At SNR = 10 dB there were generally 2-13% more errors than MNH, except for NS where both MNH and M1 produce zero errors. There were slightly fewer errors at the higher SNR. For M2 at SNR = 0 dB there was generally about 20% errors, except for dimension GV which had 32 and 34% errors. At SNR = 10 dB there were fewer errors (up to 11%), especially for NS, SB and GV. M2 was the only model that produced a substantial amount of errors in dimension NS. Model M3 generally had a very low error rates of about 10 to 23% at SNR = 0 dB and 4 to 20% and SNR = 10 dB. In dimension NS there were virtually zero errors. Errors rates were mostly lower than those produced by MNH at both SNRs, which was unexpected. It is unclear whether this reflect unrealistic simulation of degraded

auditory processing, or if the back end needs to be modified to appropriately handle the template matching after degraded auditory processing.

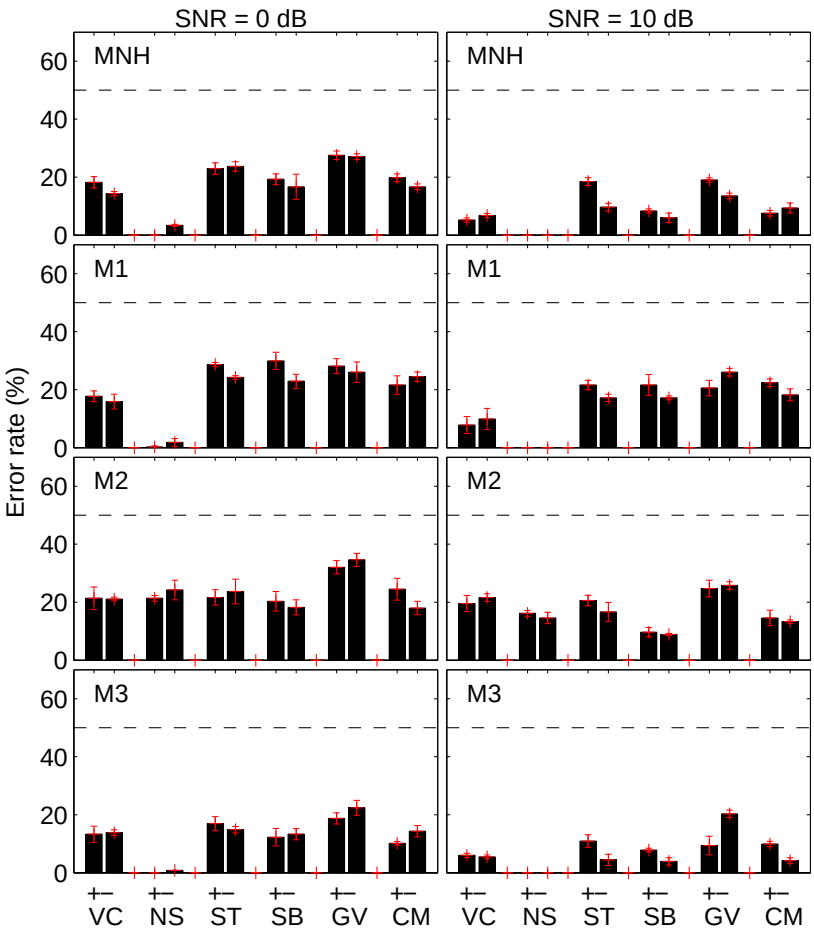

Figure 5.12: Error patterns predicted by the four models (MNH, M1, M2 and M3), corresponding to Fig. 5.11.

Comparison between human and model error patterns

The target error rates of the models were the individual human error rates. A χ^2-statistic was used to evaluate if the match between model and human error rate was significant. This metric was also used in Messing *et al.* (2009). It evaluates whether error rates were statistically similar or different. Lower values of the χ^2-statistic reflect closer matches. If the χ^2-value is lower than a critical value it cannot be rejected that the errors rates are the same. For one degree of freedom these critical value is 3.84 at confidence level of 95%. Here matches within the 95% level were considered good. Figure 5.13 shows the χ^2-values in for the acoustic-phonetic features. Formally these values can only be positive, but here a sign has been added to indicate whether errors were over- or underestimated. Negative values reflect that the model produced too few errors. The critical value is indicated by the horizontal gray lines. The bars were colored black if the values exceeded the critical value. For the two SNR conditions the MNH model produce close matches in most of the acoustic-phonetic dimensions. At the lower SNR (0 dB) for GV- the error were substantially overestimated. For the models simulating hearing imapairment different trends appear. For model M1 the matches are genrerally fair, except for the ST+ dimesnion were the amount of errors were substantially underestimated. This was also the case for the simulated errors by model M3. Model M2 oervall produced a good match at the lower SNR, but at the higher SNR the model generally produced too many errors. The mean χ^2-values (without sign change) for the individual listeners at the two tested SNRs are shown in Table 5.4. If the mean χ^2-value was lower than the critical value (3.84) the simulated error pattern was considered a fair overall match to the data. The mean critical value was lower than the critical value in six of the eight conditions. The two conditions were there was a significant difference was for M2 in the 10-dB SNR condition and for model M3 in the 0-dB SNR condition.

SNR (dB)	MNH − NH	M1 − S1	M2 − S2	M3 − S3
0	3.82	3.78	3.01	6.74
10	2.09	2.52	7.72	3.76

Table 5.4: χ^2-values between measured and predicted error patterns, averaged across acoustic-phonetic features in the DRT.

Error patterns due to reduced sensitivity alone

The error patterns from by the models that only simulate reduced sensitivity (A1, A2 and A3) are compared to those simulating hearing loss due to loss of hair-cells leading to reduced sinsetivity and suprathreshold deficits. In Fig. 5.14error patterns are compared in terms of the error rate difference in percentage points (pp). Zero error rate differences represent perfect matches. Negative bars indicate that simulated supra-threshold deficits contribute to a larger number of errors in the DRT - up to 20% in several cases. For the models simulating the peripheral processing of listener S1 and S2, it is clear that the supra-threhold deficits have a large influence, whereas for models A3 and M3 produce similar amounts of errors. The simulations from the "sensitivity-only" model are compared to the human data in the χ^2 sense and the values are shown in Table 5.5. In none of the conditions the mean χ^2-value falls within the critical limit at 3.84. Thus, the relatively fewer errors produced by the "sensitivity-only" models generally led to unreasonable macthes to the human data. The χ^2-analysis was also used to test whether the error patterns of the two models, simulating each listener, was significantly different (bottom rows of Table 5.5). Significant differences were found in only two of the six conditions (A1/M1 at 10-dB SNR and A2/M2 at 10-dB SNR).

SNR (dB)	A1 − S1	A2 − S2	A3 − S3
0	5.60	5.34	6.79
10	7.26	4.53	6.85
SNR (dB)	A1 − M1	A2 − M2	A3 − M3
0	1.80	2.02	0.53
10	4.19	7.22	0.69

Table 5.5: χ^2-values calculated to evaluate the matches between the "sensitivity-only" models and the human data (top rows), and comparing the two model configurations for the individual listeners (bottom rows)

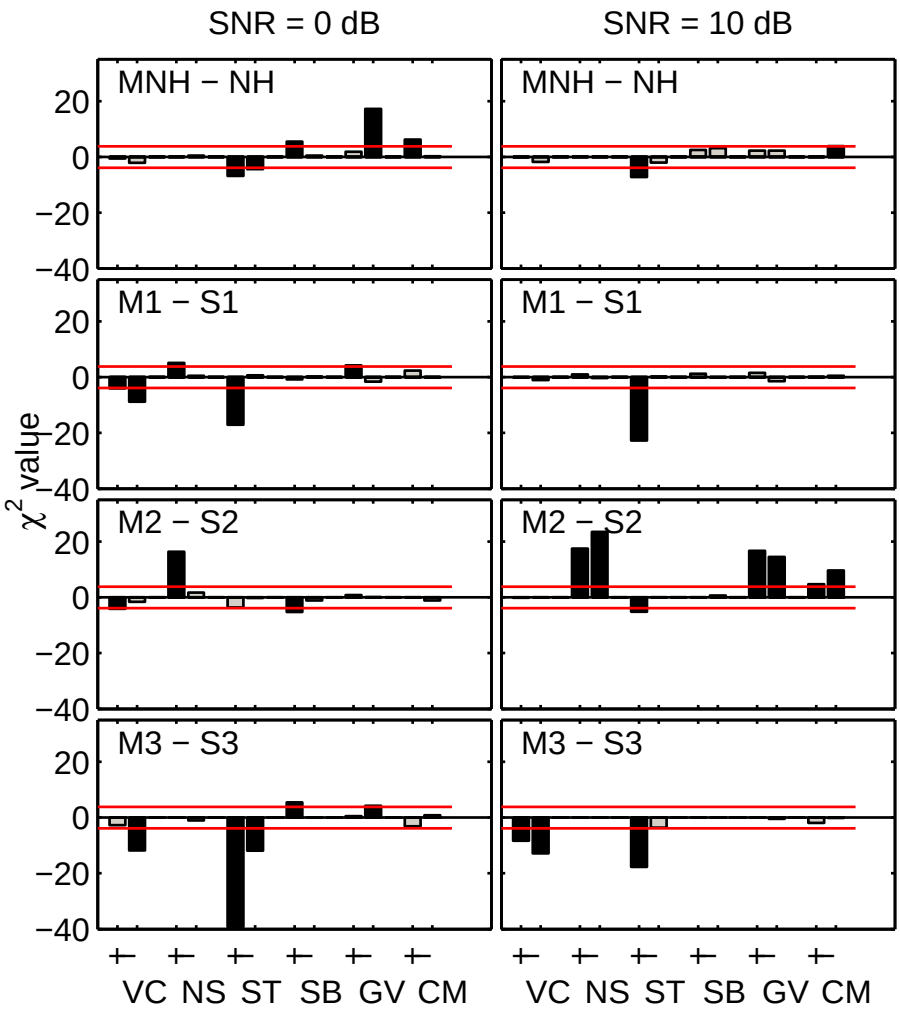

Figure 5.13: The match of predicted and human error rates in terms of χ^2-statistics. Gray bars indicate cases where the value is lower than the critical value (3.84). Black bars indicate cases where the critical value is exceeded. Negative bars reflect that errors are underestimated by the model.

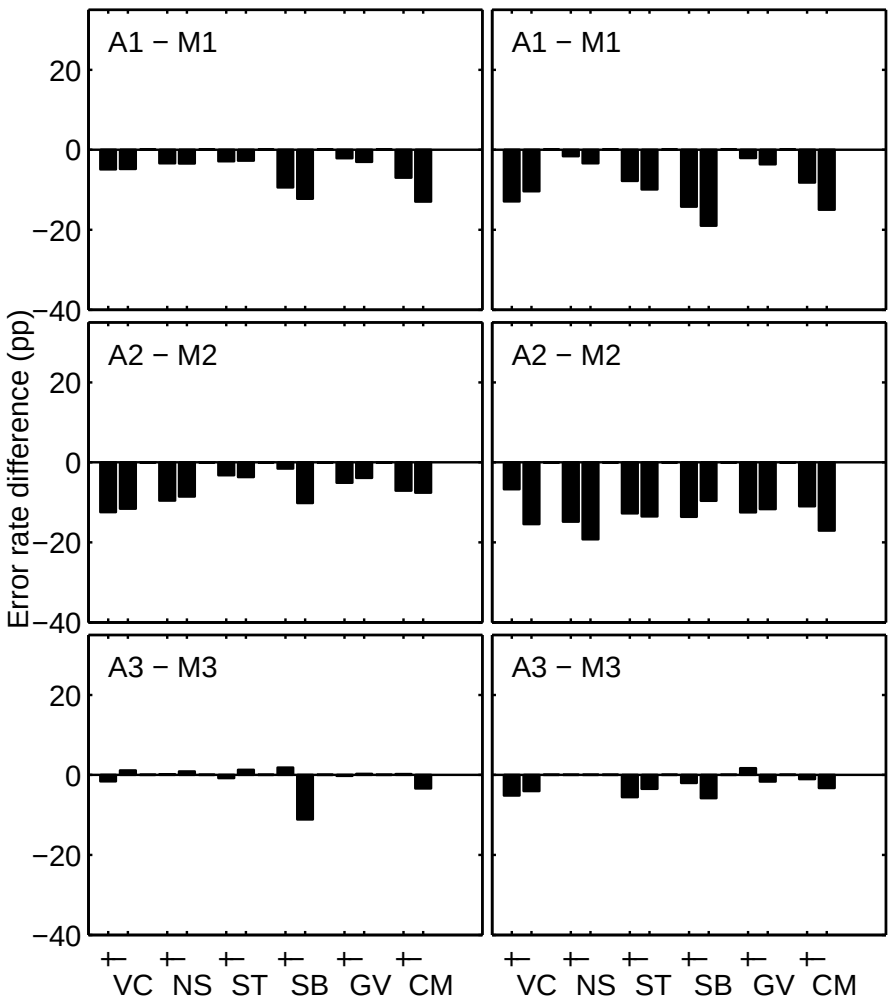

Figure 5.14: Contribution from simulated supra-threshold deficits in terms of the error rate difference in percentage points (pp). Negative bars indicate that simulated supra-treshold effects lead to more errors.

5.5 Discussion

5.5.1 Front-end processing

The predicted error patterns were in reasonable agreement with the measured error patterns, except for a few particular acoustic-phonetic dimensions. This indicates that the front-end processing, which was fitted to the hearing loss of the individual listeners, appropriately simulates internal representations in the hearing-impaired listeners. However, errors rates were systematically underestimated in three particular acoustic-phonetic dimensions. It is yet unclear if this discrepancy is due to inappropriate front-end or back-end processing. Similar results were obtained for NH listeners in Ghitza (1993) and Messing *et al.* (2009). The result of this study is, to the knowledge of the authors, the first time that a relation between speech and non-speech data has been shown in listeners with cochlear hearing loss. The IR reflects aspects of both sensitivity and supra-threshold deficits. The simulated supra-threshold effects are consistent with the current understanding of consequences of cochlear damage, that is, changes in frequency selectivity and temporal resolution. These effects are crucial for describing the variability in results of HI listeners and can presumably not be accounted for by using threshold shaped noise masking of a model of normal hearing (e.g., Holube and Kollmeier, 1996). However, this was not explicitly tested here.

The adaptation stage of the CASP model was crucial in order to account for, among other aspects, temporal masking (Dau *et al.*, 1996a, 1997a; Jepsen *et al.*, 2008). Such effects were not included in the front-end used in Messing *et al.* (2009). Another effect of adaptation was logarithmic compression for stationary inputs, e.g., for the noise used in the present study. This reduced the dynamic range of the response to the noise, and may be effectively similar to the concept of the dynamic range window introduced in Messing *et al.* (2009), which they assigned to simulate efferent control. No stages of efferent effects were considered in the CASP model. However, in terms of the predicted DRT error patterns for NH listeners, the performance of the present model and that of Messing *et al.* are comparable.

It was further found that the prediction using the modulation filterbank was better than using an energy representation (e.g., Dau *et al.*, 1996a). Aspects of, e.g., onset

timing was represented in more detail using the modulation filters and adding up to six modulation filters affected the pattern of errors. Jürgens and Brand (2009) used an earlier version of the CASP model as front-end. They used the first four modulation channels. It is unclear why they did not include filters tuned to higher modulations rates. In other auditory models intended as front-ends for speech intelligibility, the analysis was performed in time-frames. Messing *et al.* (2009) used temporal windows of about 8-12 ms to find the short term average of the output. Jürgens and Brand used down-sampling to get instantaneous output values at every 10 ms (100 Hz). In the present study, the temporal sampling rate of the IRs was 1 kHz, which means that more temporal information, e.g. fine-structure, was preserved at frequencies up to 500 Hz which could be relevant for speech perception.

By using versions of the model that was fitted to the HI listeners, and simulating only loss of sensitivity, it was explored how the simulation of supra-threshold deficits affected the DRT error patterns. It was found, that for the predictions of the data for two out of the three listeners, error rates were substantially underestimated. This indicates that simulation of reduced spectral and temporal resolution does have a considerable influence on the simulations relating to speech perception. In Holube and Kollmeier (1996) they attempted similar explorations, but they did not find large effects of simulating broader filters in their predictions of the data in their speech task. However, they did not include realistic simulation of nonlinear cochlear processing in their model.

5.5.2 Back-end processing

The underlying assumption in the detector was that the dominant source of errors produced by the model was due to insufficient information to discriminate a diphone pair, after front-end processing. The use of the synthesized DRT stimuli, combined with the template matching paradigm, allowed this assumption. However, due to the adaptation stage in the CASP model the IR depends on the previous samples over an interval of 500 ms. However, it is likely that this side-effect does not influence the predicted error rate, since major contributions to the calculated MSEs were within the time-range of the initial consonant. The contribution from the last 200 ms of the IRs to the ΔMSEs was in the range from 0 to 6%.

It remains unclear at which SNR the template should be generated. In previous studies using the CASP model to predict masking and discrimination data, the SNR of the template was usually at a high SNR compared to the expected detection threshold. Here, a SNR of 5 dB, thus between the two tested SNRs (0 and 10 dB) was chosen, similarly to Messing *et al.* (2009) who found this to be the optimal choice. This may not necessarily be optimal using the CASP model as the front end.

Jürgens and Brand (2009) used perfect *a priori* knowledge of the stimuli to obtain the best matches to human performance, that is, templates were derived from signals identical to the test stimuli. They used naturally uttered nonsense logatoms. In order to account for the variations in the stimuli they used a dynamic time-warp stage in their detector. This stage may introduce some errors, due to time-compression or expansion and it is not possible to separate if predicted confusion errors are due to this stage or the front-end. Also, information about timing differences, which may aid detection, was lost in the dynamic time-warp stage. Timing cues are of great importance in discriminating consonants (e.g., Régnier and Allen, 2008).

5.5.3 Limitations of the approach

The results obtained here with synthesized stimuli are useful, since front end and back end were clearly separated. The experimental data do not reflect aspect of natural variations of uttered diphones. These variations depend on, e.g., speaker differences, co-articulation etc. The current detector cannot account for these variations in time and frequency. Future studies should address this issue.

Here, templates were derived from signals embedded in noise. If it is assumed that human observers have stored templates of speech sounds, they may be "clean" or there may be several templates representing a broad range of speech sounds at different SNRs. It is also a question whether hearing-impaired listeners have templates reflecting a normally functioning periphery, or if they adjust templates over time due to their degraded representations (neural plasticity). The listeners here had hearing losses since early childhood, and templates were derived from their individual impaired auditory processing.

The error rates of the VC−, ST+ and ST− dimensions were substantially underestimated. This was also a general problem in the model predictions of

Messing *et al.* (2009). These are also the conditions where the NH listeners showed substantially worse performance in the DRT using synthetic diphones, compared to natural diphones (Messing *et al.*, 2009). The missing capability to predict these error rates may reflect that the detector of the present model is too sensitive to timing cues. Voicing and sustention are the features which primarily depend on timing-differences in a minimal pair, while the remaining features depend more on spectral or spectro-temporal differences. It is unclear if the human observers can use a timing precision of about 1 ms in their decision, although the information may be available in the peripheral representation.

5.6 Conclusions

- Cochlear hearing loss in three individual listeners were characterized due to their audiograms and estimated basilar-membrane I/O functions. The parameters of the cochlear stage of the CASP model were fitted to these data. The model was then used as a front end in a speech detector system.

- The model with individualized front-ends could predict most aspects of DRT error patterns measured in the same listeners, except for a few particular conditions were DRT error rates are substantially underestimated by the model. Since the modeling framework could separate front-end and back-end errors, the capability of the model to predict the error patterns shows that there is a relation between the limited auditory function, characterized on the basis of non-speech data, and speech perception.

- There were considerable differences between the predicted error patterns by the suggested model and a model that was designed to only simulate reduced sensitivity in the individuals.

- The suggested framework, combining the CASP front end with the back end based on synthetic DRT stimuli, might be interesting in applications, e.g., to objectively assess the perceptual implications of signal processing algorithms of hearing aids in HI listeners.

6

General discussion

In this thesis, a model was proposed that simulates auditory signal processing and perception. This model was first developed to simulate the normally functioning auditory system. The focus was to include a realistic cochlear processing stage into an existing modeling framework that assumed linear processing at this stage. Second, it was shown how consequences of individual cochlear hearing impairment can be characterized experimentally and accounted for by the model. Third, the peripheral part of the model was used as a front-end in a speech recognizer designed for consonant discrimination. It was shown that the model using individually fitted front-end parameters can account for many characteristics of the individual error patterns in the data from hearing-impaired (HI) listeners.

The computational auditory signal-processing and perception (CASP) model was shown to account for various data from psychoacoustic detection and masking experiments (Chapter 2). The inclusion of the nonlinear basilar-membrane (BM) stage increased the predictive power of the model, particularly in conditions where the results are affected by the level-dependent cochlear processing, such as spectral-masking patterns and forward masking. This was an important result since previous studies had raised concerns about the combination of the compressive cochlear stage and the subsequent adaptation stage assumed in the model framework (Derleth *et al.*, 2001). Here, it was shown that there was no principal limitation in combining the two stages; however, it was necessary to include a stage of level-independent expansion to account for the data in the tested experimental conditions, particularly in forward masking. Another key finding was that intensity discrimination data could be accounted for. The question was whether the compressive properties of the BM stage would results in an underestimation of intensity JNDs. However, intensity discrimination data were accurately accounted for, since the linear off-frequency

processing in neighboring channels of the cochlear filterbank model dominates the processing in this task within the model, since off-frequency channels realize a logarithmic compression. This results in JNDs of approximately 1 dB. The model was further modified in the modulation processing stage, where the sensitivity to high modulation rates (above 150 Hz) was reduced by a lowpass filter prior to the modulation filterbank stage. Here, it was shown that the model's ability to account for temporal modulation transfer functions in narrowband and wideband carriers was preserved, at least for modulation rates at up to 250 Hz.

In Chapter 4, perceptual consequences of cochlear hearing loss including sensitivity and supra-threshold limitations, were considered in individual listeners. For ten HI listeners, an individual parameter-set for the cochlear stage of the CASP model was derived, based on the experimental estimates of BM I/O functions and the audiogram. Individual frequency-specific estimates of the effect of outer hair-cell (OHC) and inner hair-cell (IHC) loss on sensitivity were obtained. One key finding was that these estimates varied largely across listeners, and could not be predicted based on the audiogram alone. Within the model, a reduced or lost BM compression associated with OHC loss had direct consequences for BM tuning. It was shown that the model could account for individual frequency selectivity as measured independently in all listeners, even though some systematic discrepancy was found at one tested frequency. The model successfully accounted for the individual thresholds in simultaneous- and forward masking conditions. The results indicate that individual BM I/O behavior combined with the audiogram provide sufficient information about cochlear hearing loss to describe the tested supra-threshold effects.

The experimental characterization of BM I/O functions in Chapter 4 showed that stable estimates of BM compression as well as the I/O-function knee point are useful quantities in order to simulate individual cochlear hearing loss. Chapter 3 described an attempt to extend the growth-of-masking (GOM) experiment (Oxenham and Plack, 1997). It was shown that the knee point of the BM I/O function could be accurately estimated with the modified paradigm in addition to estimating the amount of BM compression. The results demonstrated that an estimate of the BM I/O function could be estimated for a wider range of input levels than in the case of the original method by using two different masker-signal interval conditions. The within-

listener variability in the data was small compared to that found previously in the alternative temporal masking curve (TMC) method (Nelson *et al.*, 2001; Rosengard *et al.*, 2005). The extended GOM method thus represents a method of estimating BM I/O-functions which produces robust data. However, the capability to accurately estimate knee point depends on the appropriate choice of masker-signal interval in a particular experimental condition. For NH listeners, the knee point estimate was obtained with a constant masker-signal interval. For HI listeners, however, the choice of masker-signal interval should be chosen individually for measured ears, based on pilot experiments. The suggested method could have been used to obtain the BM I/O functions in Chapter 4, but it was decided to use the established and commonly used TMC method (Nelson *et al.*, 2001), since it was not yet explicitly shown if more stable results could be obtained in HI listeners with the new method. Furthermore the method of Chapter 3 required more testing time compared to the TMC method.

The results reported in Chapter 5 showed that consonant discrimination error patterns were mostly accounted for using auditory processing front-end that had been fitted to individual cochlear hearing loss. The model's back-end and the synthetic speech stimuli were designed such that front-end and back-end errors were separated. Otherwise it would not have been possible to assign consonant discrimination error patterns to the degraded auditory processing in the models describing hearing loss. The results indicated that it is possible to use a model of detailed auditory preprocessing as a front-end in an speech intelligibility application. The results further indicated that there is a relation between the performances of individual HI listeners in speech versus non-speech perception tasks. However, for three particular acoustic-phonetic feature dimensions the errors were substantially underestimated both for MNH and the three model of hearing impairment. It is still unclear exactly why this is the case, but the back end of the model may be too sensitive to timing cues which are important in these partilar dimensions. The current findings support that supra-thresholds consequences of cochlear damage are crucial to speech perception, and that audibility alone cannot be expected to explain degraded speech perception in HI listeners. In future studies, back-ends which can handle natural speech stimuli (instead of the synthesized stimuli considered here) may lead to models that account for data in a broader selection of speech materials.

The modeling framework suggested in this thesis may be interesting and useful for applications, such as systems which objectively assess speech intelligibility or audio quality, as perceived by hearing-impaired listeners. For example, new compensation strategies or signal-processing algorithms in hearing aids (HA) could be tested in a carefully designed system to give rough estimates of the outcome of listening tests, which are otherwise expensive and time-consuming. A scheme for the objective assessment of the effect of hearing-aid processing is suggested in Fig. 6.1. Consider an assessment system where the model, with a back-end (such as an optimal detector or speech recognizer), can account for some data (non-speech, speech intelligibility, sound quality etc.) from both NH listeners and a HI listener. If hearing-aid processing is introduced prior to the model representing the impaired periphery of the HI listeners, the implications of the HA processing can be observed at the output of the complete model. The outcome could then be compared to that of the model of normal hearing. The HA processing could subsequently be adjusted to match the performance of the NH model or to further reduce errors, e.g., in consonant discrimination error patterns (see, e.g., Chapter 5). Subjective testing cannot be expected to be completely replaced, but objective assessment tools may provide useful estimates of the effects of distortions and improvements resulting from the tested algorithms. Some of the experiments considered in this thesis to characterize individual hearing loss are time-consuming. Thus, the suggested framework is probably not applicable to HA fitting in individual patients. However, for research and development purposes, the experiments presented here should not necessarily be repeated, since the current modeling framework, including the results of this thesis, already provides parameter-sets to describe a variety of HI listeners. These may comprise a representative sample of current or potential hearing-aid users.

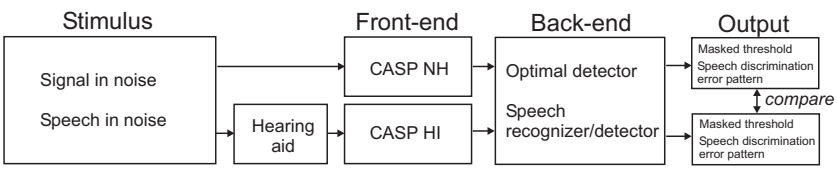

Figure 6.1: Example of a scheme to test perceptual implications of hearing-aid processing, using the auditory processing model framework suggested in this thesis

References

ANSI (**1969**). “S3.5-1969: Methods for calculation of the articulation index,” American National Standards Institute, New York .

ANSI (**1997**). “S3.5-1997: Methods for calculation of the speech intelligibility index,” American National Standards Institute, New York .

Bacon, S. P., and Gleitman, R. M. (**1992**). “Modulation detection in subjects with relatively flat hearing losses,” J. Speech Hear. Res. **35**, 642– 653.

Bacon, S. P., and Grantham, D. W. (**1989**). “Modulation masking: Effects of modulation frequency, depth and phase,” J. Acoust. Soc. Am. **85**, 2575–2580.

Bacon, S. P., and Viemeister, N. F. (**1985**). “Temporal modulation transfer functions in normal-hearing and hearing-impaired listeners,” Audiology **24**, 117–134.

Borg, E., and Engström, B. (**1989**). “Noise level, inner hair cell damage, audiometric features, and equal-energy hypothesis,” J. Acoust. Soc. Am. **86**, 1776–1782.

Breebaart, J., van de Par, S., and Kohlrausch, A. (**2001a**). “Binaural processing model based on contralateral inhibition. I. Model structure.,” J. Acoust. Soc. Am. **110**, 1074–1088.

Breebaart, J., van de Par, S., and Kohlrausch, A. (**2001b**). “Binaural processing model based on contralateral inhibition. II. Dependence on spectral parameters.,” J. Acoust. Soc. Am. **110**, 1089–1104.

Breebaart, J., van de Par, S., and Kohlrausch, A. (**2001c**). “Binaural processing model based on contralateral inhibition. III. Dependence on temporal parameters.,” J. Acoust. Soc. Am. **110**, 1105–1117.

Bruce, I. C., Sachs, M. B., and Young, E. D. (**2003**). “An auditory-periphery model of the effects of acoustic trauma on auditory nerve responses,” J. Acoust. Soc. Am. **113**, 369–388.

Buchholz, J. M., and Mourjoloulus, J. (**2004a**). "A computational auditory masking model based on signal dependent compression. I. Model description and performance analysis," Acustica - Acta Acustica **5**, 873–886.

Buchholz, J. M., and Mourjoloulus, J. (**2004b**). "A computational auditory masking model based on signal dependent compression. II. Model simulations and analytical approximations," Acustica - Acta Acustica **5**, 887–900.

Burns, E. M., and Viemeister, N. F. (**1981**). "Played-again SAM: Further observations on the pitch of amplitude-modulated noise," J. Acoust. Soc. Am. **70**, 1655–1660.

Carlyon, R. P., and Shamma, S. (**2003**). "An account of monaural phase sensitivity," J. Acoust. Soc. Am. **114**, 333–348.

Carney, L. H., Heinz, M. G., Evilsizer, M. E., Gilkey, R. H., and Colburn, H. S. (**2002**). "Auditory phase opponency: A temporal model for masked detection at low frequencies," Acta. Acust. Acust. **88**, 334–347.

Carney, L. H. (**1993**). "A model for the responses of low-frequency auditory-nerve fibers in cat," J. Acoust. Soc. Am. **93**, 401–417.

Chi, T., Gao, Y., Guyton, M. C., Ru, P., and Shamma, S. (**1999**). "Spectro-temporal modulation transfer functions and speech intelligibility," J. Acoust. Soc. Am. **106**, 2719–2732.

Colburn, H. S., Carney, L. H., and Heinz, M. G. (**2003**). "Quantifying the information in auditory-nerve responses for level discrimination," J. Assoc. Res. in Otolaryngology **4**, 294–311.

Dau, T., Puschel, D., and Kohlrausch, A. (**1996a**). "A quantitative model of the effective signal processing in the auditory system. I. Model structure," J. Acoust. Soc. Am. **99**, 3615–3622.

Dau, T., Puschel, D., and Kohlrausch, A. (**1996b**). "A quantitative model of the effective signal processing in the auditory system. II. Simulations and measurements," J. Acoust. Soc. Am. **99**, 3623–3631.

Dau, T., Kollmeier, B., and Kohlrausch, A. (**1997a**). "Modeling auditory processing of amplitude modulation. I. Detection and masking with narrow-band carriers," J. Acoust. Soc. Am. **102**, 2892–2905.

Dau, T., Kollmeier, B., and Kohlrausch, A. (**1997b**). "Modeling auditory processing of amplitude modulation. II. Spectral and temporal integration," J. Acoust. Soc. Am. **102**, 2906–2919.

de Charms, R. C., Blake, D. T., and Merzenich, M. M. (**1998**). “Optimizing sound features for cortical neurons,” Science **280(5368)**, 1439–1443.

Deng, L., and Geisler, C. D. (**1987**). “A composite auditory model for processing speech sounds,” J. Acoust. Soc. Am. **82**, 2001–2012.

Derleth, R. P., and Dau, T. (**2000**). “On the role of envelope fluctuation processing in spectral masking,” J. Acoust. Soc. Am. **108**, 285–296.

Derleth, R. P., Dau, T., and Kollmeier, B. (**2001**). “Modeling temporal and compressive properties of the normal and impaired auditory system,” Hear. Res. **159**, 132–149.

Dicke, U., Ewert, S. D., Dau, T., and Kollmeier, B. (**2007**). “A neural circuit transforming temporal periodicity information into a rate-based representation in the mammalian auditory system.,” J. Acoust. Soc. Am. **121**, 310–326.

Dubno, J. R., Horwitz, A. R., and Ahlstrom, J. B. (**2007**). “Estimates of Basilar-Membrane Nonlinearity Effects on Masking of Tones and Speech,” Ear and Hearing **28**, 2–17.

Elhilali, M., Chi, T., and Shamma, S. (**2003**). “A spectro-temporal modulation index (STMI) for assessment of speech intelligibility,” Speech Commun. **41**, 331–348.

Ewert, S. D., and Dau, T. (**2000**). “Characterizing frequency selectivity for envelope fluctuations,” J. Acoust. Soc. Am. **108**, 1181–1196.

Ewert, S. D., and Dau, T. (**2004**). “External and internal limitations in amplitude-modulation processing,” J. Acoust. Soc. Am. **116**, 478–490.

Ewert, S. D., Verhey, J. L., and Dau, T. (**2002**). “Spectro-temporal processing in the envelope-frequency domain,” J. Acoust. Soc. Am. **112**, 2921–2931.

Ewert, S. D., Hau, O., and Dau, T. (**2007**). “Forward Masking: Temporal Integration or Adaptation?,” in *Hearing - From Sensory Processing to Perception*, edited by Kollmeier, B., Klump, G., Hohmann, V., Langemann, U., Mauermann, M., Uppenkamp, S., and Verhey, J. (Springer-Verlag, Berlin) , 165–174.

Fitzgerald, M. B., and Wright, B. A. (**2005**). “A perceptual learning investigation of the pitch elicited by amplitude-modulated noise,” J. Acoust. Soc. Am. **118**, 3794–3803.

Florentine, M., and Buus, S. (**1984**). “Temporal gap detection in sensorineural and simulated hearing impairments.,” J. Speech and Hear. Res. **27**, 449–455.

Florentine, M., Fastl, H., and Buus, S. (**1988**). "Temporal integration in normal hearing, cochlear impairment, and impairment simulated by masking," J. Acoust. Soc. Am. **84**, 195–203.

Florentine, M., Reed, C. M., Rabinowitz, W. M., Braida, L. D., Durlach, N. I., and Buus, S. (**1993**). "Intensity perception. XIV. Intensity discrimination in listeners with sensorineural hearing loss," J. Acoust. Soc. Am. **94**, 2575–2586.

Formby, C. C. (**1987**). "Modulation threshold functions for chronically impaired Ménière patients," Audiology **26**, 89–102.

Ghitza, O. (**1993**). "Adequacy of auditory models to predict human internal representation of speech sounds," J. Acoust. Soc. Am. **93**, 2160–2171.

Glasberg, B. R., and Moore, B. C. J. (**1990**). "Derivation of auditory filter shapes from notched-noise data," Hear. Res. **47**, 103–138.

Glasberg, B. R., Moore, B. C. J., and Bacon, S. P. (**1987**). "Gap detection and masking in hearing-impaired and normal-hearing subjects," J. Acoust. Soc. Am. **81**, 1546–1556.

Gockel, H., Moore, B. C. J., and Patterson, R. D. (**2002**). "Asymmetry of masking between complex tones and noise: The role of temporal structure and peripheral compression," J. Acoust. Soc. Am. **111**, 2759–2770.

Goldstein, J. L. (**1990**). "Modeling rapid waveform compression on the basilar membrane as multiple-bandpass-nonlinearity filtering," Hear.Res. **49**, 39–60.

Goode, R. L., Killion, M. L., Nakamura, K., and Nishihara, S. (**1994**). "New knowledge about the function of the human middle ear: development of an improved analogue model," Am. J. Otol. **15**, 145–154.

Green, D. M., and Swets, J. (**1966**). *Signal Detection Theory and Psychophysics*. Wiley, New York.

Hall, J. L. (**1997**). "Asymmetry of masking revisited: generalization of masker and probe bandwidth," J. Acoust. Soc. Am. **101**, 1023–1033.

Hansen, M., and Kollmeier, B. (**1999**). "Continuous assessment of time-varying speech quality," J. Acoust. Soc. Am. **106**, 2888–2899.

Hansen, M., and Kollmeier, B. (**2000**). "Objective modeling of speech quality with a psychoacoustically validated auditory model," J. Audio Eng. Soc. **48**, 395–409.

Harrison, R. V., and Evans, E. F. (**1979**). "Some aspects of temporal coding by single cochlear fibres from regions of cochlear hair cell degeneration in the guinea pig," Arch. Otolaryngol. **224**, 71–78.

Heinz, M., and Swaminathan, J. (**2009**). "Quantifying envelope and fine-structure coding in auditory-nerve responses to chimaeric speech," J. Assoc. Res. Otolaryngology **10**, 407–423.

Heinz, M. G., and Young, E. D. (**2004**). "Response Growth With Sound Level in Auditory-Nerve Fibers After Noise-Induced Hearing Loss," J. Neurophysiol. **91**, 784–795.

Heinz, M. G., Colburn, H. S., and Carney, L. H. (**2001a**). "Evaluating auditory performance limits: I. One-parameter discrimination using a computational model for the auditory nerve," Neural Comp. **13**, 2273–2316.

Heinz, M. G., Colburn, H. S., and Carney, L. H. (**2001b**). "Rate and timing cues associated with the cochlear amplifier: Level discrimination based on monaural cross-frequency coincidence detection," J. Acoust. Soc. Am. **100**, 2065–2084.

Heinz, M. G., Zhang, X., Bruce, I. C., and Carney, L. H. (**2001c**). "Auditory nerve model for predicting performance limits of normal and impaired listeners," Acoust.Res. letters online **2**, 91–96.

Heinz, M. G., Colburn, H. S., and Carney, L. H. (**2002**). "Quantifying the implications of nonlinear cochlear tuning for auditory-filter estimates," J. Acoust. Soc. Am. **111**, 996–1011.

Hellman, R. P. (**1972**). "Asymmetry of masking between noise and tone," Percept. Psychophys. **11**, 241–246.

Hewitt, M. J., and Meddis, R. (**1994**). "A computer model of amplitude-modulation sensitivity of single units in the inferior colliculus," J. Acoust. Soc. Am. **95**, 2145–2159.

Holube, I., and Kollmeier, B. (**1996**). "Speech intelligibility prediction in hearing-impaired listeners based on a psychoacoustically motivated perception model," J. Acoust. Soc. Am. **100**, 1703–1716.

Houtgast, T. (**1989**). "Frequency selectivity in amplitude-modulation detection," J. Acoust. Soc. Am. **85**, 1676–1680.

Houtsma, A. J. M., Durlach, N. I., and Braida, L. D. (**1980**). "Intensity perception. XI. Experimental results on the relation of intensity resolution to loudness matching," J. Acoust. Soc. Am. **68**, 807–813.

Huber, R., and Kollmeier, B. (**2006**). “PEMO-Q - a new method for objective audio quality assessment using a model of auditory perception,” IEEE Trans. Audio, Speech and Lang. Proc. **14**, 1902–1911.

Humes, L. E., Dirks, D. D., Bell, T. S., Ahlstrom, C., and Kincaid, G. E. (**1986**). “Application of the articulation index and speech transmission index to the recognition of speech by the normal-hearing and hearing-impaired,” J. Speech Hear. Res **29**, 447–462.

Irino, T., and Patterson, R. D. (**2006**). “Dynamic, compressive gammachirp auditory filterbank forperceptual signal processing,” IEEE Intl. Conf. Acoust., Speech and Signal Proc. **V**, 133–136.

Jepsen, M. L., and Dau, T. (**2008**). “Estimating the basilar-membrane input-output function in normal-hearing and hearing-impaired listeners using forward masking,” J. Acoust. Soc. Am. **123**, 3859.

Jepsen, M. L., and Dau, T. (**2010**). “Characterizing auditory processing and perception in individual listeners with sensorineural hearing loss,” J. Acoust. Soc. Am. **-**, Submitted.

Jepsen, M. L., Ewert, S. D., and Dau, T. (**2008**). “A computational model of human auditory signal processing and perception,” J. Acoust. Soc. Am. **124**, 422–438.

Jesteadt, W., Bacon, S. P., and Lehman, J. R. (**1982**). “Forward masking as a function of frequency, masker level, and signal delay,” J. Acoust. Soc. Am. **71**, 950–962.

Jürgens, T., and Brand, T. (**2009**). “Microscopic prediction of speech recognition for listeners with normal hearing in noise using an auditory model,” J. Acoust. Soc. Am. **126**, 2635–2648.

Kates, J. M. (**1991**). “A time-domain digital cochlear model,” IEEE Trans. Signal Process. **39**, 2573–2592.

Kohlrausch, A., Fassel, R., and Dau, T. (**2000**). “The influence of carrier level and frequency on modulation and beat-detection thresholds for sinusoidal carriers,” J. Acoust. Soc. Am. **108**, 723–734.

Kryter, K. D. (**1962**). “Methods for calculation and use of articulation index,” J. Acoust. Soc. Am. **34**, 1689–1697.

Langner, G., and Schreiner, C. (**1988**). “Periodicity coding in the inferior colliculus of the cat. I. Neuronal mechanism,",” J. Neurophysiol. **60**, 1799–1822.

Langner, G. (**1981**). "Neuronal mechanisms for pitch analysis in the time domain," Exp. Brain Res. **44**, 450–454.

Langner, G. (**1992**). "Periodicity coding in the auditory system," Hear. Res. **60**, 115–142.

Lee, J., and Bacon, S. P. (**1997**). "Amplitude modulation depth discrimination of a sinusoidal carrier: effect of stimulus duration.," J. Acoust. Soc. Am. **101**, 3688–3693.

Liberman, M. C., and Dodds, L. W. (**1984**). "Single-neuron labeling and chronic cochlear pathology. III. Stereocilia damage and alterations of threshold tuning curves," Hear. Res. **16**, 55–74.

Loeb, G. E., White, M. W., and Merzenich, M. M. (**1983**). "Spatial cross-correlation. A proposed mechanism for acoustic speech perception," Biol. Cybern. **47**, 149–163.

Lopez-Poveda, E. A., and Meddis, R. (**2001**). "A human nonlinear cochlear filterbank.," J. Acoust. Soc. Am. **110**, 3107–3118.

Lopez-Poveda, E. A., Plack, C. J., and Meddis, R. (**2003**). "Cochlear nonlinearity between 500 and 8000 Hz in listeners with normal hearing," J. Acoust. Soc. Am. **113**, 951–960.

Lopez-Poveda, E. A., Plack, C. J., Meddis, R., and Blanco, J. L. (**2005**). "Cochlear compression in listeners with moderate sensorineural hearing loss," Hear. Res. **205**, 172–183.

Lopez-Poveda, E. A., Johannesen, P. T., and Merchán, M. A. (**2009**). "Estimation of the degree of inner and outer hair cell dysfunction from distortion product otoacoustic emission input/output functions," Audiological Medicine **7**, 22–28.

Lorenzi, C., Gilbert, G., Carn, H., Garnier, S., and Moore, B. C. J. (**2006**). "Speech perception problems of the hearing impaired reflect inability to use temporal fine structure," Proc. Natl. Acad. Sci. USA **103**, 18866–18869.

Lunner, T. (**2003**). "Cognitive function in relation to hearing aid use," Int. J. Audiol. **42**, S49–58.

Meddis, R., and O'Mard, L. P. (**2005**). "A computer model of the auditory-nerve response to forward-masking stimuli," J. Acoust. Soc. Am. **117**, 3787–3798.

Meddis, R., O'Mard, L. P., and Lopez-Poveda, E. A. (**2001**). "A computational algorithm for computing nonlinear auditory frequency selectivity," J. Acoust. Soc. Am. **109**, 2852–2861.

Messing, D. P., Delhorne, L., Bruckert, E., Braida, L. D., and Ghitza, O. (**2009**). "A non-linear efferent-inspired model of the auditory system; matching human confusions in stationary noise," Speech Commun. **51**, 668–683.

Miller, G. A., and Nicely, P. E. (**1955**). "An analysis of perceptual confusions among some english consonants," J. Acoust. Soc. Am. **27**, 338–352.

Miller, R. L., Schilling, J. R., Franck, K., and Young, E. D. (**1997**). "Effects of acoustic trauma on the representation of the vowel / / in cat auditory nerve fibers," J. Acoust. Soc. Am. **101**, 3602Ű3616.

Miller, G. A. (**1947**). "Sensitivity to changes in the intensity of white noise and its relation to masking and loudness," J. Acoust. Soc. Am. **19**, 609–619.

Moore, B. C. J., and Glasberg, B. R. (**1987**). "Factors affecting thresholds for sinusoidal signals in narrow-band maskers with fluctuating envelopes," J. Acoust. Soc. Am. **82**, 69–79.

Moore, B. C. J., and Glasberg, B. R. (**2003**). "Behavioural measurement of level-dependent shifts in the vibration pattern on the basilar membrane at 1 and 2 kHz," Hear. Res. **175**, 66–74.

Moore, B. C. J., Glasberg, B. R., Plack, C. J., and Biswas, A. K. (**1988**). "The shape of the ear's temporal window," J. Acoust. Soc. Am. **83**, 1102–1116.

Moore, B. C. J., Alcantara, J. I., and Dau, T. (**1998**). "Masking patterns for sinusoidal and narrow-band noise maskers," J. Acoust. Soc. Am. **104**, 1023–1038.

Moore, B. C. J., Vickers, D. A., Plack, C. J., and Oxenham, A. J. (**1999**). "Inter-relationship between different psychoacoustic measures assumed to be related to the cochlear active mechanism," J. Acoust. Soc. Am. **106**, 2761–2778.

Moore, B. C. J. (**1995**). *Perceptual Consequences of Cochlear Damage*. Oxford University Press, New York.

Moore, B. C. J. (**1996**). "Perceptual consequences of cochlear hearing loss and their implications for the design of hearing aids.," Ear Hear. **17**, 133–161.

Moore, B. C. J. (**2007**). *Cochlear hearing loss*. pp. 29-37, Wiley, New York.

Muller, M., Robertson, D., and Yates, G. K. (**1991**). "Rate-versus-level functions of primary auditory nerve fibres: evidence for square law behaviour of all fibre categories in the guinea pig," Hear. Res. **55**, 50–56.

Nelson, P. C., and Carney, L. H. (**2004**). "A phenomenological model of peripheral and central neural responses to amplitude-modulated tones," J. Acoust. Soc. Am. **116**, 2173–2186.

Nelson, D. A., and Schroder, A. (**2004**). "Peripheral compression as a function of stimulus level and frequency region in normal-hearing listeners," J. Acoust. Soc. Am. **115**, 2221–2233.

Nelson, D. A., and Swain, A. (**1996**). "Temporal resolution within the upper accessory excitation of a masker," Acustica - Acta Acustica **82**, 328–334.

Nelson, D. A., Schroder, A. C., and Wojtczak, M. (**2001**). "A new procedure for measuring peripheral compression in normal-hearing and hearing-impaired listeners," J. Acoust. Soc. Am. **110**, 2045–2064.

Oxenham, A. J., and Moore, B. C. J. (**1994**). "Modeling the additivity of nonsimultaneous masking," Hear. Res. **80**, 105–118.

Oxenham, A. J., and Plack, C. J. (**1997**). "A behavioral measure of basilar-membrane nonlinearity in listeners with normal and impaired hearing," J. Acoust. Soc. Am. **101**, 3666–3675.

Oxenham, A. J., and Plack, C. J. (**2000**). "Effects of masker frequency and duration in forward masking: further evidence for the influence of peripheral nonlinearity," Hear. Res. **150**, 258–266.

Oxenham, A. J., and Shera, C. A. (**2003**). "Estimates of Human Cochlear Tuning at Low Levels Using Forward and Simultaneous Masking," J. Assoc. Res. Otolaryngology **4**, 541–554.

Oxenham, A. J., Moore, B. C. J., and Vickers, D. A. (**1997**). "Short-term temporal integration: evidence for the influence of peripheral compression," J. Acoust. Soc. Am. **101**, 3676–3687.

Oxenham, A. J. (**1998**). "Temporal integration at 6 kHz as a function of masker bandwidth," J. Acoust. Soc. Am. **103**, 1033–1042.

Oxenham, A. J. (**2001**). "Forward masking: Adaptation or integration?," J. Acoust. Soc. Am. **109**, 732–741.

Palmer, A. R., and Russell, I. J. (**1986**). "Phase locking in the cochlear nerve of the guinea-pig and its relation to the receptor potential of inner hair-cells," Hear. Res. **24**, 1–15.

Palmer, A. R. (**1995**). “Neural signal processing,” in *Hearing*, edited by Moore, B. C. J. (Academic).

Patterson, R. D., and Moore, B. C. J. (**1986**). “Auditory filters and excitation patterns as representations of frequency resolution,” in *Frequency Selectivity in Hearing* (Academic, London).

Patterson, R. D., and Nimmo-Smith, I. (**1980**). “Off frequency listening and auditory filter asymmetry,” J. Acoust. Soc. Am. **67**, 229–245.

Patterson, R. D., Allerhand, M. H., and Giguere, C. (**1995**). “Time-domain modeling of peripheral auditory processing: a modular architecture and a software platform,” J. Acoust. Soc. Am. **98**, 1890–1894.

Phatak, S. A., and Allen, J. B. (**2007**). “Consonant and vowel confusions in speech-weighted noise,” J. Acoust. Soc. Am. **121**, 2312–2326.

Phatak, S. D., Lovitt, A., and Allen, J. B. (**2008**). “Consonant confusions in white noise,” J. Acoust. Soc. Am. **124**, 1220–1233.

Pickles, J. O. (**2008**). *An Introduction to the Physiology of Hearing*. pp. 56-63, Emerald, Bingley, U.K.

Piechowiak, T., Ewert, S. D., and Dau, T. (**2007**). “Modeling comodulation masking release using an equalization-cancellation mechanism.,” J. Acoust. Soc. Am. **121**, 2111–2126.

Plack, C. J., and Oxenham, A. J. (**1998**). “Basilar-membrane nonlinearity and the growth of forward masking,” J. Acoust. Soc. Am. **103**, 1598–1608.

Plack, C. J., and Oxenham, A. J. (**2000**). “Basilar-membrane nonlinearity estimated by pulsation threshold,” J. Acoust. Soc. Am. **107**, 501–507.

Plack, C. J., Oxenham, A. J., and Drga, V. (**2002**). “Linear and nonlinear processes in temporal masking,” Acustica - Acta Acustica **88**, 348–358.

Plack, C. J., Drga, V., and Lopez-Poveda, E. A. (**2004**). “Inferred basilarmembrane response functions for listeners with mild to moderate sensorineural hearing loss,” J. Acoust. Soc. Am. **115**, 1684–1695.

Plasberg, J. H., and Kleijn, W. B. (**2007**). “The sensitivity matrix: Using advanced auditory models in speech and audio processing,” IEEE Trans. Audio, Speech and Lang. Proc. **15**, 310–319.

Pralong, D., and Carlile, S. (**1996**). “The role of individualized headphone calibration for the generation of high fidelity virtual auditory space,” J. Acoust. Soc. Am. **100**, 3785–3793.

Püschel, D. (**1988**). *Prinzipien der zeitlichen Analyse beim Hören*. PhD thesis , University of Göttingen.

Reed, C. M., Braida, L. D., and Zurek, P. M. (**2009**). “Review of the literature on temporal resolution in listeners with cochlear hearing impairment: A critical assessment of the role of suprathreshold deficits,” Trends Amplif. **13**, 4–43.

Régnier, M. S., and Allen, J. B. (**2008**). “A method to identify noise-robust perceptual features: Application for consonant /t/,” J. Acoust. Soc. Am. **123**, 2801–2814.

Rhode, W. S., and Cooper, N. P. (**1996**). “Nonlinear mechanics in the apical turn of the chinchilla cochlea in vivo,” Aud. Neurosci. **3**, 101Ű121.

Rosen, S., Baker, R. J., and Darling, A. M. (**1998**). “Auditory filter nonlinearity at 2 kHz in normal listeners,” J. Acoust. Soc. Am. **103**, 2539–2550.

Rosengard, P. S., Oxenham, A. J., and Braida, L. D. (**2005**). “Comparing different estimates of cochlear compression in listeners with normal and impaired hearing,” J. Acoust. Soc. Am. **117**, 3028–3041.

Ru, P., and Shamma, S. A. (**1997**). “Representation of musical timbre in the auditory cortex,” J. New Music Res. **26**, 154–169.

Ruggero, M. A., and Rich, N. C. (**1991**). “Furosemide alters organ of corti mechanics: Evidence for feedback of outer haircells upon the basilar membrane,” J. Neuroscience **11**, 1057–1067.

Ruggero, M. A., Rich, N. C., Recio, A., Narayan, S. S., and Robles, L. (**1997**). “Basilar-membrane responses to tones at the base of the chinchilla cochlea,” J. Acoust. Soc. Am. **101**, 2151–2163.

Ruggero, M. A. (**1992**). “Physiology and coding of sound in the auditory nerve,” In A. N. Popper and R.R. Fay (Eds.), The Mammalian Auditory Pathway: Neurophysiology **Springer-Verlag, New York.**, pp. 34–93.

Schreiner, C. E., and Calhoun, B. (**1995**). “Spectral envelope coding in cat primary auditory cortex: Properties of ripple transfer functions,” J. Auditory Neuroscience **1**, 39–61.

Schroeder, M. R., and Hall, J. L. (**1974**). “Model for mechanical to neural transduction in the auditory receptor,” J. Acoust. Soc. Am. **55**, 1055–1060.

Schuknecht, H. F., and Woellner, R. C. (**1953**). “Hearing losses following partial section of the cochlear nerve,” Lyrangoscope **63**, 441–465.

Shamma, S. (**2001**). “On the role of space and time in auditory processing,” Trends Cogn. Sci. **5**, 340–348.

Shera, C. A., Guinan, J. J., and Oxenham, A. J. (**2002**). “Revised estimates of human cochlear tuning from otoacoustic and behavioral measurements,” Proc. Nat. Acad. Sci. U.S.A. **99**, 3318Ű3323.

Siebert, W. M. (**1965**). “Some implications of the stochastic behavior of primary auditory neurons.,” Kybernetik **2**, 206–215.

Siebert, W. M. (**1968**). “Quarterly no. 88,”. Technical Report pp. 330-334 MIT Research Lab of Electronics 1968.

Siebert, W. M. (**1970**). “Frequency discrimination in the auditory system: place or periodicity mechanism,” Proc. IEEE **58**, 723–730.

Smith, R. L. (**1977**). “Short-term adaptation in single auditory-nerve fibers: Some post-stimulatory effects,” J. Neurophysiology **49**, 1098–1112.

Stainsby, T. H., and Moore, B. C. J. (**2006**). “Temporal masking curves for hearing-impaired listeners,” Hear. Res. **218**, 98–111.

Steeneken, H., and Houtgast, T. (**1980**). “A physical method for measuring speech-transmission quality,” J. Acoust. Soc. Am. **67**, 318–326.

Stein, A., Ewert, S. D., and Wiegrebe, L. (**2005**). “Perceptual interaction between carrier periodicity and amplitude modulation in broadband stimuli: a comparison of the autocorrelation and modulation-filterbank model,” J. Acoust. Soc. Am. **118**, 2470–2481.

Strelcyk, O., and Dau, T. (**2009**). “Relations between frequency selectivity, temporal fine-structure processing, and speech reception in impaired hearing,” J. Acoust. Soc. Am. **125**, 3328–3345.

Strube, H. W. (**1985**). “Computationally efficient basilar-membrane model,” Acustica **58**, 207–214.

Tchorz, J., and Kollmeier, B. (**1999**). “A model of auditory perception as front end for automatic speech recognition,” J. Acoust. Soc. Am. **106**, 2040–2050.

Thompson, E., and Dau, T. (**2008**). “Frequency selectivity in binaural processing of fluctuations in interaural level difference,” J. Acoust. Soc. Am. **123**, 1017–1029.

van der Heijden, M., and Kohlrausch, A. (**1995**). "The role of envelope fluctuations in spectral masking," J. Acoust. Soc. Am. **97**, 1800–1807.

Verhey, J. L., Dau, T., and Kollmeier, B. (**1999**). "Within-channel cues in comodulation masking release (CMR): Experiments and model predictions using a modulation-filterbank model," J. Acoust. Soc. Am. **106**, 2733–2745.

Verhey, J. L. (**2002**). "Modeling the influence of inherent envelope fluctuations in simultaneous masking experiments," J. Acoust. Soc. Am. **111**, 1018–1025.

Viemeister, N., and Wakefield, G. (**1991**). "Temporal integration and multiple looks," J. Acoust. Soc. Am. **90**, 858–865.

Viemeister, N. F. (**1979**). "Temporal modulation transfer functions based upon modulation thresholds," J. Acoust. Soc. Am. **66**, 1364–1380.

Viemeister, N. F. (**1983**). "Auditory intensity discrimination at high frequencies in the presence of noise," Science **221**, 1206–1208.

Voiers, W. D. (**1983**). "Evaluating processed speech using the diagnostic rhyme test," Speech Technol. **1**, 30–39.

Wagener, K., Josvassen, J. L., and Ardenkjaer, R. (**2003**). "Design, optimization and evaluation of a Danish sentence test in noise," Int. J. Audiol. **42**, 10–17.

Wakefield, G. H., and Viemeister, N. F. (**1990**). "Discrimination of modulation depth of sinusoidal amplitude modulation (SAM) noise," J. Acoust. Soc. Am. **88**, 1367–1373.

Westermann, L. A., and Smith, R. L. (**1984**). "Rapid and short-term adaptation in auditory nerve responses," Hear. Res. **15**, 249–260.

Williams, E. J., and Bacon, S. P. (**2005**). "Compression estimates using behavioral and otoacoustic emission measures," Hear. Res. **201**, 44–54.

Wojtczak, M., and Oxenham, A. J. (**2009**). "Pitfalls in behavioural estimates of basilar-membrane compression in humans," J. Acoust. Soc. Am. **125**, 270–281.

Woolf, N. K., Ryan, A. F., and Bone, R. C. (**1981**). "Neural phase-locking properties in the absence of cochlear outer hair-cells," Hear. Res **107**, 335–346.

Yates, G. K., Winter, I. M., and Robertson, D. (**1990**). "Basilar membrane nonlinearity determines auditory nerve rate-intensity functions and cochlear dynamic range," Hear. Res. **45**, 203–220.

Zhang, X., Heinz, M. G., Bruce, I. C., and Carney, L. H. (**2001**). "A phenomenological model for the responses of auditory-nerve fibers: I. Nonlinear tuning with compression and suppression," J. Acoust. Soc. Am. **109**, 648–670.

Zilany, M. S. A., and Bruce, I. C. (**2006**). "Modeling auditory-nerve responses for high sound pressure levels in the normal and impaired auditory periphery," J. Acoust. Soc. Am. **120**, 1446–1466.

Zilany, M. S. A., and Bruce, I. C. (**2007**). "Representation of the vowel /ϵ/ in normal and impaired auditory nerve fibers: Model predictions of responses in cats," J. Acoust. Soc. Am. **122**, 402–417.

Contributions to Hearing Research

Vol. 1: *Gilles Pigasse*, Deriving cochlear delays in humans using otoacoustic emissions and auditory evoked potentials, Dec. 2008.

Vol. 2: *Olaf Strelcyk*, Peripheral auditory processing and speech reception in impaired hearing, Jun. 2009.

Vol. 3: *Eric R. Thompson*, Characterizing binaural processing of amplitude-modulated sounds, Aug. 2009.

Vol. 4: *Tobias Piechowiak*, Spectro-temporal analysis of complex sounds in the human auditory system, Sept. 2009.

Vol. 5: *Jens Bo Nielsen*, Assessment of speech intelligibility in background noise and reverberation, Dec. 2009.

Vol. 6: *Helen Connor Sørensen*, Hearing aid amplification at soft input levels, Jan. 2010.

Vol. 7: *Morten Løve Jepsen*, Modeling auditory processing and speech perception in hearing-impaired listeners, May 2010

Vol. 8: *Sarah Verhulst*, Characterizing and modeling dynamic processes in the cochlea using otoacoustic emissions, Jun. 2010

Vol. 9: *Sylvain Favrot*, A loudspeaker-based room auralization system for auditory research, Jun. 2010